Ultra-precision Abrasive Machining of Functional Structured Surfaces

Christian Thomas Young

A thesis submitted to the University of Huddersfield in partial fulfilments of the requirements for the degree of Doctor of Philosophy

The University of Huddersfield

Submission date June 2018

Abstract

This thesis details the research undertaken to investigate the feasibility of the adaption of macro-scale grinding techniques to the production of micro-scale surface structures. The ability to utilise these techniques in conjunction with equipment normally associated with ultra-precision grinding presents an opportunity to increase the manufacturing capability of existing ultra-precision machining centres at relatively low cost. Grinding is a process well suited to the manufacture of surface structures in substances such as hard or brittle materials, for example tool steels and ceramics, which can be difficult or costly to work. This is of particular value when considering the production of moulds for parts incorporating functional surface structures, which are becoming increasingly common.

A wide variety of parts can incorporate functional structured surfaces which utilise micro and nano scale structures to provide beneficial characteristics. Structured surfaces are currently being used to affect properties such as drag reduction, wettability and reflectivity. However, the manufacture of structured surfaces either directly onto the part or onto moulds and other forming tools presents several challenges. The manufacture of the individual micro and nano scale features requires specialist production techniques which can prove costly and difficult to apply over larger areas.

Recently macro-scale grinding techniques using grinding wheels incorporating specialised geometry have been demonstrated which can be used in the production of deterministic surface textures. Adapting these techniques for micro-scale production of surface structures presents several challenges. The tools and equipment used must be sufficiently accurate and capable of a high degree of control while also being cost effective and rugged enough to be utilised in a typical CNC ultra-precision machining environment. The scalability of the process also presents a unique challenge in the physical interaction of the tool and workpiece. Conventional techniques used to analyse the performance of ultra-precision grinding are unsuitable or insufficient to characterise the micro-scale structures generated by such a process.

The original contribution of this work is to address these challenges and demonstrate a system capable of dressing grinding wheels by utilising a novel offset technique with a continuously rotating single point dressing nib. Grinding wheels have been dressed with specialised geometry and used to produce micro patches with aspect ratios of 10:1 and feature heights of 40+ μm. The system presented is cost effective and could be retrofitted onto an existing CNC ultra-precision machining centre for approximately £10,000 to £15,000. While not capable of producing every distinct type of surface structure; this system has the potential to greatly increase the ability of small manufacturing companies to incorporate a specific range of functional surface structures into their products without the expense of large capital outlay on specialised equipment. This would greatly impact on their ability to manufacture high value added parts.

1 Contents

List of Figures

List of Tables

Acknowledgements and Dedication

First and foremost, I would like to thank my supervisory team of Professor Liam Blunt and Dr Leigh Fleming for their guidance and support throughout the project. You have helped me develop not only as a researcher but as a person by providing opportunities to engage in a wide range of activities. I would also like to thank Dr Zhen Tong. As leader of the Ultra Precision Manufacturing Group, your enthusiasm for the project and help and advice have been greatly appreciated. As the people around me know, the machine I have been working on has not always proven the most reliable, it is only with the help of Chris Dawson and John Allsop that I have been able to keep it going. You have both provided me with an excellent technical education and I have no doubt that without your support I would still be scratching my head and trying to figure out how the Nanoform 250 works! Finally, I would like to thank all my friends and colleagues within the Centre for Precision Technologies for making it such a pleasant place to work. In particular, I must thank my firm friends Zavid, Katie and Duo Li. Together we've worked towards our PhDs, travelled around the world, taken part in competitions and drunk more tea than I care to think about! The author gratefully acknowledges the UK's Engineering and Physical Sciences Research Council (EPSRC) funding of the EPSRC Centre for Innovative Manufacturing in Advanced Metrology (Grant Ref: EP/I033424/1).

This work is dedicated to my long suffering partner and soon to be wife, Lorna, who allowed me to remain a student just a little while longer. Your support and encouragement have kept me going through good times and through tough times and without it I certainly wouldn't be where I am now. Thank you.

Abbreviations

ARS:	Anti-Reflection Structured
CBN:	Cubic Boron Nitride
CNC:	Computer Numerical Control
CVD:	Chemical Vapour Deposition
DTI:	Dial Test Indicator
EDM:	Electrical Discharge Machining
ELID:	Electrolytic In-process Dressing
FIB:	Focused Ion Beam
FTS:	Fast tool Servo
HBN:	Hexagonal Boron Nitride
MOA:	Minute of Angle
NIL:	Nanoimprint Lithography
PC:	Personal Computer
PCD:	Polycrystalline Diamond
PGA:	Passive Grinding Area
RPM:	Revolutions Per Minute
SPDT:	Single Point Diamond Turning
SCD:	Single Crystal Diamond
SEM:	Scanning Electron Microscope
STS:	Slow Tool Servo
USB:	Universal Serial Bus
UcBN:	Ultrafine-crystalline cubic Boron Nitride

Chapter One

Introduction

This chapter details the background to the project, its aims and objectives. The challenges being addressed, and the benefits of the work are briefly introduced. The chapter concludes with a summary of the contribution and an outline of the thesis structure.

Compared to conventional methods of machining micro-scale functional surface structures, grinding has several advantages such as low cost and the ability to machine relatively large surfaces in a single operation. These advantages could potentially increase the viability of incorporating functional surfaces on a broader range of products.

1 Introduction

1.1 Research Background

The ability of functional micro-scale surface structures to impart beneficial characteristics on to manufactured parts presents a great opportunity to increase the capability of a wide range of items and devices. These beneficial characteristics range from improvements in performance, such as the incorporation of drag reducing riblets which can be applied to surfaces such as turbine blades to increase efficiency, through to new functionality such as super hydrophobicity which facilitates the control and positioning of liquids in micro-fluidic medical devices. In addition to these exotic, high value added applications, surface structures are increasingly used in everyday products, for example smart phones use optical de-pixelators in their screens, while sports clothing may incorporate super-reflective patches to improve visibility. The most common means of large volume manufacture of parts with surface structures is moulding. This is well suited to the manufacture of parts in plastics but for parts made from metals or ceramics it is necessary to machine, or otherwise apply, the structures directly onto the surface of the part.

A variety of techniques are used to manufacture parts or moulds incorporating functional surface structures; typically, these can be classified as either direct machining or applied coatings. Direct machining techniques such as Fast Tool Servo (FTS) assisted diamond turning, micro milling or laser ablation are generally used to machine individual structures over the surface of the part. Direct machining is well suited to the production of deterministic surface structures of well-defined, regular form and it is highly versatile, capable of producing a wide variety of forms. However, these processes can be very time consuming, particularly over larger areas, as each structure is individually formed. Coatings can be applied over large areas using techniques such as Chemical Vapour Deposition (CVD) but these processes are generally only capable of producing stochastic textures, limiting the type of additional functionality that can be achieved. For both techniques, an initial high

capital outlay is required to purchase specialist equipment and tooling which can be especially prohibitive for smaller companies.

Recently several techniques for specialised grinding using structured grinding wheels to generate deterministic surface textures on a macro-scale have been demonstrated (Stepien, 2007a). The principal challenge in each of these techniques has been the development of a method to accurately dress the required profile geometry onto the surface of the grinding wheel. For the most part the textures produced have very low aspect ratios i.e. the depth of the features created is a fraction of the length and width of the feature. For example, both the Stępień (2007a) technique and the technique developed by Oliveira, et al. (2010) have created features with lengths of 2mm+ and depths of approximately 20µm yielding an aspect ratio of approximately 100:1 However, other techniques, particularly those developed by Denkena, et al. (2009) have shown promise for the manufacture of functional surface structures, albeit using highly specialised grinding wheels and profile rollers, which have achieved limited success in generating features with aspect ratios in the region of 2:1. Modifying and adapting these techniques to produce features with aspect ratios of 10:1 or greater, utilising conventional super-abrasive ultra-precision grinding wheels could represent a more accessible method of manufacturing some types of structured surfaces.

While there are limitations to the types of forms that could be achieved, the potential to use grinding to directly machine surface structures has several benefits. The use of specially profiled wheels to selectively grind material means that larger areas can be machined more quickly, in reduced operations. Tooling costs would also be comparatively low if it were possible to retrofit the required equipment onto existing CNC machining centres. This would make the use of functional surface structures more cost effective on a wider range of parts and more accessible to smaller manufacturing companies.

1.2 Aims and Objectives

The aim of this project is to investigate the potential for structured abrasive machining to be used in the production of artefacts incorporating functional surface structures and to use the findings to develop a cost-effective method to implement this technique on a conventional CNC ultra-precision machining centre.

To achieve the aim the following objectives have been identified:

- Investigate the different types of types of functional structured surfaces that exist and identify which profiles would be suitable for production using structured grinding.
- Examine the various macro-scale structured grinding techniques which have previously been developed and evaluate their potential to be adapted for use in the micro-scale.
- Identify a suitable technique(s) to dress profiles onto ultra-precision grinding wheels.
- Develop mathematical models to describe the relationship between the dressing process, grinding wheel profile and structured surface profile which can be used to determine a grinding solution for a given surface design.
- Adapt the Precitech Nanoform 250 Ultra Grind CNC diamond turning lathe and grinding centre, available at the University of Huddersfield, to be capable of carrying out the developed techniques.
- Carry out machining trials using the techniques developed to produce surface structures with useable aspect ratios and demonstrate the capability of the setup,
- Evaluate the performance of the manufacturing process to determine the accuracy of the dressing process and the capability to reproduce surface structures based on the nominal design; and
- Identify any areas for further development.

1.3 Summary of Contribution

Presented in this thesis are several contributions to the field of structured grinding.

Firstly, a technique for using a single point diamond dressing nib to true an ultra-precision grinding wheel and then dress a specified profile in-situ on the machine has been developed and refined. The process developed utilises a novel method of positioning the dressing nib offset from the centreline of the grinding wheel and continually rotating the nib throughout the dressing process. This results in significant reductions to the wear rate of the dressing nib while also allowing it to maintain a more uniform radiused profile.

Secondly, this technique has been used to dress micro-scale profiles onto a number of ultra-precision grinding wheels. Strategies for using these specially profiled grinding wheels to directly machine micro-scale features with pitch lengths of approximately 400µm onto the surface of a workpiece to depths of greater than 40µm; the resultant features having aspect ratios of approximately 10:1. These trials have been used to evaluate the performance of the techniques developed. The technique developed is not suitable for producing all structured surface profiles, forms with sharp flat edges cannot be created due to the limitations of using a rotating tool. However, for the profiles that can be generated, performance is similar to existing manufacturing techniques.

Finally, a cost-effective method of retrofitting the equipment required to enable the use of these techniques has been designed. This system allows any ultra-precision CNC machining equipped with two or more linear axes and a rotary workpiece axis to be adapted for use in the manufacture of parts incorporating a range of functional surfaces. The total cost of retrofitting the system as described would range between £10,000-£15,000 depending on the specification of the existing equipment. Further refinement of the techniques developed in this project will allow a broader spectrum of manufacturing companies to access the capability to produce artefacts incorporating functional structured surfaces.

1.4 Structure of Thesis

The thesis is presented in three sections.

The first section is a review of the existing literature surrounding functional surface structures, grinding technology and existing structured grinding techniques. This section provides a brief background to the research which informed the design of the techniques developed.

The second section details the mathematical modelling processes necessary to design the structured grinding operations described and the changes made to the Precitech Nanoform 250 Ultra Grind to develop the capability to carry out micro-scale structured grinding. This section aims to enable the reader to replicate the process on similar equipment.

The final section details the experimental procedures carried out, and the results generated, to develop the capability for ultra-precision grinding of functional surface structures. The section ends with a discussion of the success of the work and recommendations for future follow on work to further enhance the capability of these processes.

Chapter Two

Literature Review

This chapter presents a consideration of the major technical elements relating to this project and summarises the relevant research carried out in these fields.

Firstly, structured surfaces are examined to demonstrate what constitutes a structured surface and what kind of beneficial characteristics they are capable of delivering. Examples of manufactured surfaces and instances of their presence in nature are presented along with their applications. The methods of producing these surface structures are also shown.

Secondly, grinding as a manufacturing process is examined in detail to determine the advantages and disadvantages of this technique for production of surface structures. Macro scale structured grinding has received significant interest recently and an examination of these techniques, in particular the methods of dressing the grinding wheels, is under taken to identify the most suitable avenues for investigation in this process.

2 Literature Review

2.1 Functional Structured Surfaces

When designing a part, the designer will usually represent the surface, the boundary between the workpiece and its environment, as a clean, smooth line. This is referred to as the nominal surface. However, when the component is made the manufacturing process inevitably results in a surface texture with features and imperfections which deviate from the nominal design (Mummery, 1992). Typically, these surfaces are non-functional and can be quantified by measures such as surface roughness (*Ra*). Historically measurement techniques have focussed on linear measurements and, to a greater or lesser extent, these are still commonplace in industry. However, there is a trend towards the adoption of 3D areal measurement as this provides a more comprehensive approach to surface characterisation and is better able to represent the functional properties of a part (Blunt & Jiang, 2003).

Surfaces can generally be classified as engineered or non-engineered. Non-engineered implies that, provided the part is manufactured to the tolerances for surface finish, no additional processing is necessary. Non-engineered surfaces are typically generated as a result of the manufacturing process used and may range from very rough, for example from investment casting, through to very smooth, for example a polished finish. A specific level of surface finish may be specified when it is relevant to the parts function, for example the production of smooth bearing surfaces, but beyond this specific criterion the surface characteristics do not impact upon the functionality of the part. Engineered surfaces are surfaces designed with a specific function in mind which is integral to the function of the part incorporating the surface. These can be structured or unstructured. An example of an unstructured engineered surface would be a honed cylinder bore. Honing provides functional grooves for oil retention and lubrication, but the process is stochastic. A structured surface is one which, through the application of deterministic high aspect ratio micro and nano scale geometric features, has a specific designed function. Structured surfaces can further be

classified as directional or non-directional based on the orientation and distribution of the features (Stout & Blunt, 2001).

Engineered surfaces have many functional properties which, broadly speaking, can be separated into three main domains; physical, biological and technological. Within these domains further sub-divisions exist which are each relevant to different characteristics. For example, surface energy is a physical property which affects a surfaces capillarity, wettability and adhesive qualities. By creating structured geometry on the surface of a part it is possible to alter these properties and manipulate the characteristics to achieve an outcome beneficial to a specific application. To exploit the functional properties of a surface it is necessary to follow a structured design-manufacturing process as shown in Figure 2-1 (Bruzzone, et al., 2008).

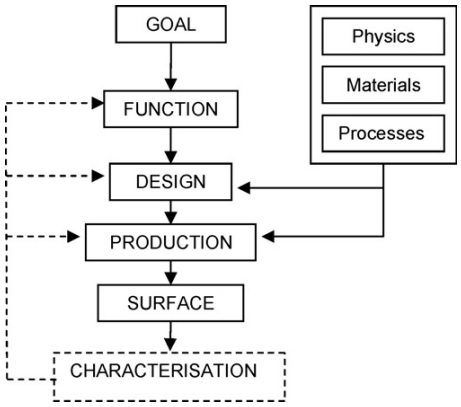

Figure 2-1: Development process for 'surfaces-based' applications (Bruzzone, et al., 2008)

Many manufactured structured surfaces take their inspiration from nature. Over the course of millions of years plants and animals have evolved characteristics which provide a competitive advantage in their environment. By determining the functional aspects of these advantages and the mechanisms through which they act, it is possible to design and manufacture surfaces which also incorporate these beneficial characteristics. The term “biomimetics” is used to refer to designs inspired by, or adapted from, nature. (Bhushan, 2012). Examples of different biomimetic structured surfaces are discussed below.

Superhydrophobicity is the ability of a surface to repel water. The same effect can be achieved with other liquids, in which case the term is changed to reflect the liquid, for example oil repellent surfaces would be referred to as oleophobic. There are two types of superhydrophobic surfaces which differ in the degree of contact angle and contact angle hysteresis. Surfaces with a static contact angle above 150 degree and low contact angle hysteresis will exhibit extreme water repellence and very low wettability (Hisler, et al., 2014). This causes water droplet on the surface to ball up and roll or slide over the surface. This phenomenon is referred to as the lotus effect after the plant which exhibits this property. The effect allows the beads of water to remove contaminant particles from the surface and is useful in applications where self-cleaning is desirable. Rose petals exhibit a similar effect with high contact angle hysteresis. In this case, liquids will still bead up but as the micro and nano structures have a larger pitch value, liquids can partially penetrate in a process referred to as the Cassie impregnating wetting regime (Lee, et al., 2018). The beads of liquid display a strong adhesion to the surface and will not roll off even if the surface is inclined. This property is useful in applications requiring retention of liquid such as lubrication of the processing and analysis of liquid microdroplets in microfluidic devices. Both these surfaces are examples of a hierarchical structure, an example of which can be seen in Figure 2-2. Hierarchical surfaces incorporate features of significantly different sizes. In the lotus example shown the micro pillars are themselves covered in a nano structure of wax tubules.

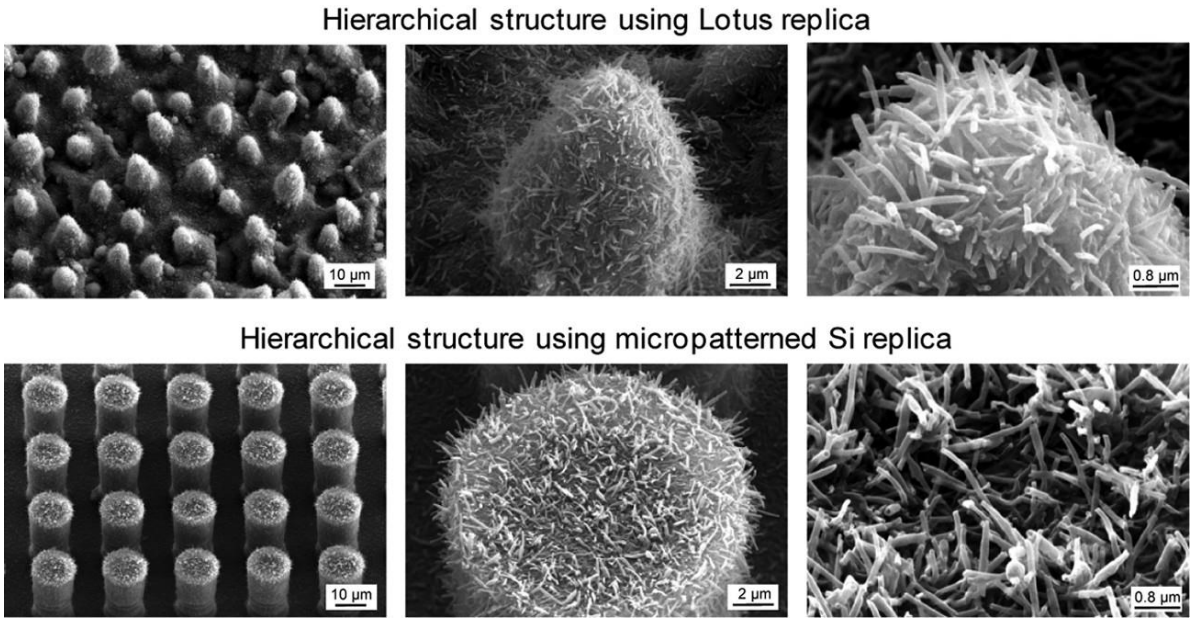

Figure 2-2: Comparison of natural and manufactured hydrophobic surfaces (Bhushan, 2012)

Counter to hydrophobicity is hydrophilicity, the characteristic of a surface to attract liquids so that they spread completely over the surface. This is sometimes referred to as superwetting or hemi-wicking. This characteristic has several potentially beneficial applications and could be used to facilitate surface drying or to reduce bubble formation in fluid handling systems. A technique to allow graphite to demonstrate superwetting has been demonstrated using arrays of square pillars with side lengths of 390µm and a height of 420µm and treated to render them lyophilic. This example demonstrates how structured surfaces can impart beneficial characteristics which would not otherwise be present, and the inherent wettability of the graphite did not impact on the end result. Varying the geometry of the surface structures, such as the spacing and the height of the features, it was possible to control the degree of wicking (Extrand, et al., 2007)

One of the more well-known types of structured surfaces are the so called “shark skin” drag reducing surfaces. The skin of fast swimming sharks is covered in tiny scales called dermal denticles, these are illustrated in Figure 2-3. These form a surface of micro riblets aligned in the direction of flow and act to reduce viscous drag by up to 9.9 per cent (Dean & Bhushan, 2010). Shark skin surfaces were brought to the public’s attention when they were

controversially used on the rowing shell hull of the United States rowing team at the 1984 Olympic games and on the hull of the winning yacht in the 1987 America's cup race. They were subsequently banned from competition. The idea was revived for competitive swimwear, once again for the Olympic games, by Speedo™ in 2004 with their introduction of FASTSKIN swimsuits. These swimsuits incorporate a fabric weave which creates grooves mimicking riblets. The drag reduction, and competitive advantage, these suits provide has caused some controversy, but they are still commercially available (Favret & Nestor, 2009).

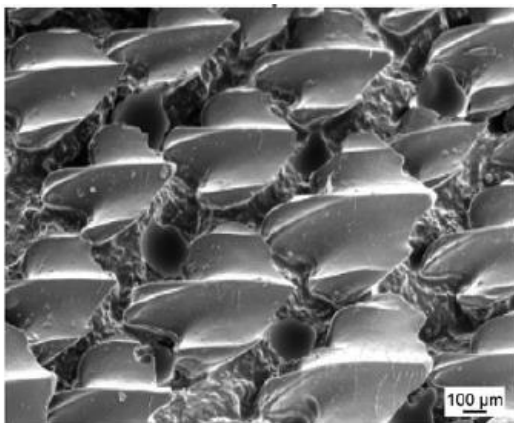

Figure 2-3: Shark skin showing drag reducing micro riblets (Bhushan, 2012)

Outside of competitive water sports drag reducing riblets have many other applications. Manufactured riblets with varying profiles such as those shown in Figure 2-4 have been applied to parts ranging from the body of a commercial aeroplane to the surfaces of aerofoils and turbine blades (Garcia-Mayoral & Jimenez, 2011). The drag reduction benefits and consequent improvements in efficiency are highly desirable. However, for the riblets to be effective the surface structure must be applied to the majority of the part exposed to fluid flow. Developing a cost effective manufacturing method capable of being applied to large surface areas, potentially with complex geometries, is a significant challenge and presents a definite barrier to widescale adoption.

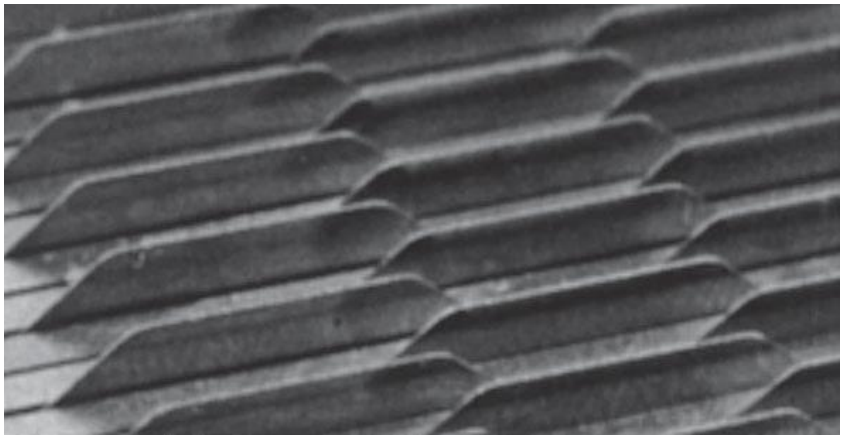

Figure 2-4: Manufactured trapezoidal blade riblets (Dean & Bhushan, 2010)

Antireflection structured (ARS) surfaces such as those found on the corneas of certain species of moth are effective at suppressing the reflections of both linearly polarised and randomly polarised light. This is achieved by the production of structured arrays of subwavelength size and by varying the size of the features it is possible to select which portions of the spectrum will not be reflected. The ideal profile for an ARS surface is an array of square based pyramids (Raguin & Morris, 1993). However, profiles with such sharp points and edges are difficult to produce and prone to damage. The natural surface in a moth's eye is more akin to a sine wave, and this type of feature has been successfully replicated experimentally as shown in Figure 2-5. The typical period and depth of the features necessary to achieve useful antireflective properties is 200-250nm which presents a significant challenge to manufacturing however areas of 2500mm^2 have been created (Abbott & Gaskell, 2007). Currently antireflective coatings are applied to parts using additive methods such as Nanoimprint Lithography (NIL) to achieve the effect however this has some limitations including a lack of suitable liquid coating materials and the unavailability of commercial scale NIL processes (Buskens, et al., 2016). Therefore, the ability to create parts with antireflective properties through processes such as injection moulding has some advantages.

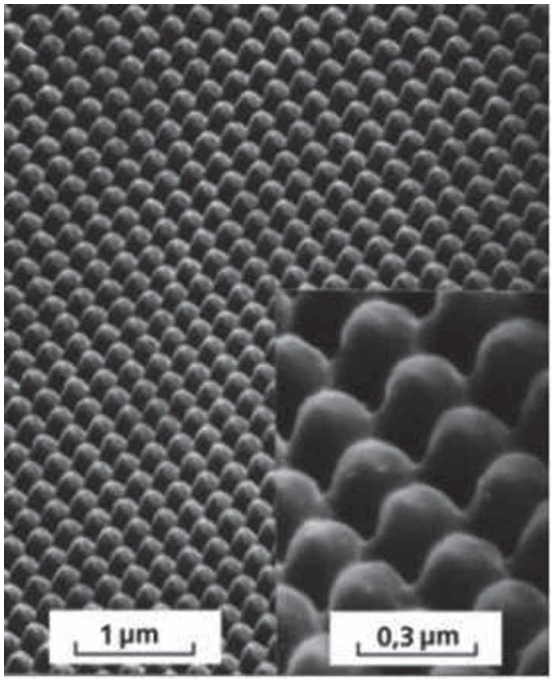

Figure 2-5:Antireflective Moth eye structure replicated in polymer (Abbot & Caskell, 2007)

One type of structured surface which is not present in nature is the saw tooth ratchet profile utilised in the propulsion of liquid droplets using the Leidenfrost effect. The Leidenfrost effect occurs when a droplet of liquid is placed on a heated surface and levitates on a film of gas produced by evaporation. It has been shown that when the surface is structured with a ratchet profile, as shown in Figure 2-6, a force can be induced in the droplet propelling it over the surface. This has a range of potential applications in micro-fluidics and thermal management. The propulsion effect is significantly enhanced when the period and height of the ratchet profile is reduced to the micro and sub-micron scale, an example of which can be seen in Figure 2-7 (Ok, et al., 2011). Additionally, directional control of the droplet can be improved if a hierarchical surface structure is adopted and further micro structures are incorporated on to the surface of the ratchet profile (Grounds, et al., 2012).

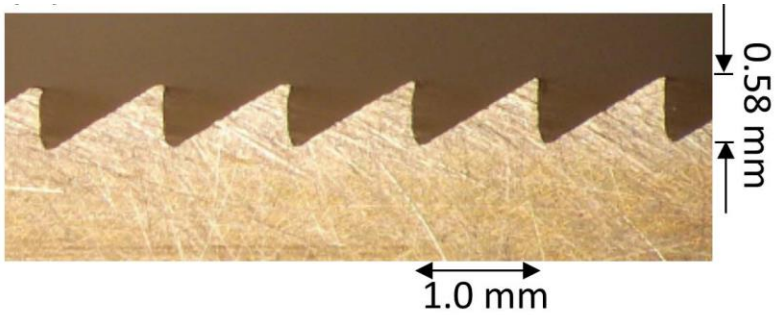

Figure 2-6: Saw Tooth Ratchet Profile (Grounds, et al., 2012)

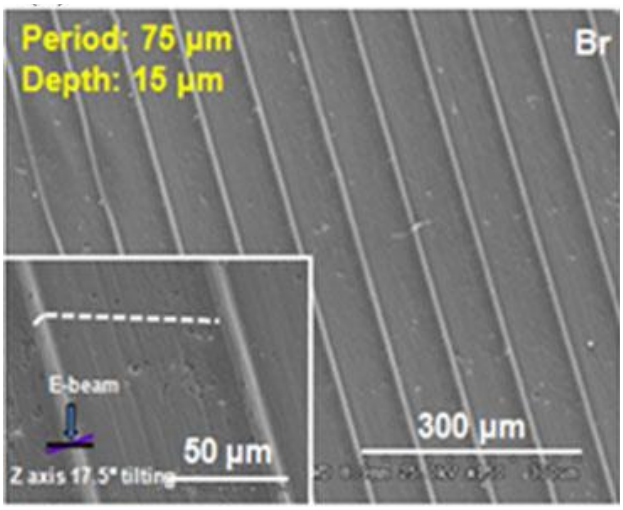

Figure 2-7: Micro scale ratchet surface in brass (Ok, et al., 2011)

A variety of methods have been used in the manufacture of surfaces structures ranging from conventional machining techniques such as diamond turning and micro milling through to more advanced methods such as focussed ion beam or laser ablation. For structured surfaces to be viable on manufactured parts they must not only provide a technological advantage, they must also be economical to produce. Micro manufacturing techniques which are used to produce each surface feature individually are suitable for individual items or the manufacture of very small batches, but they are not capable of mass production due to the lengthy machining times (Kirsch, et al., 2017). For nano scale surfaces with random feature orientation techniques such as Chemical Vapour Deposition or nanosuspension coating can be used rather than machining the surface directly (Gao, et al., 2012). This is beneficial as it is capable of coating large surface areas. However, for features which rely on orientation for their function or are in the micro scale this technique cannot be used and micro machining

techniques are better suited. (Abbott & Gaskell, 2007). However, there are geometric and kinematic limitations associated with physical manufacturing processes (De Chiffre, et al., 2003).

For larger surfaces with relatively simple geometry such as the saw tooth ratchet surface profile previously discussed, a mixture of conventional and ultra-precision techniques may be used to achieve the desired effect. For example, producing a stepped surface by micro-milling is a simple process which does not require complex tool setting. By then using conventional machining on the reverse of the workpiece it is possible to reorient the stepped surface so that it acquires the correct ratchet profile (Ok, et al., 2011). Ratchet profiles have also been manufactured to a height of 200µm by wire-electrode cutting (Feng, et al., 2012).

2.2 Methods of manufacturing structured surfaces

Several methods of manufacturing micro scale surface structures exist, each suited to the production of structures with different forms. The techniques can broadly be separated into subtractive methods, where material is selectively removed from the stock, and additive methods where material is added to a substrate to create a new surface profile.

2.2.1 Subtractive Methods

In subtractive machining processes, material is selectively removed from piece of stock material that is larger than the desired final form. There are three main mechanisms for the removal of material: cutting, abrading and eroding.

Many ultra-precision machining techniques make use of diamond cutting tools. Superficially these resemble conventional machining processes such as turning, fly cutting or planning. In cutting processes, single or multi-point cutting tools are passed over the surface of a part at a set depth to shear material away as chips. The size, shape and volume of the chips formed varies with each cutting process and the tool geometry being used. There are two main types of cutting diamond cutting tool which can be used to directly cut structures. Form

tools are shaped to match the profile of the desired structures and use simple tool paths to replicate the features on the surface of the part. Radius tools are shaped to provide an efficient cutting edge which is smaller than the desired feature and must be moved using a tool path which matches the form of the desired feature. In general, form tools provide greater form accuracy at the cost of reduced surface finish (Steinkopf, et al., 2015). This is illustrated in Figure 2-8. Beyond simple tool paths, it is possible to use radius tools to generate more complex arrays such as convex or concave dome arrays. This can be achieved by using Slow Tool Servo (STS) and Fast Tool Servo (FTS) motion control, in conjunction with workpiece rotation, to generate more complex tool paths (Zhu, et at., 2016)

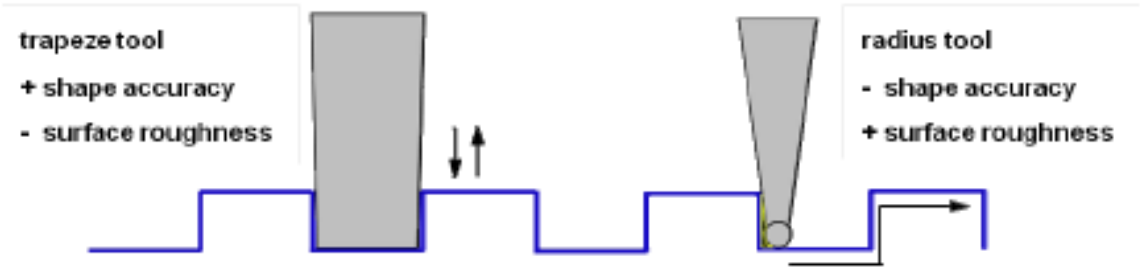

Figure 2-8: Form Tool (left) and Radius Tool (right) showing typical tool paths (Steinkopf, et al., 2015)

The unique properties of diamond make it ideal for cutting operations designed to produce micro scale features. As a superhard material, diamond can be shaped to an extremely fine cutting edge with a high degree of accuracy. In addition, it is highly resilient, displaying high wear resistance and thermal stability while maintaining a low coefficient of friction. These factors make it a highly efficient cutting tool. When used in macro scale machining processes to generate surfaces with very high surface finishes, typically less than Ra 10nm, a Single Crystal Diamond (SCD) tool is most frequently used. These are often referred to as having a single point, as in Single Point Diamond Turning (SPDT). However, in reality the cutting edge is usually shaped to a radius or other profile similar to conventional cutting tools. In some applications SCD can be prone to chipping leading to tool damage. In these cases, Polycrystalline Diamond (PCD), created using powdered diamond fused under high temperature and high pressure can be used. PCD is significantly more resistant to chipping

or fracture though, while it is almost as hard as SCD, the edge will not be as sharp (Zhang, et al., 2017). Diamond tooling can be used to cut a wide range of non-ferrous materials from metals such as aluminium, copper and electroless nickel, through to other ductile material such as plastics. However, other materials such as titanium, pure nickel or alloys containing carbon, such as steel, cannot be machined using diamond as the tool wears and becomes dull quickly due to a material interaction that is not currently fully understood (Davies, et al., 2003). To machine these materials the same processes can be used with different superhard materials such as Cubic Boron Nitride (CBN) though quality of surface finish is typically somewhat poorer than can be achieved with diamond tooling.

For the production of micro scale geometries, conventional diamond tooling is not suitable as the tool geometry is too large to be used to create the required profiles. It is therefore necessary to create specialised tools by shaping the cutting edge according to requirements. For relatively simple geometries such as V grooves, square profile grooves or through rotation of the workpiece, straight sided pyramidal structures, this could be achieved by shaping the cutting edge to match the required profile. Techniques such as these have been used successfully in the creation of micro-grooves (Liu, et al., 2017) and micro-pyramids (Zhu, et al,. 2016) to a depth of 20μm using a fly cutting process as shown in Figure 2-9.

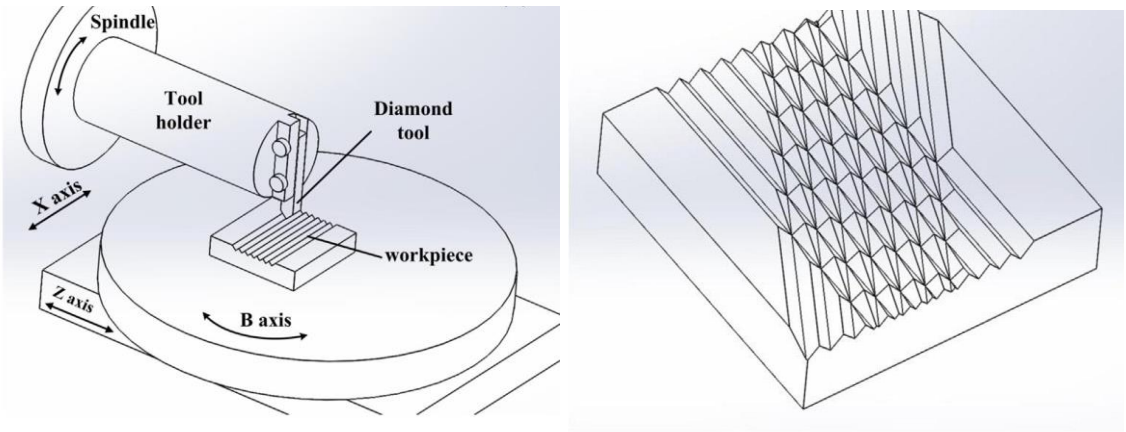

Figure 2-9: Diamond fly cutting arrangement and resultant surface (Zhu, et al., 2016)

The techniques described thus far use macro scale geometries for the cutting edge, albeit sharpened to very small tolerances. It is also possible to shape micro scale cutting

geometries onto the edge of a diamond cutting tools using Focused Ion Beam (FIB) sputtering (Tong & Luo, 2015). These tools can be used to directly machine individual features onto the surface of a part. This technique has been sucessfully demonstrated in a diamond turning process to create micro V groove arrays on a cylindrical face (Picard, et al., 2003). Figure 2-10 shows the shaped tool and resultant surface from this procedure.

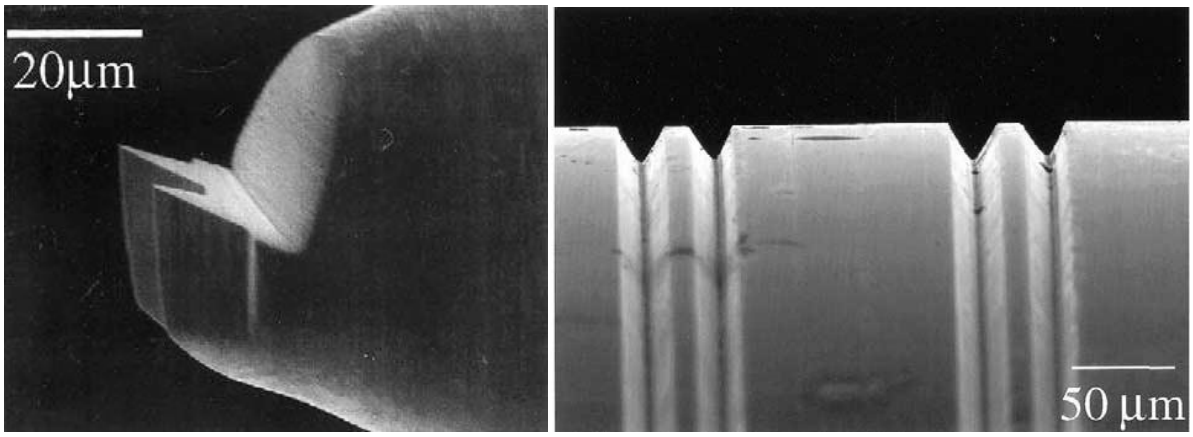

Figure 2-10: FIB shaped tool (left) and Micro-grooves (right) (Picard, et al., 2003)

In conventional machining, milling is one of the most common methods of manufacturing parts with 3D forms. Milling tools are rotary cutting tools with multiple continuous cutting edges. Because milling tools can cut in multiple directions while they are rotating, they can be used to selectively remove material along tool paths which match the profile of the part being created. Milling tools have specific geometry which is optimised for the cutting process being carried out. One of the most common and versatile profiles for a milling tool is the ball-end mill (Pratap & Patra, 2018). Figure 2-11 shows a macro scale ball-end milling tool and a part produced by such a tool, clearly showing the versatility of the process and the ability to cut in multiple directions to generate a complex form.

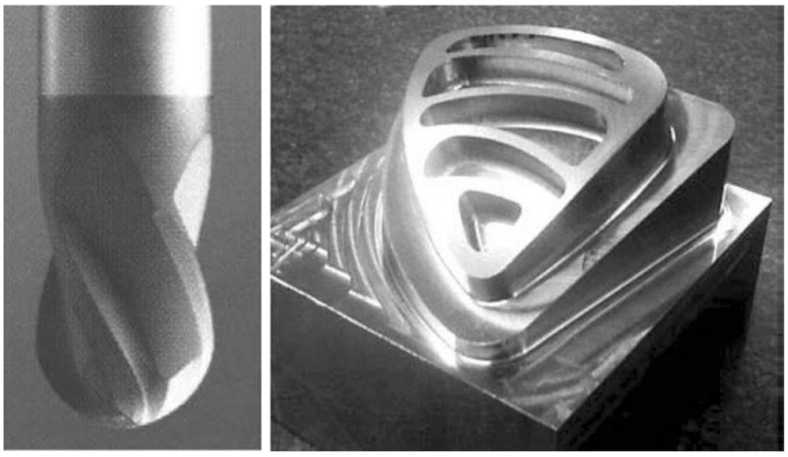

Figure 2-11: 6mm Ball-end milling tool and part produced by high speed ball-end milling (Pratap & Patra, 2018)

Micro-milling utilises similarly shaped tools at a micro scale to create individual features with complicated shapes on the surface of a part. Examples of the types of features which can be generated include micro-dimple, micro-groove and micro-pyramid arrays. Figure 2-12 Shows false-colour 3D topology of such arrays.

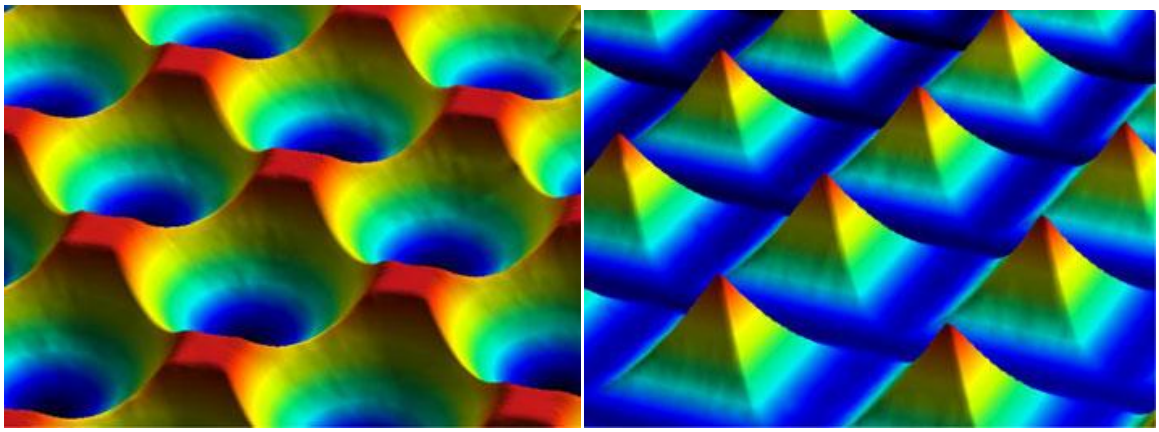

Figure 2-12: 5μm deep arrays of micro-dimples (left) and micro-pyramids (right) (Yan, et al., 2010)

The position of the features can be varied by changing the tool path used. The form of the features is also a result of the tool path but the range of profile which can be generated is limited by the form of the tool being used. As each feature is individually machined, the processing times to produce large arrays can be prohibitive. To produce high quality surface finishes on the produced forms, micro-milling tools can be fabricated using single diamond crystals sharpened to two cutting edges (Yan, et al., 2010).

Abrasive processes such as grinding and polishing are also cutting processes but they differ from those described already in that they make use of abrasive particles to remove material from the surface of the part. The abrasive particles act as a distributed set of discontinuous cutting edges which, individually, remove small amounts of material. In grinding the abrasive particles are fixed and bonded together in a statistically distributed fashion, wheras in polishing the abrasive particles are loose (Brinksmeier, et al., 2010).

Grinding wheels can be shaped with specific geometry to create matching profiles on the surface of a part using linear tool paths (Curtis, et al., 2009). Structures manufactured in this way might best be described as meso scale in that the are a functional element of the surface of the part they are machined onto, but the individual features have geometries with dimensions in the 1mm range. Examples of structures manufactured using superabrasive grinding wheels shaped in this way would include so called fir tree grinding wheels used to grind meso scale root mounting slots on turbine blade roots (Aspinwall, et al., 2007). For machining individual micro scale structures and arrays, highly specialised grinding wheels have been developed, reffered to as micro-pencil grinding tools. These tools have been manufactured using a variety of methods, with diameters of between 5μm to 200μm. The tools can be used in a similar fashion to micro-milling tools and share many of the advantages and disadvantages. Figure 2-13 shows several examples of these micro-pencil grinding tools.

Figure 2-13: Examples of micro-pencil grinding tools produced by CVD coating (left), sintering (centre) and electroplating (right) (Brinksmeier, et al., 2010)

Polishing uses loose abrasive particles to remove small amounts of material from the surface of a part and is usually used to increase surface finish. The abrasive particles are usually suspended in a liquid or a paste to be supplied to the process and are forced into contact with the workpiece using a polishing tool. When polishing surface structures, the primary challenge is to avoid rounding of the corners and edges. This can be achieved by using specially shaped polishing tools manufactured from materials sufficiently hard to avoid form deviation whilst also being tough enough to carry the abrasive particles. This process has been demonstrated by Brinksmeier et al. (2006) to increase the quality of the surface finish of V grooves features created using a fly cutting process without significantly impacting on the form accuracy. Structures can also be created by varying the tool path, swing angle and speed and pressure of a conventional polishing tool. Using this technique Zhong-Chen et al. (2017) have created patterned features on the surface of parts. The primary limitation of polishing as a means to produce structured surfaces is the limited number of profiles which can be created with the tools available and the degree to which the process can be controlled due to the random distribution and motion of the abrasive particles.

In addition to methods of removing material from a part using cutting mechanisms, several methods of eroding material directly exist which have been used to create surface structures. Electrical Discharge Machining (EDM) uses a shaped electrode, brought into close proximity to the workpiece surface in the presence of a dielectric liquid, to remove material by spark erosion. Currently this process can only be carried out on conductive materials as an electrical current must be passed between the tool electrode and the workpiece electrode. As material is erroded from both electrodes, tool wear is a significant challenge. When this process is carried out on a micro scale it is usually reffered to as μEDM and this process has been used to sucessfully machine different profiled grooves into the surface of a part (Yan, et al., 2010). This technique has been used to sucessfully machine a number of profiles into stainless steel as shown in Figure 2-14 to a depth of 30μm

though the tools experienced significant tool wear during use limiting their potential to produce large arrays of features.

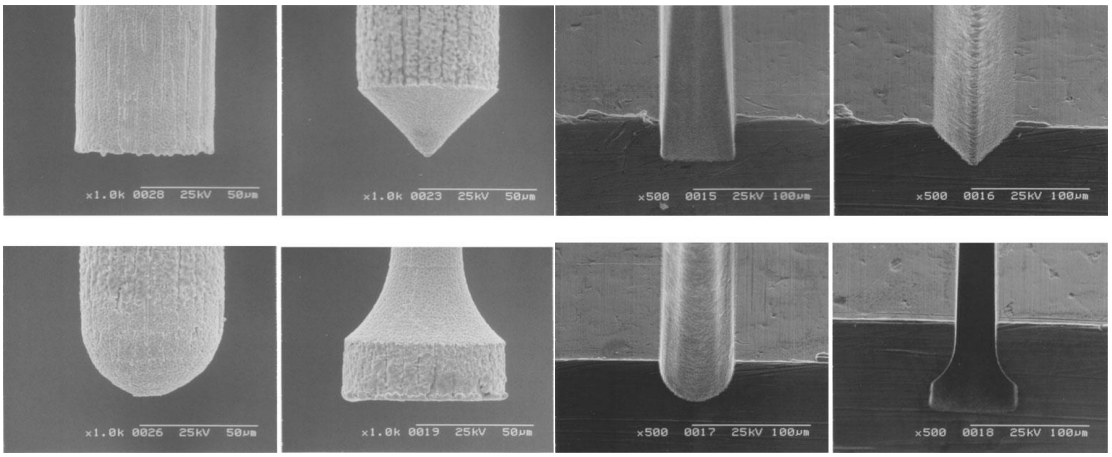

Figure 2-14: µEDM electrode profiles and the corresponding machined grooves (Yan, et al., 2010)

Lasers are used in several manufacturing processes and present possess many advantages such as high speed, process controlability, reduced heat affected zone and versatile machining processes. Laser Ablation is a technique used to remove material from a surface by using a high energy laser pulse to heat a small area of material to the point of melting and eventually vapourisation. A portion of the material is ejected from the formed cavity by vapor and plasma pressure while the remaining liquid material quickly cools and solidifys forming a recast layer (Scholz, et al., 2017). By controlling the path of the pulsed laser beam, it is possible to machine forms directly into the surface of a substrate material over a large area with relative speed. For example this technique has been used effectively to create arrays of grooves to depths of 25µm in stainless steel to create moulds for super-hydrophobic surfaces (Wang, et al., 2016).

2.2.2 Additive Methods

Additive manufacturing processes involve depositing material onto a substrate to selectively build up areas resulting in a surface form. These processes invariably involve very high cost, highly specialised production equipment and require well controlled environment to prevent contamination from outside materials. As such they are not generally considered machining

processes and are not suitable for retrofitting or incorporating into existing machining centres. Hence, they are outside of the scope of this work. Examples of additive processes and the structures that can be manufactured using them would include: Chemical Vapour Deposition (CVD) which has been used to used to generate nano scale antireflective coatings (Buskens, et al., 2016), Lithography has demonstrated the capability to produce stochastic surface textures with feature heights of 25μm (Blas Romero, et al., 2017) and electroforming which has been used to produce 500μm micro-dome arrays over a wide surface area (Hernandez-Castellano, et al., 2017)

2.2.3 Comparison of advantages and disadvantages

Each of the various machining processes described has a range of advantages and disadvantages and is more or less suited to the production of specific feature types. As a continually developing field, methods of manufacturing micro scale structures are constantly evolving. The level of research activity in this area is very high novel methods of utilising existing techniques are constantly being developed and increased levels of performance are achieved. Table 2-1 presents a consideration of the most important consideration when selecting a machining technique to investigate. The details given are fundamental limitation of the technique. Specific consideration has been given to the ease to which a system can be retrofitted or incorporated into existing equipment. When assessing this, it has been assumed that aspects such as motion control and accuracy are a factor of the existing equipment that the technique would be adapted to and are thus equal for all techniques. Therefore, this assessment is based on the need for additional equipment, control of the processing environment and ease of integration.

Machining Technique	Suitable Features	Advantages	Disadvantages	Ease of Retrofitting
Diamond Cutting	grooves, ribs, pyramids	tool longevity, fast machining times, defined tool geometry	high tooling cost, limited range of materials	Moderate
Micro Milling	grooves, ribs, pyramids, pillars, dimples, domes	versatility and range of features possible, defined tool geometry, machine a wide range of materials	high tooling cost, high rates of tool breakage, slow machining times	High
Micro Grinding	grooves, ribs, patches	machine a wide range of materials, fast machining times, low tooling cost	tool wear, challenge of modelling randomly distributed abrasive particles	High
Micro Polishing	grooves, patches	Improved surface finish, machine a wide range of materials	limited form accuracy, challenge of modelling randomly distributed abrasive particles	Low
μEDM	grooves, ribs, pyramids, pillars, dimples, domes	versatility and range of features possible, suitable for difficult to machine materials	limited range of materials, high tooling costs, tool wear, high power consumption	Very Low
Laser Ablation	grooves, ribs, patches, dimples	Low marginal costs, no tool wear, highly controllable process, machine a wide range of materials including difficult to machine materials	Initial high tooling cost, Limitation in producing sharp edges due to recast layer formation	moderate

Table 2-1: Comparison of machining processes

2.3 Ultra-precision machining and grinding processes

Ultra-precision (UP) machining can be divided into two fields. Firstly, the production of parts with very high tolerances for surface finish, typically surface roughness of less than 10nm, and form accuracy in the order of 0.2μm or better (Zhang, et al., 2015) and secondly the production of parts or geometries in the micro and nano scales. Historically the primary drive behind the development of UP Machining has been the fields of optics and computing. Many UP machining techniques bear significant similarity to their conventional counterparts; the major difference being the quality and stability of the tools used and the accuracy of the

machine control elements. For example, Single point diamond turning is superficially similar to conventional turning on a CNC lathe. However, on closer inspection several differences become apparent. For example, the cutting edge in diamond turning is a single diamond crystal shaped to the required geometry. This is much more stable than a conventional carbide cutting tool. The chuck will utilise an air bearing with a very high stiffness figure and superior position accuracy (due to the lack of friction and backlash) and linear actuators will be used in the place of ball bearing based feed mechanisms for the same reason (Chapman, 2004). The exact performance of each machine will vary by specification. The workholding spindle utilised in the Nanoform 250 Ultra Grind has a quoted axial stiffness of 230 N/µm, radial stiffness of 130 N/µm with a position accuracy of ± 1 arc-sec (Precitech, 2014) however extremely high stiffness figures in the order of 4000 N/µm have been reported in some applications (Lihua, et al., 2010)

UP Grinding is a technique used to create parts with high levels of surface finish, form accuracy and surface integrity. UP Grinding can be used on most types of materials however, it is particularly well suited to hard or brittle materials. UP Grinding is most frequently used to manufacture parts used in electronic and optical applications. Ultra-precision grinding is a process using fixed abrasives (as opposed to polishing which uses loose abrasives), in interrupted contact with the workpiece surface and where the abrasive surface is characterised by at least one statistically distributed parameter. The ideal ultra-precision grinding process has been defined as yielding a surface finish with the following characteristics

- Root mean squares figure accuracy $<\lambda/10$ with $\lambda<1\mu m$
- Surface roughness $Sq < \lambda/100$
- A damage free sub-surface zone.

These figures represent the current state of the art when considering the ability of ultra-precision grinding to produce macro scale surface and are relative to the size of the part. The implication is that form errors are no more than ten times greater than deviations in

surface roughness. While this is achievable for macro scale surfaces, for micro scale structures this cannot be achieved. This is because it is much more difficult to distinguish between what is surface roughness and what is a deviation in form accuracy. At present, there is no similar universal definition for performance characteristics of surface roughness on the faces of micro scale features.

Development of ultra-precision grinding has been motivated primarily by a desire for it to replace time consuming secondary processes such as fine grinding, lapping or polishing which can increase production costs.

For ultra-precision grinding to be possible several elements of machine tool design must be present. The machine tool must be capable of precise, smooth vibration and backlash free motion to ensure that form errors are reduced to a minimum. Very low levels of synchronous and asynchronous spindle errors are necessary especially when complex tool paths, such as those used in the generation of freeform surfaces, are employed. The machine tool must also possess high static/dynamic loop stiffness; despite the low levels of material removal Ultra-precision grinding uses micrometer scale abrasives which results in a high normal to tangential force ratio. (Brinksmeier, et al., 2010)

A variety of abrasives and bonding methods are used in ultra-precision grinding. The most common are natural or synthetic diamonds and Cubic Boron Nitride (CBN). Diamond abrasives are normally used in the grinding of brittle non-ferrous materials such as silicone or glass due to an adverse reaction with certain metallic materials which causes the transformation of diamond into graphite (Marinov, 2010). CBN can be used for most applications and has superior thermo-chemical stability when compared to diamond however diamond abrasives are more readily available in smaller grain sizes. Bonding types can broadly be divided into metal, resin and vitreous. Metal bonding is most commonly used with super abrasives such as CBN and diamond while resinous and vitreous bonds are typically used with conventional abrasives. Resin bonded wheels typically have very small pore fractions which leads to low protrusion of the abrasives and increases friction between the

bond and the workpiece while vitrified bonds have larger pores which reduces friction. However, they are more prone to wear. Multi-layer metal bonded wheels have significantly higher resistance to tool wear and consequently have greater profile stability (Denkena, et al., 2018). This would be beneficial in grinding processes where the surface of the grinding wheel is non-uniform and shaped to produce a corresponding profile on the workpiece. The greater profile stability will lead to a longer service life before the grinding wheel must be re-dressed to account for deviations in the profile resulting from wheel wear.

Abrasive grains utilised in ultra-precision grinding wheels can vary greatly in size and composition. Readily available ultra-precision grinding wheels utilise grains ranging in size from 18μm (1000 Grit) down to 8-12μm (1800 Grit) (Brinksmeier, et al., 2010). Smaller grit sizes are available in lapping and polishing compounds (ranging from 1-8μm) but these are rarely utilised in grinding wheels except in specialist applications.

For this project the ratio of the grain size to the feature created is of critical importance and using too large a grain size will result in poor form accuracy of the surface structures. A technique has been described for the production of polycrystalline CBN grains developed from Hexagonal Boron Nitride (HBN) of high purity using a chemical vapour deposition process. These Ultrafine-crystalline cubic Boron Nitride (UcBN) abrasives have a grain size smaller than 500nm. When compared with conventional CBN wheels these UcBN abrasives have been shown to produce a high quality mirror finish (roughness level <Rz 0.2μm and < Ra 0.018 μm) with greater efficiency than the conventional mono-crystalline CBN abrasives. In addition, the fracture strength of the grains has been determined to be significantly higher, reducing wear and leading to a wheel life approximately three times longer than a conventional CBN wheel (Ishida, 2015).

UP Grinding has been used in the manufacture of micro structures, specifically on hard to machine materials such as tungsten carbide, glass and ceramics. Significant effort has been made into reducing tool dimensions. Currently two types of tool are used for micro grinding structures. Peripheral grinding wheels are used in the production of continuous structures

with a regular repeated pattern. Pin type grinding tools are used to produce irregular or discontinuous features, at this scale the pin type grinding wheels are analogous to a conventional milling operation (Brinksmeier, et al., 2010).

2.3.1 Dressing Techniques and Structured Grinding

Ultra-precision grinding wheels use grains of hard abrasive material held in a bonding matrix. For the wheel to be affecting the abrasive grains must be presented so that their cutting faces come into contact with the workpiece. There are generally three ways in which tool wear occurs; Grain fracture where a portion of the abrasive grain breaks off exposing fresh sharp cutting material but reducing the overall size of the grain, attritious wear in which the grains become dull through the creation of flat spots or rounded edges and bond fracture in which the bond retaining the grain breaks due to high cutting force (usually the result of a dull grain) (Marinov, 2010) (Jackson, 2004). When wear occurs there is a loss of cutting ability and a reduction in the quality of the surface finish achieved on the workpiece (Chen, et al., 1998)

To ensure that the tool remains efficient it is necessary to condition the wheel to refresh the working surface (Khangar, et al., 2006). The conditioning operation used are of primary importance when determining the manufacturing results and will to a large extent determine the efficiency of cutting, surface finish and sub-surface zone state (Klocke & Linke, 2008). In general, the operations can be separated into dressing and truing/profiling. Dressing is the removal of material to expose fresh abrasive grains and remove material clogging the pores. Truing or profiling is used to determine the form of the grinding wheel to ensure a consistent straight surface or impart a specific profile for use in creating shaped workpieces (Wegener, et al., 2011). There are many techniques for dressing and truing grinding wheels. Some rely on a tool physically contacting the grinding surface to break the bonding material through brittle fracture while other processes such as Electrolytic In-process Dressing (ELID) can be

applied to metal bonded wheels to erode the bond material away through electrolysis (Itoh & Ohmori, 1996).

Crush dressing is the process of forcing a grinding wheel and dressing tool into contact to generate high normal forces, break the bonds between the grains and hence causing whole grains and bond material to fall away. This removes the very top layer of material, exposing the fresh grains beneath. In conventional grinding a specialist carbide dressing tool may be used which is wedged between the machine base and the wheel by hand. For CNC processes such as ultra-precision grinding a specialised grinding wheel is used as the dressing tool. For crush dressing to be successful it is necessary to synchronise the wheel and tool speeds otherwise there will be significant wear of the dressing tool. Crush dressing can be used to profile grinding wheels however the process is not easily varied, and each new profile will require a new dressing wheel to be created (Derkx, et al., 2008).

The crush dressing procedure has been adapted for use in the creation of grinding wheels to produce micro riblets on turbine blades. Diamond dressing wheels have been created which incorporate V grooves with varying profile angles (45°, 60° and 90°). Figure 2-15 shows the setup of this equipment. A profiled diamond wheel was used to selectively dress Silicon Carbide (SiC400) wheels with grain sizes varying from 9-60μm.

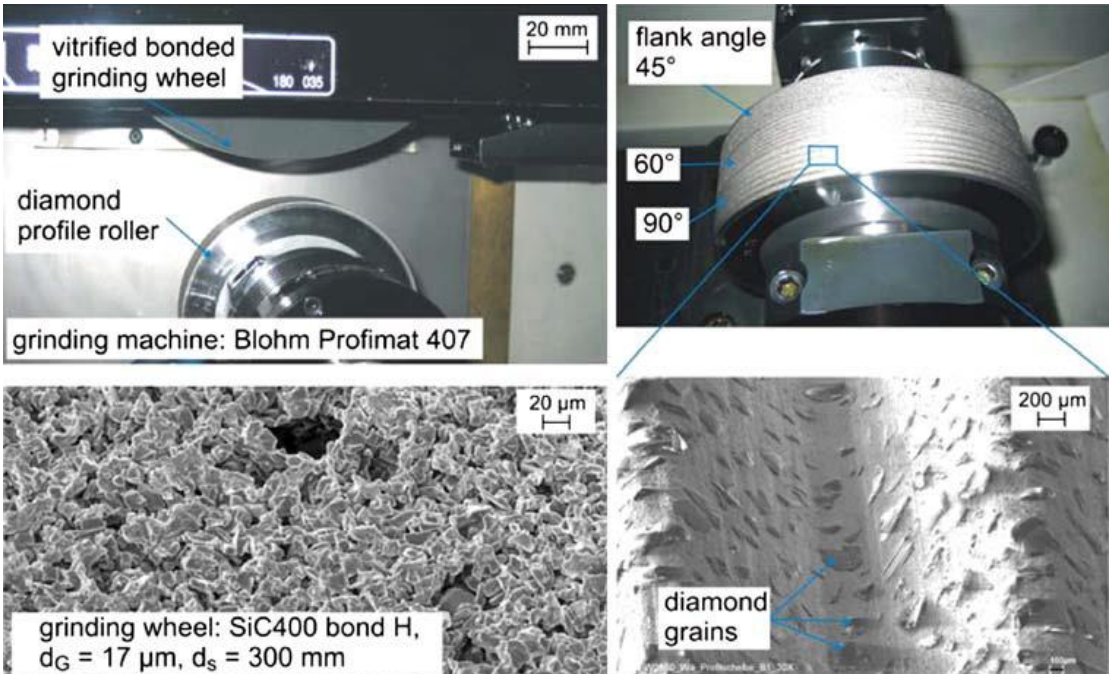

Figure 2-15: structured diamond profile rolling (Denkena, et al.,2009)

By using multiple passes as shown in Figure 2-16 it is possible to generate riblets with a profile width of 50µm and a profile height of 20µm. This high aspect ratio is possible because the riblets are aligned along the direction of travel of the workpiece. Consequently, there are no groove side curve length considerations and the resultant profile is a direct transfer of the wheel profile (albeit inverted) (Denkena, et al., 2009). The limiting factor for the riblet geometry is the minimum size of V groove that can be created on the profile roller. At present grinding wheels with a profile height of 500µm and a profile distance of 600µm with axial shifting is required to produce the riblets described. Using the profile roller technique, the time to dress a wheel with 20 microprofile grooves drops from 15mins (using a single dicing blade) to 1min (Denkena, et al., 2010). Due to the specially constructed dressing rollers and the number of axial dressing paths necessary to form the required profile this process lacks flexibility. The number of dressing paths required is a function of the spacing of features on the diamond profile roller and the desired spacing of the resultant features on the grinding wheel. Effectively, the dressing profile roller is shifted axially a fraction of the pitch distance between features. To calculate the number of axial shifts required, the pitch of the features on the dressing profile roller is divided by the desired pitch of the resultant

features on the grinding wheel. Therefore, to create a uniform profile across the grinding wheel, the spacing of features on the grinding wheel can only be set to values which would require a whole number of axial shifts. This process is illustrated in Figure 2-16. Production of diamond profile rollers requires specialist knowledge and equipment and may prove costly. However, once a diamond profile roller with the correct profile is available the process has the potential to achieve good processing times.

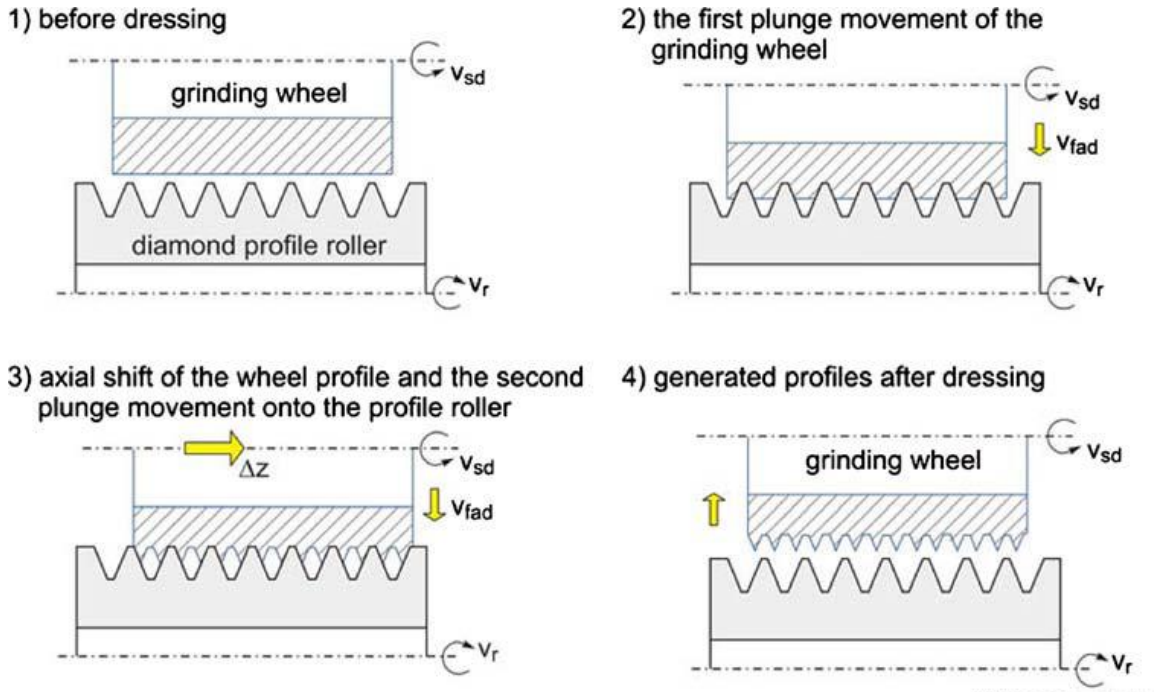

Figure 2-16: Axial dressing path necessary to create microprofile grooves (Denkena, et al., 2010)

Single point diamond dressing is mostly used in the truing of grinding wheels. The principal mechanism for material removal is the breaking of bond material by introducing high stresses. This is similar to crush dressing however the stresses are not generated through high normal forces but by point loading (Chen & Brian Rowe, 1996). A single diamond grain is bonded or brazed to the dressing tool tip and then sharpened to a point. By dragging this point across the surface of the part it is possible to create highly localised stresses. Because bonds are only broken over the small area in contact with the tool, single point diamond dressing is not suitable for creating profiles which require large amounts of material removal. The speed of the grinding wheel must be carefully controlled and matched to the feed rate of

the dressing tool to ensure that the entire surface is dressed (Wegener, et al., 2011). The dressing operation is a harsh process and the dressing tool will gradually be worn away (Zhang & Shin, 2002) (Oliveira, et al., 2009). If too high a speed is used, then the dressing tool tip will be worn away very quickly. This wear occurs due to brittle structural fracture of the diamond. The profile of the changes as the tool is worn and the effective tip width increases dramatically as the dib height decreases. This is important as it has been shown that the residual profile of the dressed grinding wheel surface is closely related to the geometry of the dressing tool (Liu, et al., 2017).

Because it is a highly localised process single point diamond dressing is well suited to the creation of profiles that require highly deterministic material removal. This technique has been used in the past to create microdiscontinuities on the surface of grinding wheels. Microdiscontinuities are grooves or pits shaped into the surface of a grinding wheel surface that do not interfere with the macro geometry to facilitate the removal of chips, improve coolant flow (Denkena, et al., 2015) and reduce wear. Tools incorporating a Passive Grinding Area (PGA), a portion of the grinding wheel not in contact with the workpiece, have been shown to reduce the temperature generated in grinding. The textures used range from horizontal/inclined grooves to zigzags and crosses (Li & Axinte, 2018). These PGAs show many similarities to microdiscontinuities.

A method for the dressing of micro-scale geometries has been described which uses a single point diamond dressing nib or a dressing wheel. The dressing tool selected is mounted on an electronically controlled module to achieve the required motion. Figure 2-17 shows how a single point tool so mounted can be moved across the surface of a wheel to create a deterministic pattern. In this example the tool is mounted in such a way that in can be moved in two ways; firstly, in a linear fashion along the profile of the wheel and secondly by oscillating through an arc. Several other configurations have been described using this method (Nadolny & Kaplonek, 2012).

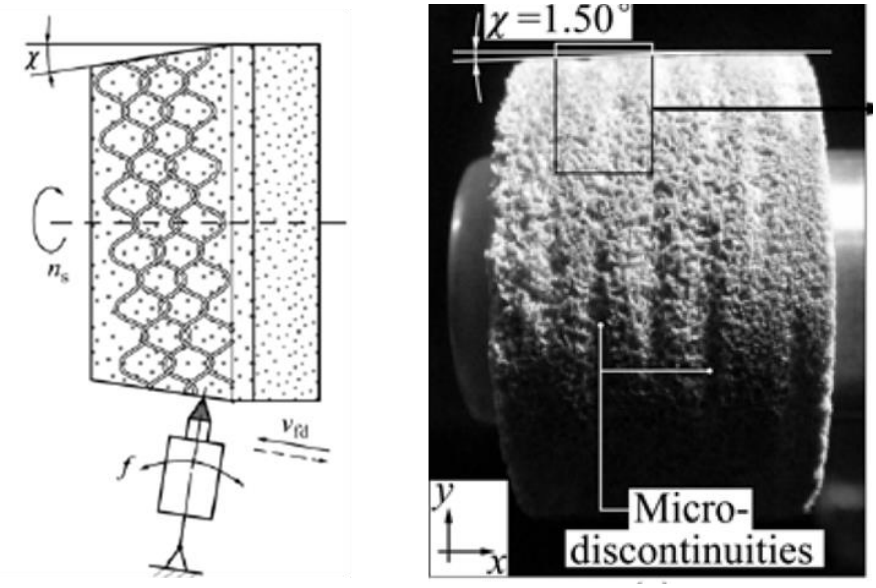

Figure 2-17: Micro-discontinuities created by movement of a single point diamond dressing nib (Nadolny & Kaplonek, 2012)

Single point diamond dressing has also been used in the creation of macro scale helical grooves in conventional grinding wheels. In this process the dressing tool is passed along the surface of the wheel at a given depth and feed rate in a process very similar to machining a screw thread (Stepien, 2011). Helical grooves can be used to generate three distinct types of surface geometry. A single helical groove can be used to generate type I and type II profiles. Type I profiles consist of a single groove ground on a diagonal to the direction of travel and are created in a single pass. It is possible to create a type II profile by using the same grinding wheel and using a double pass (once in the forward direction and once in the reverse). This creates diagonally opposed grooves, leaving pillars of unmachined material. A third type of regular surface can be generated by using grinding wheels shaped with double helical grooves. Type III profiles consist of a regular arrangement of elliptical cuts into the workpiece surface (Stepien, 2007a). Examples of the different surface textures that can be generated this way are shown in Figure 2-18.

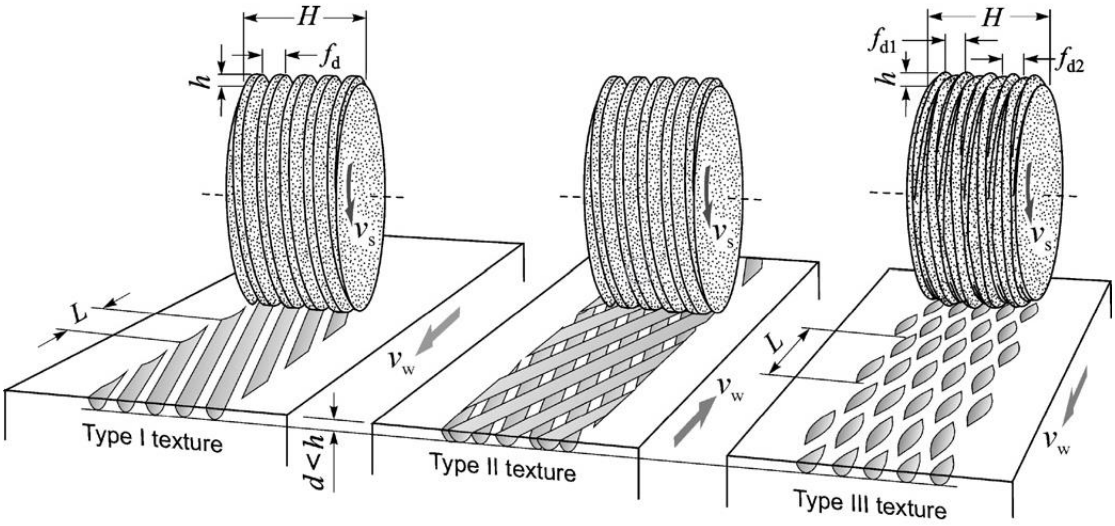

Figure 2-18: Single and double helical grooves producing different surface textures (Stępień, 2011)

Previous experimentation with helical grooves has shown that the produced surface will display both the deterministic aspects of the designed surface and the stochastic elements associated with conventional grinding. The abrasive grains follow a cycloidal path however due to the profile of the wheel only a small portion of the available grains come fully into contact with the work piece (Stepien, 2011)

Similar techniques for the production of regular surface geometries which do not utilise helical grooves have also been described. A single point diamond tool can also be used in conjunction with piezo electric oscillation to create deterministic patterns on the surface of a grinding wheel. In a process very similar to micro chiselling the tool is plunged into the surface of the grinding wheel at depth between 2-25μm. The rate of oscillation is controlled relative to the wheel position as it moves and pattern sizes of up to 2mm in the circumferential direction and 0.5mm in the axial direction can be dressed at wheel surface speeds of up to 45m/s. Figure 2-19 shows how this set up is arranged (Oliveira, et al., 2010) (Silva, et al., 2013).

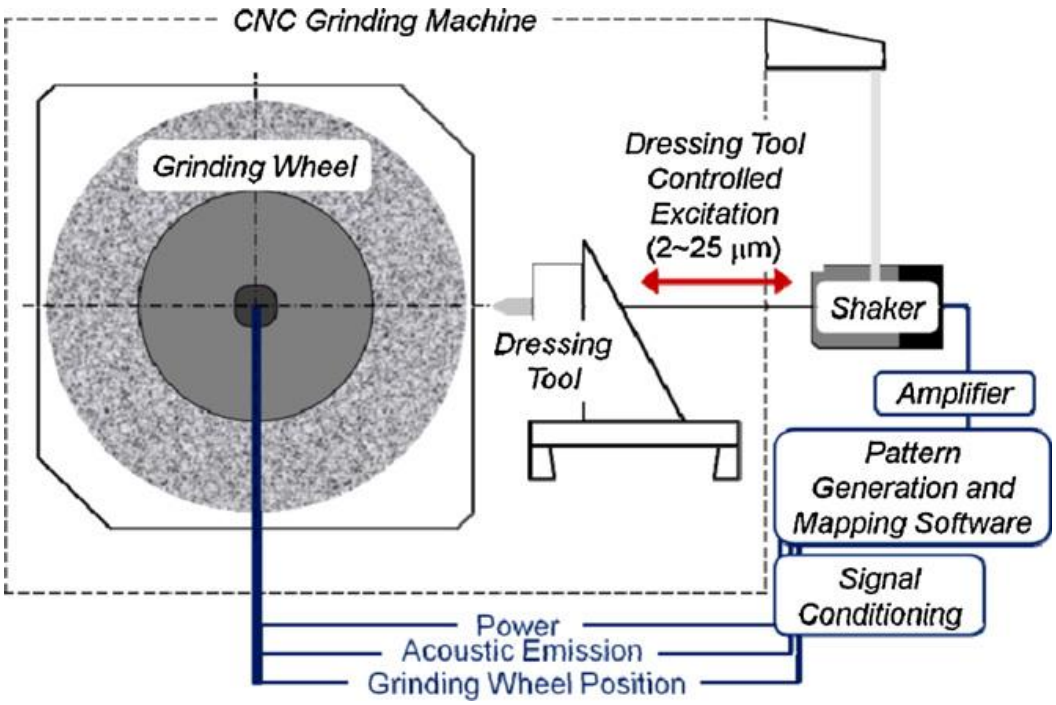

Figure 2-19: Dressing station with piezo electric excitation (Oliveira, et al., 2010)

This procedure can be used to create a number of complex geometries on the surface of the grinding wheel as shown in Figure 2-20 and could be very well suited to the production of micro scale geometries. However, accurate control of the wheel speed and oscillation of the tool is essential to ensure that the pattern is properly replicated. If this equipment is not already available to an operator the costs of implementation will be high and significant changes will be required to the setup of the grinding rig.

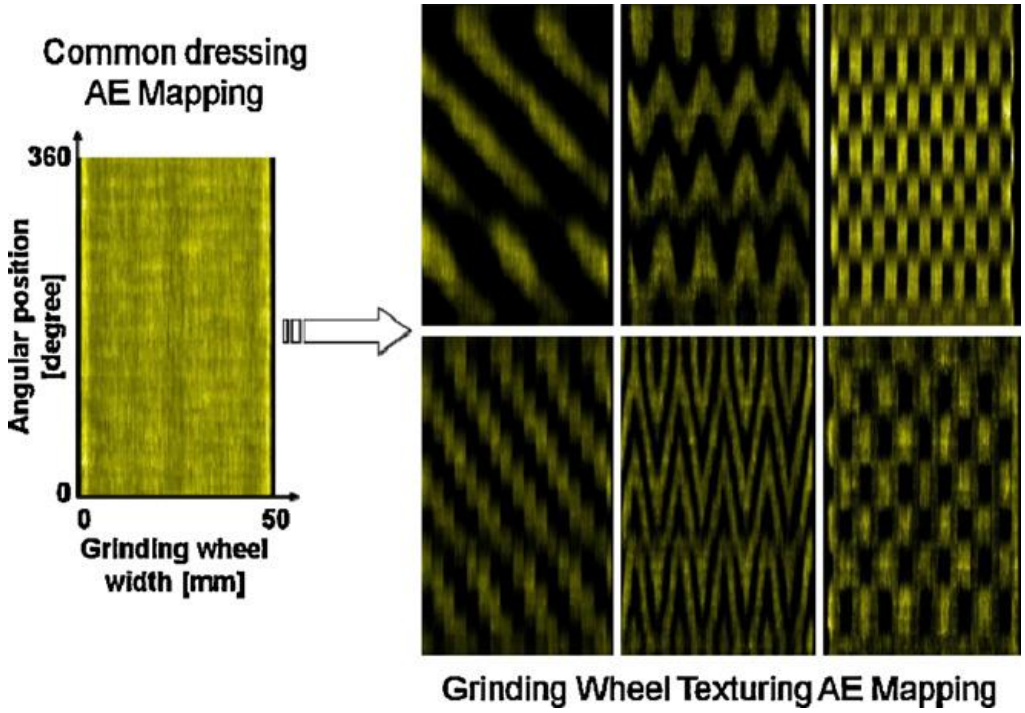

Figure 2-20: Examples of surface texture dressed onto the surface of a grinding wheel with oscillating dressing (Oliveira, et al., 2010)

Techniques which rely on selective removal of material from the surface of the grinding wheel generate a specific texture, such as the processes developed by Stępień (2011) and Oliveira, et al. (2010) share two common aspects. Firstly, they rely on interrupted contact between the surface of the grinding wheel and the workpiece to generate the required geometry. Secondly, the pattern transfer is scaled in the circumferential direction by the ratio of the grinding and workpiece speeds. Therefore, for accurate replication of the desired surface geometry it is necessary to accurately synchronise the grinding/workpiece speed.

The principle of ELID is that an electrical current can be passed through a metal bonded grinding wheel and electrolytic coolant and pass into an electrode placed close to the surface of the wheel. This allows for continuous electrolytic erosion of the bond material at the surface of the grinding wheel to ensure constant protrusion of the abrasive grains. The system is relatively easy to retrofit onto existing grinding equipment as no specific equipment beyond a power source from a conventional electro-discharge machine is required (Ohmori, et al.,1996). ELID offers significant advantages in that it can reduce downtime and ensure a more uniform surface. Where online processes have been implemented better surface

finishes and higher form accuracy are usually achieved (Bifano, et al., 1999). However, neither of these techniques is currently suitable for structured grinding as they can only create uniform surfaces.

The use of lasers as a tool for dressing grinding wheels is a relatively recent development. Laser dressing is similar to single point dressing in that it is a highly localised process. The high power of focussed lasers can be used to address several of the primary wheel wear issues either by modifying the surface to refresh worn out grains or by dislodging the chips in loaded pores (Khangar, et al., 2006). There are several potential benefits over traditional dressing methods such as selective removal of material, remote dressing, which can be achieved through the use of an optical fibre, and no wear of the dressing tool. Using techniques such as pulsed laser dressing it is possible to selectively remove material from the surface of the wheel (Xie, et al., 2004). These factors, in addition to fine control of the spot size, make the process ideal for use in dressing specific geometry onto the surface of a grinding wheel. However, specialist equipment that is extremely costly is necessary to carry out this procedure limiting its use to the manufacture of very high value parts where the additional cost is offset by the improved functionality offered. Figure 2-21 demonstrates the basic layout of a laser dressing set up.

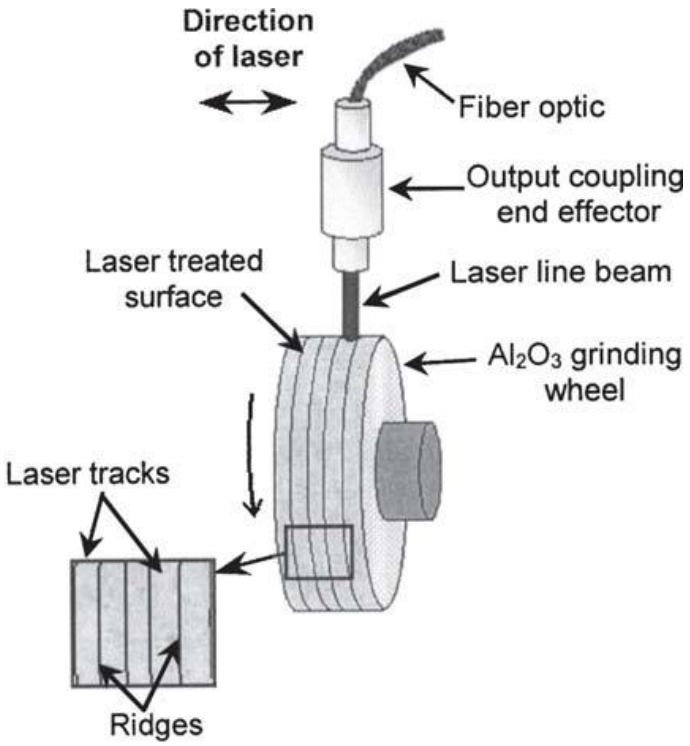

Figure 2-21: Example of a laser dressing setup (Khangar, 2006)

An alternative method of using a laser to assist in single point dressing has been put forward which uses a laser to heat the material before it passes in front of the diamond dresser this leads to a move from brittle fracture to more ductile behaviour which increases dressing accuracy. It is also possible by directly controlling the tip temperature of the dressing tool to reduce wear and prolong life (Zhang & Shin, 2002). Figure 2-22 shows the arrangement of the laser and dressing tools.

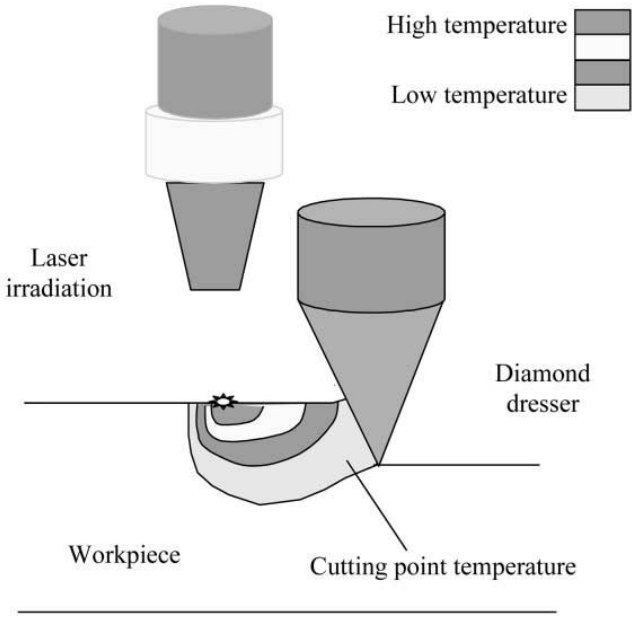

Figure 2-22: Basic laser assisted dressing principle (Zhang, 2002)

Chapter Three

Mathematical process Modelling

After determining the desirable surface geometry for a particular application, it is necessary to design a profile for the surface of the grinding wheel which is capable of generating that geometry. Before the grinding wheel can be dressed the correct parameters for the dressing operation must be determined to account for the pitch of the features, the dressing nib dimensions and the required dressing depth. In this chapter the calculations necessary to design a grinding wheel profile and dressing solution are demonstrated. A consideration of a structured grinding process making use of interrupted contact between the grinding wheel and the workpiece is presented along with a worked example at a micro scale. The technique presented is an adaptation of the helical groove process developed by Stępień and detailed in a series of papers from 2007 (Stepien, 2007a and b). The equations developed are derived primarily from Euclidean geometry and do not require complex calculation steps. They can be used with simple computational tools such as Microsoft Excel to model the grinding wheel and resultant surface profile.

3 Mathematical Process Modelling

The terminology given in Table 3-1 is used throughout the thesis. Consistency of units is crucial to accurate calculation. The units given in brackets may be used in certain equations for convenience.

Variable	Symbol	Units
Grinding Speed	v_s	m/s
Workpiece Speed	v_w	m/s
Velocity Ratio	v^*	N/A (ratio)
Grinding Depth	d	m (µm)
Grinding Wheel Radius	R	m (µm)
Dressing Depth	h	m (µm)
Functional Arc Length	AB	m (µm)
Dressing Tool Radius	r_D	m (µm)
Groove Pitch	L	m (µm)
Groove Total Length	l	m (µm)
Groove Side Length	l_c	m (µm)
Length of Bearing Segment	l_b	m (µm)
Groove Bottom Length	b	m (µm)
Dresser Feed Pitch	f_d	m (µm)
Active portion of Wheel	c	N/A (ratio)
Relative Linear Position on Workpiece	x_{equiv}	m (µm)
Local Wheel Radius	ρ(α)	m (µm)
Start of Indentation Phase	α_1	Radians
Start of Idle Phase	α_2	Radians
Start of Exit Phase	α_3	Radians
Characteristic Angle	tgk	Radians
Relative Depth of Cut	d_{cut}	m (µm)
Permissible Scalloping	S_{per}	m (µm)
Preliminary Dresser Feed Pitch	f_{prelim}	m (µm)
Feed rate	F	mm/min
Spindle Speed	RPM	Revs/min
Dressing Nib Angle	ϑ	Degrees
Interior Angle	φ	Degrees
Radiused Depth	E_r	m (µm)
Groove Enlargement	G	m (µm)

Table 3-1: Terminology

3.1 Dressing Operation

There are several parameters which affect the accuracy of the dressing operation and the life of the dressing nib.

Whilst dressing with the nib perpendicular to the surface of the grinding wheel would provide the most accurate means of generating the required geometry, this has a severely

detrimental effect on the lifespan of the dressing nib as it is quickly worn flat. To prolong the lifespan of dressing nibs they are typically presented to the grinding wheel at an angle of 15 to 20 degrees. This is normally achieved by angling the dressing nib, however this is not possible in this process as the nib is retained in the machines C axis to allow for positioning and rotation. A similar effect can be achieved with the dressing nib offset from the centreline of the grinding wheel as shown in Figure 3-1. The required height and offset to achieve the correct dressing angle can be calculated using Equations 1 and 2.

Height Offset

$$H = R \sin \theta$$

(Equation 1)

Depth offset

$$o = R - \left(\sqrt{R^2 - H^2}\right)$$

(Equation 2)

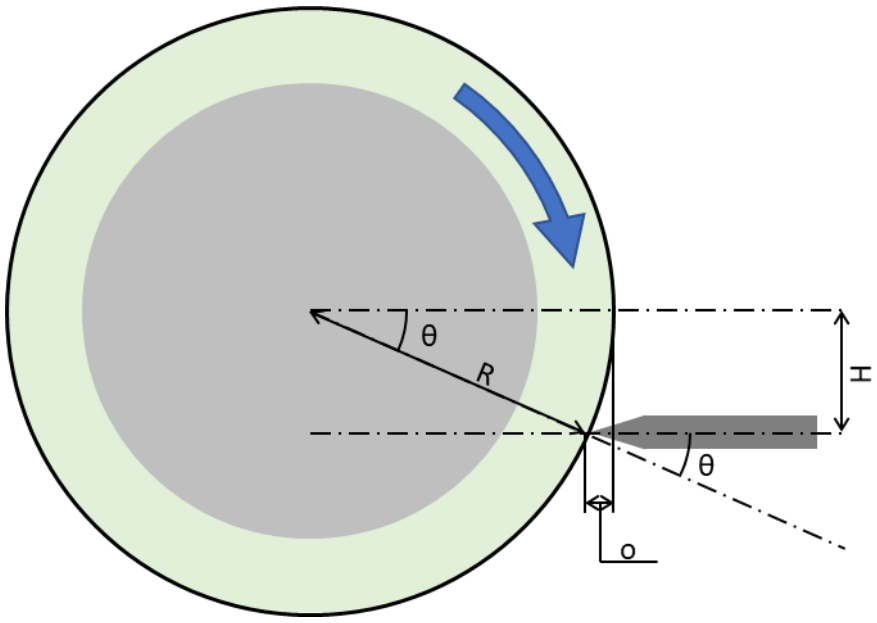

Figure 3-1: Offset dressing of the grinding wheel

Before the grinding wheel can be dressed with a specialised profile it is necessary to prepare it. Truing is carried out to ensure that the grinding wheel surface is consistent, has no taper and is parallel to the axis of rotation, while dressing is the process of refreshing the surface of the grinding wheel to expose fresh sharp grains. Both these processes can be carried out

in a single preliminary dressing operation. The process of removing individual abrasive grains will naturally yield a very rough surface however the nominal profile of the grinding wheel after preliminary dressing can be seen in Figure 3-2. A degree of overlap will occur as the dressing nib is passed over the surface of the grinding wheel while it is rotating. This creates a characteristic feature called scalloping. It is possible to calculate the optimum feed pitch for preliminary dressing using the maximum permissible height of the scallop and the radius of the dressing nib as shown in Equation 3. It is then possible to calculate the necessary feedrate for a given rotational speed using Equation 4.

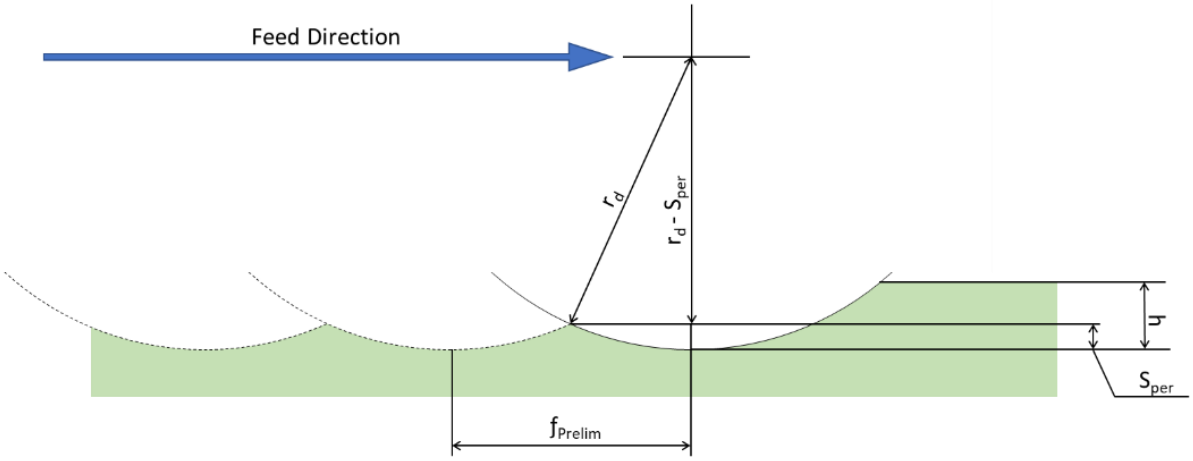

Figure 3-2: Preliminary dressing feed

Preliminary Dressing Feed Pitch

$$f_{prelim} = 2\sqrt{{r_d}^2 - \left(r_d - S_{per}\right)^2}$$

(Equation 3)

Preliminary Dressing Feedrate (mm/min)

$$F = \frac{f_{prelim}}{1000} \times RPM$$

(Equation 4)

For final dressing, to create functional geometry on the surface of the grinding wheel, the dressing nib is plunged into the surface to create a series of grooves. The features on the resultant ground surface are determined by the profile of the groove. When designing the profile of the groove the geometry of the dressing nib and the tool path are the primary

controlling variables. The dressing nib has a conical form, with an opening angle denoted by ϑ, and terminates in a radius. The sides of the cone meet the radius at tangents as shown in Figure 3-3. To calculate the depth of the radiused portion of the tip it is first necessary to determine the interior angle created perpendicular to the sides of the cone. This is easily calculated as shown in Equation 5 as the profile of the tip is that of an isosceles triangle. The radiused depth can then be calculated using trigonometry as shown in Equation 6.

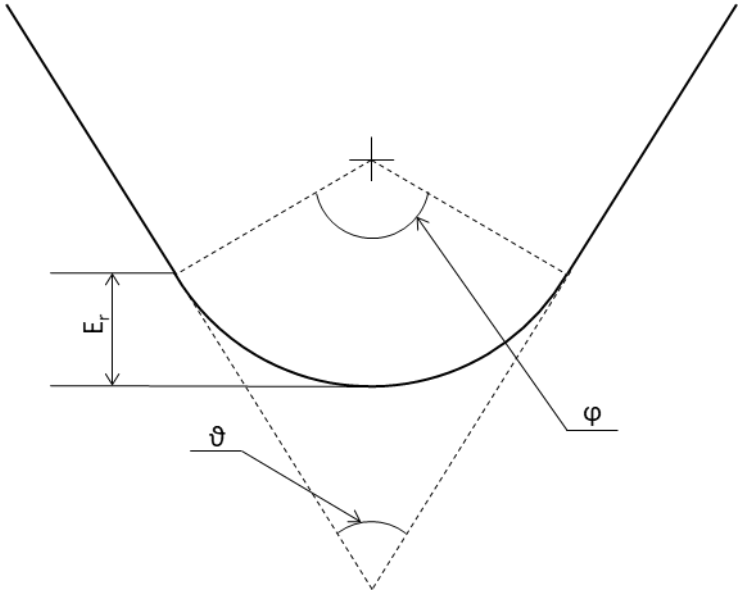

Figure 3-3: Dressing Nib Geometry

Interior Angle

$$\varphi = 180 - \vartheta$$

(Equation 5)

Radiused Depth

$$E_r = r_d - \sqrt{{r_d}^2 - \left(r_d \sin\frac{\varphi}{2}\right)^2}$$

(Equation 6)

Once the geometry of the dressing nib has been determined it is possible to calculate the profile of the groove that can be dressed with it. A simple plunging operation will replicate the

profile of the tip, in negative, on the surface of the grinding wheel. If a wider profile is necessary the tool can be moved horizontally before being withdrawn, this is illustrated in Figure 3-4. The length to which the groove is enlarged is defined as G.

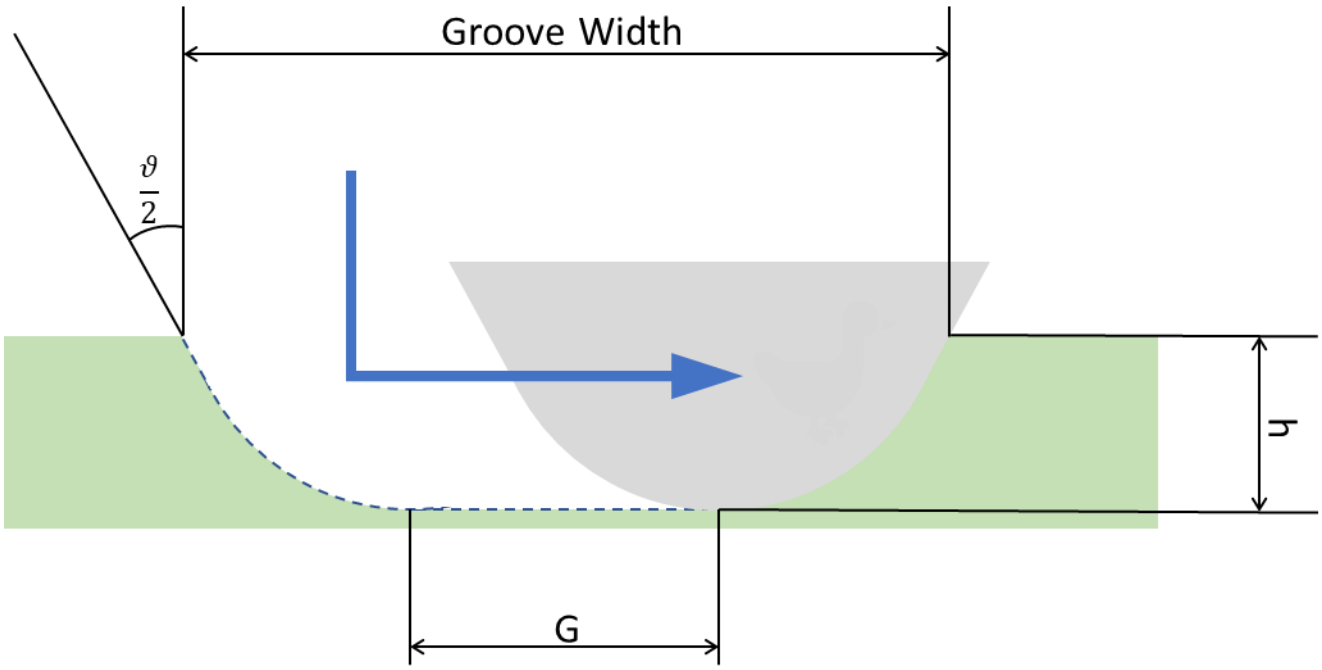

Figure 3-4: Groove Profile

The width of the groove at the surface of the grinding wheel is dependent on the dressing depth. If the dressing depth is lower than the radiused depth the groove width can be calculated using Equation 7 while when the dressing depth is equal to the radiused depth the groove width can be calculated from the chord length as shown in Equation 8. In both cases the profile of the side of the grove will match the radius of the nib. If the dressing depth is deeper than the radius depth the additional profile of the conical taper must be taken into account as shown in Equation 9. The profile of the groove will also reflect the conical profile.

Groove Width

When h < E_r

$$Groove\ Width = 2\sqrt{{r_d}^2 - (r_d - h)^2} + G$$

(Equation 7)

When h = E_r

$$Groove\ Width = 2r_d \sin\left(\frac{\varphi}{2}\right) + G$$

(Equation 8)

When h > E_r

$$Groove\ Width = \ 2r_d \sin\left(\frac{\varphi}{2}\right) + 2\left((h - E_r)\tan\left(\frac{\vartheta}{2}\right)\right) + G$$

(Equation 9)

3.2 Developed Stepien Equations

The following mathematical description is a development of the work previously presented by Stępień in various works describing the use of grinding wheels shaped with helical grooves (Stepien, 2007a) (Stepien, 2007b). Many of the formulae described are relevant to any structured grinding process which relies on interrupted contact the generate features on the workpiece surface.

Table 3-2 shows the outputs from a worked example created using a Microsoft Excel spreadsheet tool developed to allow different potential configurations to be modelled. The figures given for tool dimensions and process variables are examples of tools and equipment that are readily available for use. However, other configurations would also be available provided that a suitable grinding solution can be found. All graphs and comparisons given below are drawn from this data set.

Tool Dimensions			
Feature	**Symbol**	**Value**	**Units**
Radius	R	8	mm
Dressing Depth	h	5	µm
Dresser Feed Pitch	fd	100	µm
Functional Arc	AB	24	mm
Functional Arc Angle	α1	171.8873385	Degrees
Process Outputs			
Feature	Symbol	Value	Units
Grinding Speed	Vs	0.837758041	m/s
Velocity Ratio	v*	0.009947184	
Groove Features			
Feature	**Symbol**	**Value**	**Units**
Groove Pitch	L	500	µm
Groove Bottom Length	b	238.7324146	µm
Groove Depth	d	1	µm
Groove Side curve length	lc	126.4871142	µm
Groove Total Length	l	491.706643	µm
Length of Bearing Segment	lb	8.293357008	µm

Process Variables			
Feature	**Symbol**	**Value**	**Units**
Spindle RPM	RPM	1000	RPM
Feed Rate	Vw	500	mmpm
Grinding Depth	d	1	µm
Dressing Tool Radius	rd	70.7	µm
Process Constant	C	47.77	
Stepien Formula Geometry			
Feature	Symbol	Value	Units
Alpha 1	α1	3.001461	Rads
Alpha 2	α2	3.169322	Rads
Alpha 3	α3	6.115325	Rads
Angle K	tgk	0.397491	Rads

Table 3-2: Worked example values

In interrupted grinding processes only a portion of the grinding wheel surface actively contacts the workpiece for material removal. Figure 3-5 shows a section of a grinding wheel shaped with Stępień type helical grooves. The fully active portion of the grinding wheel, AB, is effectively unaffected by the profile dressed into the wheel, BC and EF are the sides of the groove and CDE is the groove bottom and does not contact the workpiece. The following mathematical description of the profile can be used in determining the geometry of both the grinding wheel and the resultant surface.

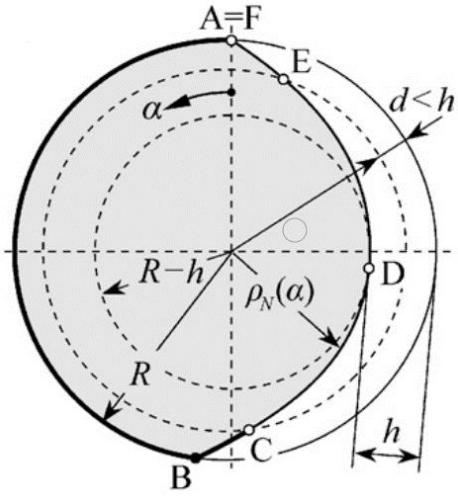

AB – Extending phase – Fully utilised
BC – Indentation Phase – Partially Utilised
CDE – Idle Phase – Not utilised, no contact with workpiece
EF(A) – Exit Phase – Partially Active

Figure 3-5: Grinding wheel section (Stępień, 2011)

Velocity Ratio

$$v^* = \frac{v_w}{v_s}$$

(Equation 10)

The velocity ratio, shown in Equation 10, is a crucial component of any structured grinding operation in which there is interrupted contact between the workpiece surface and the grinding wheel; it is directly responsible for the length of the feature being created. Due to the nature of grinding there will always be a differential between the surface speed of the grinding wheel and the workpiece feed rate. In conventional grinding this ratio is optimised to provide the required surface finish and process time. However, in structured grinding only part of the wheel is fully utilised with the profile of the remaining sections dictating the profile of the partially/unground material. It is crucial that the velocity ratio is matched to the wheel profile and required surface geometry. If the ratio is too high the fully active phase of the wheel will rotate complete more than one rotation in the space of the desired feature meaning that the surface will be ground flat. If the ratio is too low the feature will become elongated and the grinding process will rapidly loose efficiency. The impact that the velocity ratio has upon the various aspects of the ground surface groove geometry, and hence the reason it must be carefully controlled, are shown in Equations 11 to 14.

Ground Surface Groove Bottom Length

$$b = ABv^*$$

(Equation 11)

Ground Surface Groove Pitch

$$L = 2\pi R v^*$$

(Equation 12)

Ground Surface Groove Slope Length (Up Grinding Process)

$$l_{cug} = \sqrt{2Rd - d^2(1 + v^*)}$$

(Equation 13)

Ground Surface Groove Slope Length (Down Grinding Process)

$$l_{cdg} = \sqrt{2Rd - d^2(1 - v^*)}$$

(Equation 14)

The equation for slope length adds grinding depth and tool radius as process variables; as the grinding depth and/or tool radius is increased so too does the slope length. In this respect it is a limiting factor to the potential performance of the structured grinding operation. For structured micro-grinding it is desirable to use the smallest radius tool possible to minimise this effect and maximise the possible grinding depth. For example, taking the worked example in Table 3-2, if the tool radius was reduced to 4mm then grinding depth could be doubled to 2µm while maintaining the other ground surface groove geometry parameters.

Equations 15 to 18 are used to determine the angular component of the polar coordinates describing the dressing operation. The critical factors affecting these angles are the dressing depth, dressing feed pitch and the dressing tool radius. Of all these factors the dressing tool radius of the single point diamond dresser used in this application, is the hardest to control for. There are two reasons for this; firstly, dressing tools are generally supplied with geometry set for general applications and it is not possible to manufacture tools with specific geometry for individual applications without going to great expense. The second factor is that dressing tips wear throughout their service life which results in a change of geometry. It is therefore necessary to assume a nominal value for the dressing tool radius and control the dressing operation by adjusting the dressing depth and the dresser feed pitch. It should be noted that the dressing depth must always be greater than the grinding depth. Figure 3-6 demonstrates the relationship between the dressing depth and the characteristic angles graphically.

Angle α1

$$\alpha_1 = 2\pi(1 - \frac{2\sqrt{h(2r_D - h)}}{f_d}$$

(Equation 15)

Angle α2

$$\alpha_2 = 2\pi(1 - \frac{\sqrt{h(2r_D - h)} + \sqrt{(h-d)(2r_D - h + d)}}{f_d}$$

(Equation 16)

Angle α3

$$\alpha_3 = 2\pi(1 - \frac{\sqrt{h(2r_D - h)} - \sqrt{(h-d)(2r_D - h + d)}}{f_d}$$

(Equation 17)

Characteristic Angle k_1 and k_2

$$tgk = \sqrt{\left(\frac{r_D}{r_D - h}\right)^2 - 1}$$

(Equation 18)

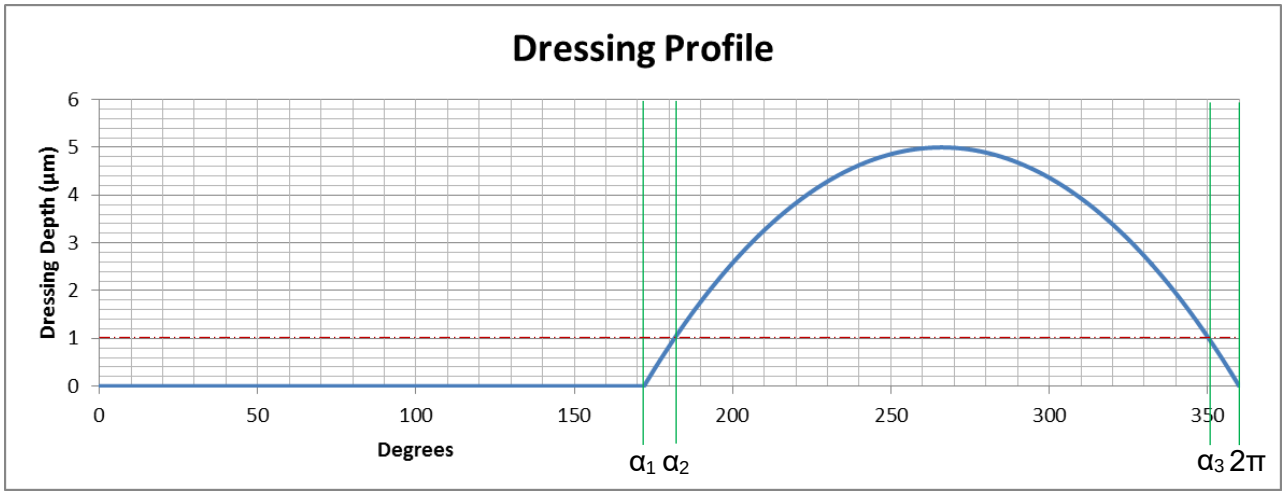

Figure 3-6: Dressing profile

Equations 19 and 20 mathematically describes, in polar coordinates, the local wheel radius. This is the relative distance of the grinding surface from the centre-point of the wheel. This is analogous to a 2D section of the wheel viewed head on such as the one shown in Figure 3-5.

Local Wheel Radius (Polar Co-ordinates)

For $0 \leq \alpha < \alpha_1$

$$\rho(\alpha) = R$$

(Equation 19)

For $\alpha_1 \leq \alpha < 2\pi$

$$\rho(\alpha) = R - \left(\sqrt{{r_D}^2 - \left(\alpha \frac{f_d}{2\pi} - \frac{f_d + c}{2} \right)^2} - r_D + h \right)$$

(Equation 20)

When modelling the grinding wheel and resultant ground surface a 3D point cloud is created by combining a number of 2D sections of the wheel with each section separated by a nominal distance and rotated fractionally by an amount determined by the separation distance between each section and the feed pitch. This point cloud is then used to model the resultant ground surface using the relative depth of cut Equations 21 to 24. As different parts of the grinding wheel profile are active at different points in the grinding process it is necessary to use a different equation for each zone. The relationship between the equations and the grinding zones is illustrated graphically in Figure 3-7.

Relative Depth of Cut

$0 \leq x_{eqiv} \leq b$

$$d_{cut} = 0 - d$$

(Equation 21)

$b < x_{eqiv} \leq (b + l_c)$

$$d_{cut} = (-1 \times d) + (R - (\sqrt{R^2 - (x_{eqiv} - b)^2}$$

(Equation 22)

$(b + l_c) < x_{eqiv} \leq (b + l_c + l_b)$

$$d_{cut} = 0$$

(Equation 23)

$(b+l_c+l_b) < x_{eqiv} \leq L$

$$d_{cut} = (-1 \times d) + (R - (\sqrt{R^2 - (L - x_{eqiv})^2}$$

(Equation 24)

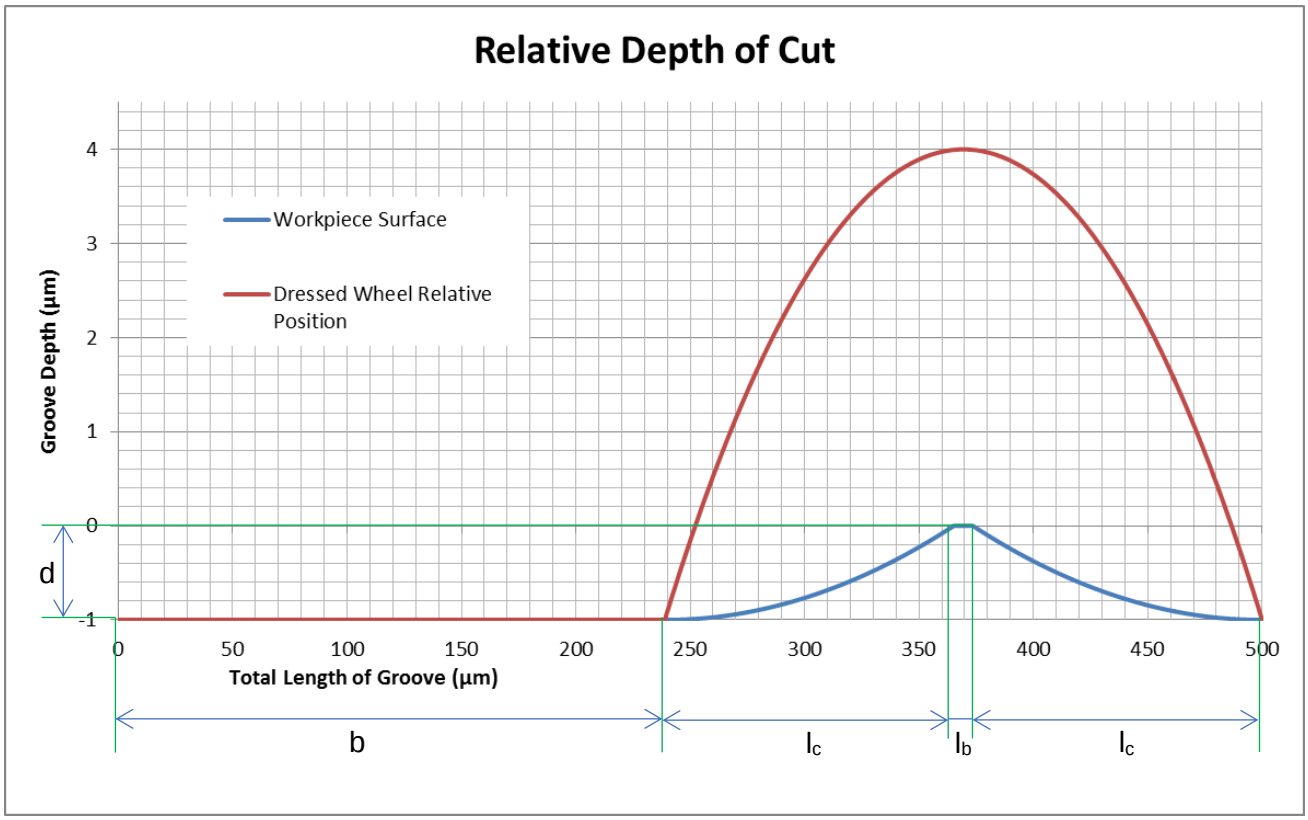

Figure 3-7: Relative depth of cut

The resultant surface profile can be converted into an XY Table format and exported to various software packages for visualisation and analysis. An example of a plot of the surface generated in the worked example is shown in Figure 3-8, this image was generated using

Surfstand 3D surface topography package. Potentially these plots could be used in comparison with the actual ground surface to evaluate performance.

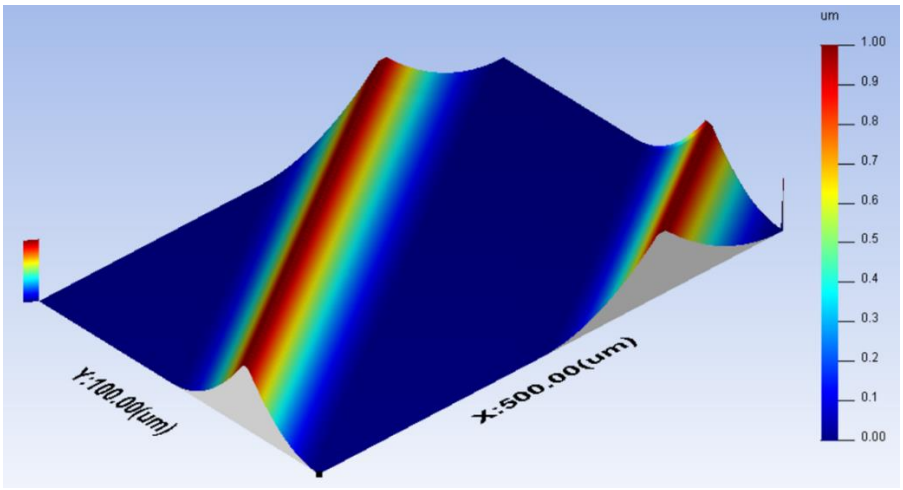

Figure 3-8: Resultant surface profile example

Chapter Four

Developing Grinding Capability

This chapter details the specifications of the equipment available through the project and the modifications that have been necessary to adapt the Precitech Nanoform 250 Ultra Grind CNC ultra-precision machining centre for micro-scale structured grinding. The techniques and procedures necessary to utilise this equipment are also described. The aim of this chapter is to allow the reader to be able to carry out similar modifications to other CNC machining centres in order to replicate the process.

4 Developing Grinding Capability

4.1 Precitech Nanoform 250 Ultra Grind Machining Centre

The Precitech Nanoform 250 Ultra Grind, henceforth referred to as the Nanoform 250, is primarily a Single Point Diamond Turning (SPDT) lathe equipped with two linear axes and a rotational workpiece axis. The machine is also equipped with a mounting station and air line feeds for a high-speed turbine spindle to enable it to be used in ultra-precision grinding operations. The Nanoform series of small frame lathes are designed primarily for the production of optical lenses and mould inserts in a range of materials. The machine utilises hydrostatic oil bearing sideways to provide high static and dynamic loop stiffness, while linear holographic glass scales provide very high feedback resolution. The high degree of form accuracy and surface finish that can be achieved on the Nanoform 250 qualify it as an ultra-precision machining centre. The key performance figures for the Nanoform 250 are summarised in Table 4-1.

Precitech Nanoform 250 Ultra Grind	
Programming Resolution	0.01nm Linear 0.0000001° Rotary
Form Accuracy	< 0.15µm (SPDT) <0.15µm (High speed grinding Tungsten Carbide)
Surface Roughness (Ra)	<1.5nm (SPDT) <5nm (High Speed Grinding)
Linear Axes	
Slide Travel	220mm (X and Z axes)
Axis Straightness	0.2µm Full Travel 0.05µm/25mm
Position Feedback Resolution	0.016nm
Maximum Feedrate	4000mm/min
Workholding/Positioning Spindle	
Standard Swing Capacity	250mm
Ultimate load Capacity	114kg (50mm from spindle nose)
Axial Stiffness	230 N/µm
Radial Stiffness	130 N/µm
Motion Accuracy	15nm
C Axis Feedback Resolution	0.010 arc-sec
C Axis Position Accuracy	1 arc-sec
Max Speed	Work Holding Spindle – 7000RPM C Axis – 1500 RPM

Table 4-1: Precitech Nanoform 250 Ultra Grind Summary

The SPDT and high-speed grinding processes which are normally carried out on the Nanoform 250 are not utilised in this technique and as such, the performance characteristics achieved using these methods are not relevant to this project. However, the high dynamic loop stiffness and positional accuracy of the axes make it an ideal platform for a structured grinding process. With two linear axes and a rotary axis the Nanoform 250 represents the most basic layout available for a CNC machining centre and the lack of a third linear axis has introduced additional challenges in positioning the grinding spindle for different operations. Development of the technique on a basic setup such as this is beneficial as it allows the processes to be easily transferred; The process can be carried out on any CNC machine capable of sufficiently accurate motion control. Indeed, machines with a greater number of axes will have increased capability.

4.2 Spindle Selection

The Loadpoint turbine spindle supplied with the Nanoform 250 for ultra-precision grinding operations was not utilised in the structured grinding process. The turbine spindle is equipped with an air bearing which provides very low run-out and high axial stiffness making it ideally suited for ultra-precision grinding. However, it does not have the necessary degree of speed control to facilitate the structured dressing and grinding operations. In operation the speed is set by regulating the air pressure to the turbine. This provides a coarse degree of speed control with different pressures corresponding to an approximate RPM value. Using this process, it is only possible to set the speed to within 10% of the desired value. Additionally, the turbine is not able to operate at low speeds, with the operational speed range of 20,000 RPM to 80,000 RPM too high for an interrupted grinding process where achieving a desirable velocity ratio would require unfeasibly high workpiece feedrates. The lack of low speed control also makes it impossible to utilise deterministic single point dressing due to the severe nib wear which would occur within the operational range. Dressing the wheel in this spindle require a passive crush dressing process not suitable for the structured grinding techniques being developed.

To allow for more accurate speed control an electrically driven spindle, such as the Nakanishi E3000 range, must be used. For initial experiments a Nakanishi EMR-3008-K spindle, already available within the research group, was trialled. This model is powered by a 32,000 RPM motor with an integral 1:4 reduction gearbox. Motor speed can be controlled in 100 RPM increments which results in an output speed that can be varied by 25 RPM. Ceramic bearings provide high stiffness and the quoted spindle run-out of 1µm is ideal for the structured grinding process. The operating speed range of 500 – 8000 RPM is adequate for structured interrupted grinding. However, the minimum recommended speed was found to be still too high for optimum dressing, and while it was possible to dress a profile at this speed there was still a significantly accelerated rate of wheel wear.

To address the issue of accelerated dresser nib wear, a spindle capable of very low speed operation was desirable. To achieve this, a modular system based around the Nakanishi E3000 range was specified. An EM-3060J motor was selected to power the unit due to its wide speed range of 1000 – 60,000 RPM. Speeds above 32,000 RPM are not useful for the grinding operation but do add to the versatility of the system allowing it to be used in other applications such as micro milling. At maximum RPM the motor has a power of 350W and a consistent output torque of 8.8 cN.m is available throughout the operating speed range for grinding. A removable ARG-031E intermediate gearbox with a 1:16 reduction is placed between the motor and spindle. This gearbox has an operating output range of 62.5 – 2000 RPM which is well suited to the dressing operation while still providing enough speed for grinding. There are two additional benefits of such a high gear reduction; firstly, the significant increase in torque is beneficial when grinding at slow speeds to relatively high depths and secondly it allows very fine control of the output speed in 6.25 RPM increments. Finally, a NR-3060S modular spindle is used for tool holding. This spindle is capable of operating at up to 60,000 RPM with a 1µm static runout and incorporates a CHK type collet system for use with tool shanks ranging from 0.5mm to 6.35mm. The quoted static runout of the CHK collet is within 2 µm.

Using the laser displacement sensor, it was possible to measure the static runout of the grinding tool on the tool shank close to the collet face. This was done to confirm performance of the spindle when used with the grinding tools available. The runout was measured with the spindle rotating at a speed of 100 RPM under no load. The measured data can be seen in Figure 4-1. For clarity four complete revolutions are shown however data was continually collected over a longer period with no variation. The square edged profile of the wave form is a result of the displacement sensor resolution being set to 1μm.

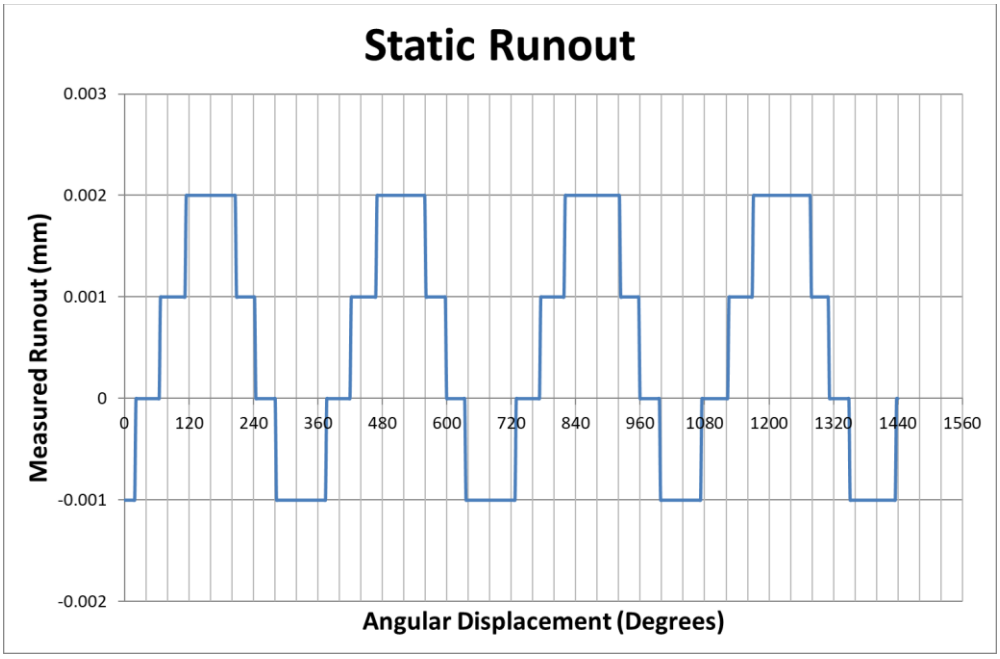

Figure 4-1: Static run out (axial and radial combined)

The runout measured is cyclical and due to the small area available for measurement (the grinding wheel surface being too rough to achieve meaningful measurement) it was not possible to separate the radial and axial elements. The peak to valley measurement of 3μm is within the quoted performance albeit at the top specification limit.

The grinding spindle set up is operated using an E3000 series controller which connects to the motor via a 3m joint type motor cord and separate air hose. For all experiments the controller was operated as a standalone unit to control the speed and direction of rotation of the grind spindle. It is possible to provide an external input, allowing the system to be integrated into an autonomous manufacturing process if desired. Bearing in mind the original

remit of producing a cost effecting solution for the manufacture of structured surfaces, the grinding spindle and controller represent a low cost and highly versatile system which has the potential to significantly enhance the capability of the Nanoform 250.

4.2.1 Spindle Mounting and Tool Alignment

The standard mounting station supplied with the machine uses a separate clamp which is attached to a face plate in a vertical, horizontal or 45°diagonal orientation. This face plate can be adjusted vertically for tool height setting before being locked in place. The entire station is attached to the bed of the Z axis using a single, central pivot bolt and a series of T-slot nuts. This allows the station to be rotated around the central pivot bolt to set the tool at an angle. In the standard configuration, when the spindle is in the vertical orientation the spindles axis is aligned over the pivot bolt meaning that rotating the grinding station does not affect the position of the grinding wheel. The base of the grinding station can be seen in Figure 4-2, the mounting bolts and T slots on the Z axis base are clearly visible.

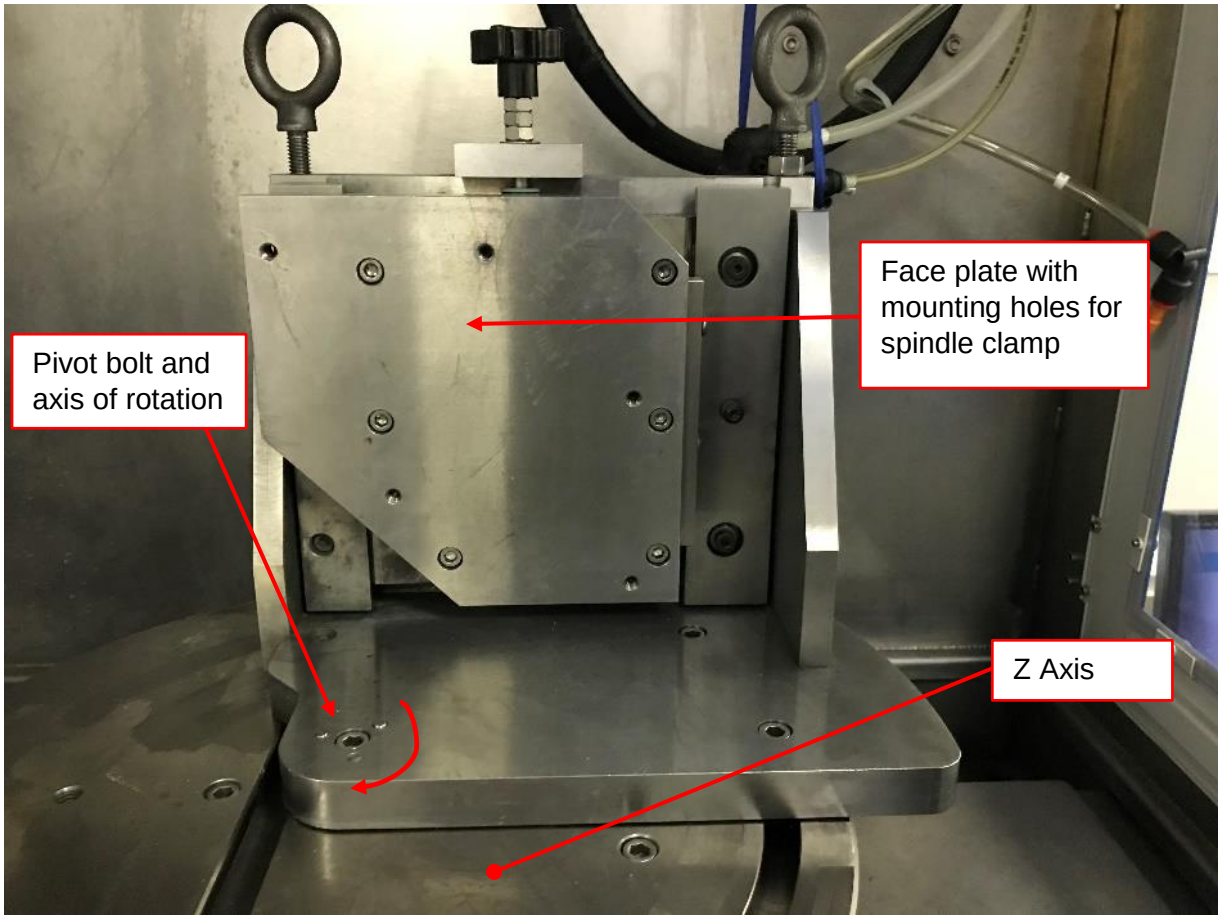

Figure 4-2: Grinding station base

The major limitation of the standard grinding station is the distance to the workpiece spindle. Because the pivot bolt is located in the centre of the Z axis bed, the front of the bed prevents the grinding spindle from moving completely up to the workpiece without using very large workpiece holders. To resolve this, a large cast iron L bracket was purchased and modified to position the spindle 150mm forward of the centre point, this is shown in Figure 4-3. While bulky, this approach has two major advantages; control of the tool height by the fine adjustment screw mechanism is retained and the interface between the spindle clamp and L bracket provides a means of adjusting the tool alignment. A small knob is attached to the screw height adjustment which is suitable for coarse adjustment. For the fine adjustment necessary when setting the dressing height, a spanner can be used on the nut to provide greater leverage and control. Once the correct height is achieved the face plate is clamped to secure it in position. The grinding wheel, retained in the spindle clamp attached to the face

plate is shown in the vertical and horizontal orientations in Figure 4-4, a 45 degree orientation is also possible using the hole arrays on the faceplate.

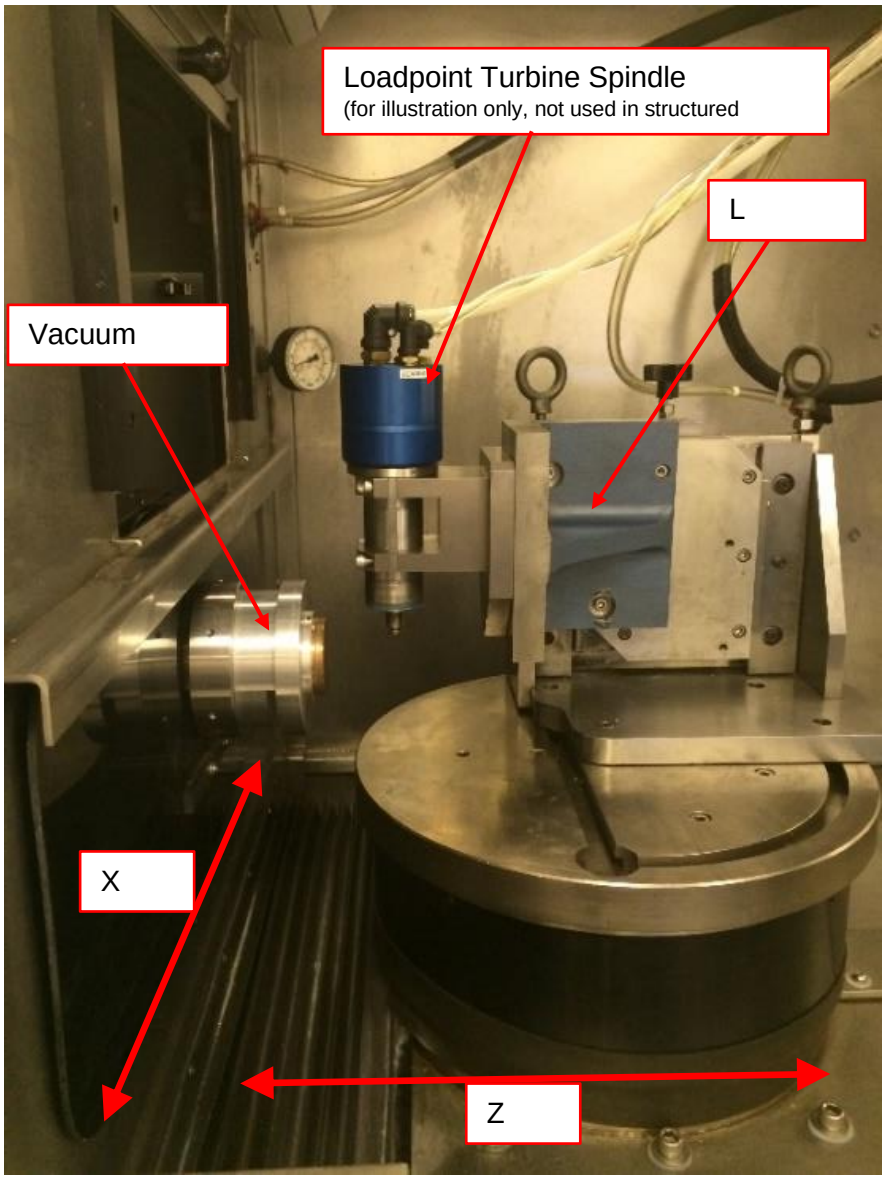

Figure 4-3: L Bracket increasing forward reach of grinding station

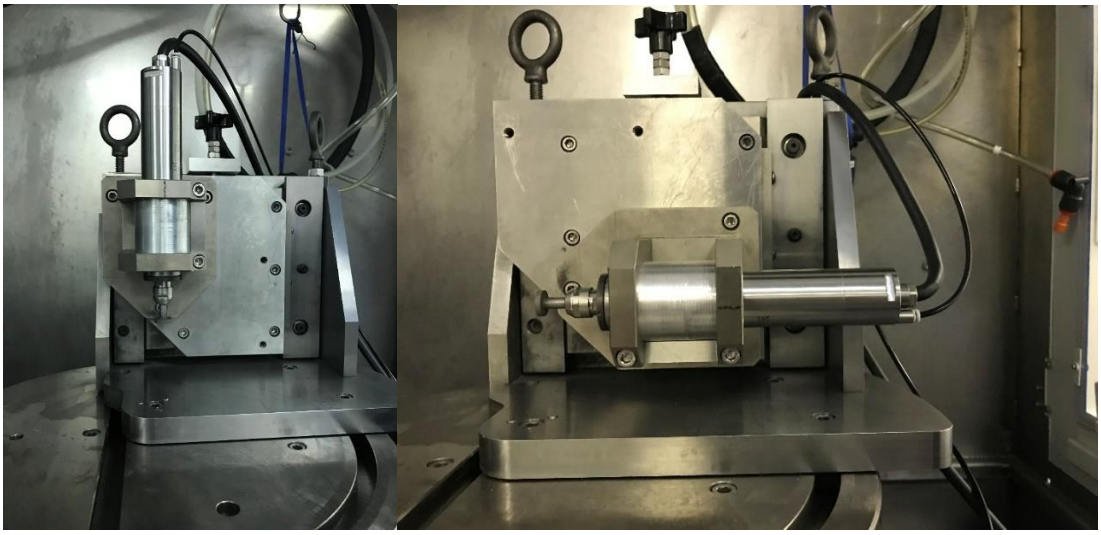

Figure 4-4: Grinding spindle in vertical and horizontal orientation

To give confidence that the insertion of the L Bracket between the faceplate has not negatively impacted the stiffness of the grinding rig, the total stiffness of the arrangement has been tested experimentally. This was achieved by measuring the displacement of forwardmost edge of the spindle clamp when a known load was applied to the topmost surface. Stiffness can be calculated as shown in Equation 25.

$$K = \frac{F}{Y} = \frac{3EI}{L^3}$$

(Equation 25)

The stiffness of the setup was measured by placing 1kg and 5kg loads on the top surface of the spindle clamp resulting in downward forces, denoted in equation 25 by F, of 9.81N and 49.05N respectively. When the 1kg load was applied a displacement, Y, of 0.48µm was measured using the integrated gauge amplifier. With this load the calculated stiffness, K, was 20.44 N/µm. When the 5kg load was applied, the measured displacement was 2.65µm yielding a calculated stiffness of 18.51 N/µm. The very low displacement measured under the 1kg load was difficult to verify as the reading was continually fluctuating however, under the heavier load, the displacement, once settled, was constant making this a more reliable measure of the true stiffness of the rig.

The grinding wheel mounted in the grinding spindle acts as a simply supported beam and the stiffness of this arrangement can also be calculated using Equation 25. To do this, two assumptions must be made; firstly, the Young's Modulus of the steel shank, denoted by E, is assumed to be 200 GN/m^2 which is a typical value for tool steel. Secondly, it is assumed that maximum displacement will occur at the unsupported edge of the grinding wheel and that this is nominally at a distance, L, of 20mm from the collet face. The area moment of inertia, I, can be calculated using Equation 26.

$$I = \frac{\pi D^4}{64}$$

(Equation 26)

The diameter, D, of the tool shank is 6mm, therefore the area moment of inertia for the tool shank is 63.62mm^4. Using these values, the calculated stiffness of the tool is 4.771N/μm. With this in mind it can be seen that the limiting factor for the stiffness of the grinding set up is the grinding tool itself. The mounting rig is approximately 3.5 times stiffer than the grinding tool and can therefore be considered suitable. It would be possible to design a stiffer arrangement by removing the ability to adjust the position of the grinding spindle however this would be undesirable as it would limit the adaptability of the set up.

When dressing the grinding wheel, the spindle is mounted in the horizontal position. The L bracket is not required as there is sufficient reach for the dressing nib to interact with the wheel. The grinding wheel in position for dressing is shown in Figure 4-5. Tool alignment is carried out by using the laser displacement sensor, mounted on the X axis, to measure along a known straight surface which lies in parallel with the spindle's axis; for example, the body of the spindle. If required the misalignment angle can be calculated using basic trigonometric functions by zeroing the sensor at one point, moving a set distance and observing the difference in measurement. This can be used to calculate the required adjustment directly however, in practice, it quicker to use the laser to repeatedly scan over a known length and make incremental adjustments until a consistent reading is achieved.

Adjustments are made by tapping on the front or back face of the grinding station with a plastic headed mallet. This process requires some operator skill but once proficient, it is possible to make very small adjustments in the order of 1-2µm. While making adjustments the central pivot bolt and T-slot nuts should be screwed down but not tightened; once satisfied that the tool is aligned, these can be progressively tightened to secure the station. Experience has shown that tightening the bolts invariably causes some slight movement of the station. For this reason, it can be beneficial to leave a small degree of anti-clockwise misalignment which, as the bolts are tightened, will come back into true. Once secure a final check of alignment can be carried out by re-measuring the original straight edge.

Figure 4-5: Grinding wheel in horizontal orientation for dressing

To align the tool vertically the grinding wheel is first brought into close proximity with the surface of the workpiece. A piece of 50µm plastic gauge strip, broader that the tool length, is placed between the grinding wheel and gently moved up and down while the grinding wheel is incrementally brought forward in small steps, ideally no more than 5µm at a time. As the operator is moving the gauge strip it will be felt when it becomes pinched between the tool and workpiece. Once this occurs the 50µm strip is removed and replaced with a thinner strip, in these experiments 13µm was used. This strip should be no more than a quarter of the tool

height. Once again, the strip is moved from the bottom of the tool to the top as the tool is advanced forward in small increments. Using this technique, it is possible to determine if the top or bottom of the tool is closer to the workpiece.

To adjust the alignment of the tool the three mounting bolts attaching the tool clamp to the L bracket are loosened and the pusher bolt behind the clamp can be wound in or out to achieve the required adjustment. The most effective method to quickly align the tool is to use shims placed under the bottom edge of the clamp to ensure that the bottom of the tool is forward. This establishes a known baseline before alignment starts. The top pusher screw, as shown in Figure 4-6, can then be wound in against tension from the mounting bolts until the correct alignment is determined using the thin piece of gauge strip. The tool is aligned when the gauge is pinched evenly along the length of the tool.

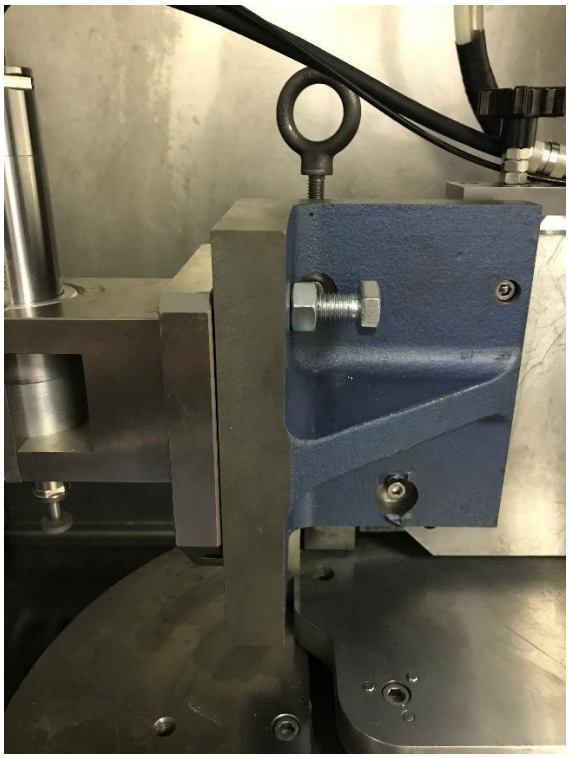

Figure 4-6: Vertical alignment screw

4.3 Integration of a USB microscope and Laser Displacement Measurement

To aid the dressing and machining processes additional equipment have been incorporated onto the Nanoform 250 Ultra Grind. These additions are used to monitor the process and assist in tool setting and alignment by providing additional non-contact measurement capability. To facilitate their inclusion on the machine a single 30mm grommeted hole was created in the body of the machine to allow cables to be passed through without compromising the safety of the equipment.

4.3.1 Laser Displacement Sensor

A method of measuring the surface of the grinding wheel in operation is required to facilitate tool setting and alignment. This method must be non-contact as the superabrasive particles in the grinding wheel would cause significant damage to the tip of a contact measurement system. The laser displacement sensor used throughout this project was a Keyence LK-H022 with a 20mm reference distance, ±3mm measurement range and sampling cycles from 2.5µs to 1000µs. The sensor head is positioned inside the machine and connected via a cable running through the side of the machine to the control unit. The control unit incorporates a small display for live data and basic function controls. Data logging and advanced set up are achieved by connecting a PC to the control unit. The basic components of the system can be seen in Figure 4-7.

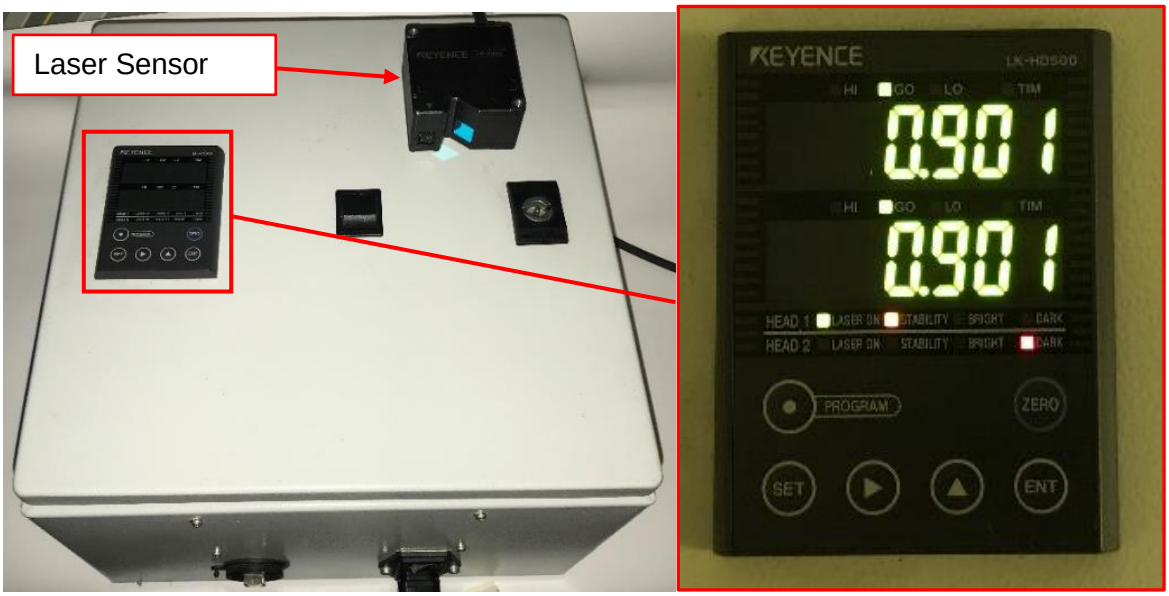

Figure 4-7: Laser Displacement Sensor control box with sensor head and close up of display

The sensor used is a 1D spot type sensor used for measuring linear displacement with a circular spot diameter of 25μm. To obtain a measurement value the sensor takes a number of averaging measurements to generate a nominal value for the point. The repeatability of the sensor head is 0.02μm when measured at the reference distance and the number of averaging measurements set to 16,384 (Keyence, 2010). To generate a linear profile measurement the spot is moved over the surface of the part in such a way that the averaging measurements continually overlap thus generating a nominal profile. This is ideal for applications such as tool setting and measuring tool run-out and deflection due to its high sampling rate and large reference distance. This model was selected as it is a low cost, highly robust self-contained unit which could easily be incorporated into the machining environment without suffering adverse effects. Additionally, the measurement system was already available within the research group and the capabilities well understood. The default minimum display resolution of 0.001mm (1μm) was deemed sufficiently accurate for the purposes of tool setting and process monitoring due to the noisy surface of the grinding wheel and the need to generate a linear profile. However, the system can be set to display measurements down to a resolution of 0.001μm if required. Use of the higher resolutions available would offer no benefit when using the system for tool setting but could facilitate

other advantageous characteristics such as on machine measurement of the finished part. Figure 4-8 shows the laser head in position for process monitoring.

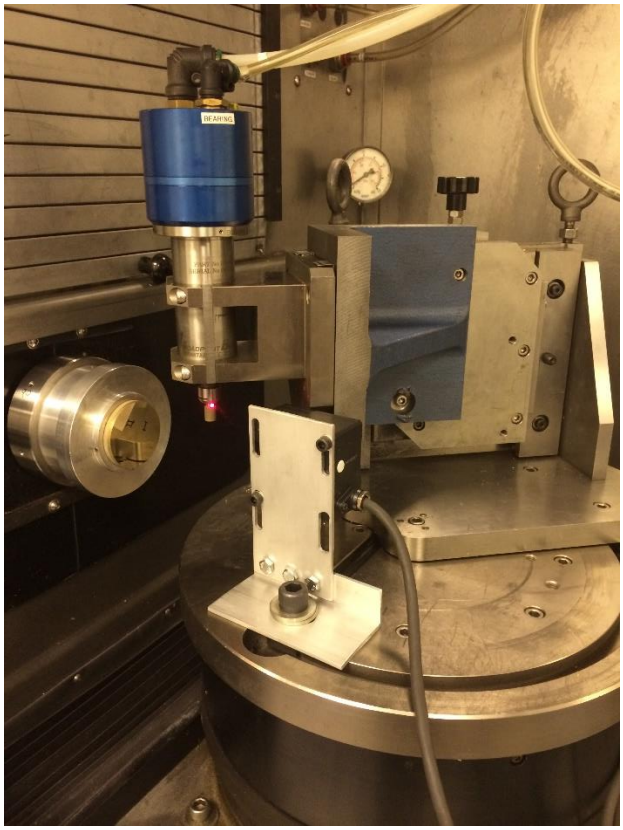

Figure 4-8: Laser Displacement Sensor mounted to the Z axis bed and positioned for process monitoring

The laser displacement sensor was originally mounted to a flat plate which could be mounted, by means of various brackets, to T-slots on the Z axis base or the vacuum chuck on the X axis. This allowed to be used in tool alignment and to measure tool displacement and run-out in process. While this data was valuable the mounting solution had severe limitations; it was not possible to use the sensor on the X axis without removing what was originally mounted there, either the dressing nib or workpiece. The sensor head affixed to the vacuum chuck can be seen in Figure 4-9.

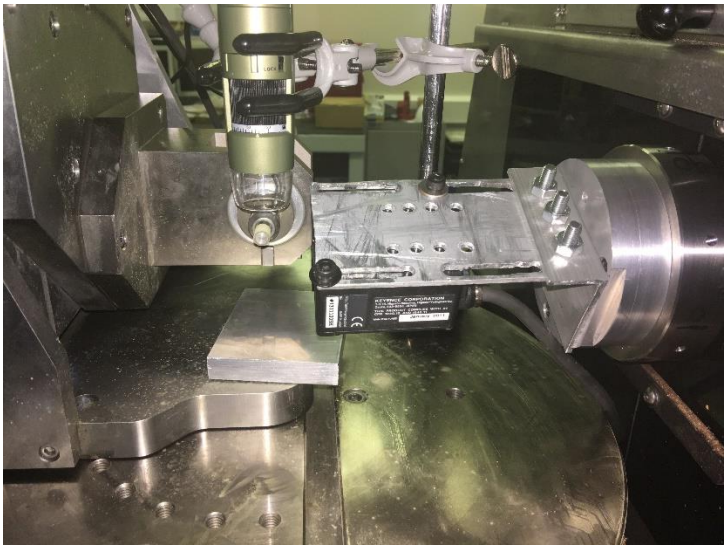

Figure 4-9: Sensor mounted to vacuum chuck

To enable the sensor to be used between dressing operations a new mounting solution was designed which makes use of the mounting points and arm used by the tool setting camera supplied with the machine. Using a small window, the arm can be mounted directly atop the X axis spindle block. The sensor can then be mounted on a plate alongside the dresser nib or workpiece enabling measurements in between processes without disturbing the experimental set up. The sensor can be mounted in multiple orientations and is adjustable for height. The mounting solution allows the sensor head to be positioned in a range of different orientations, examples are shown in Figure 4-10.

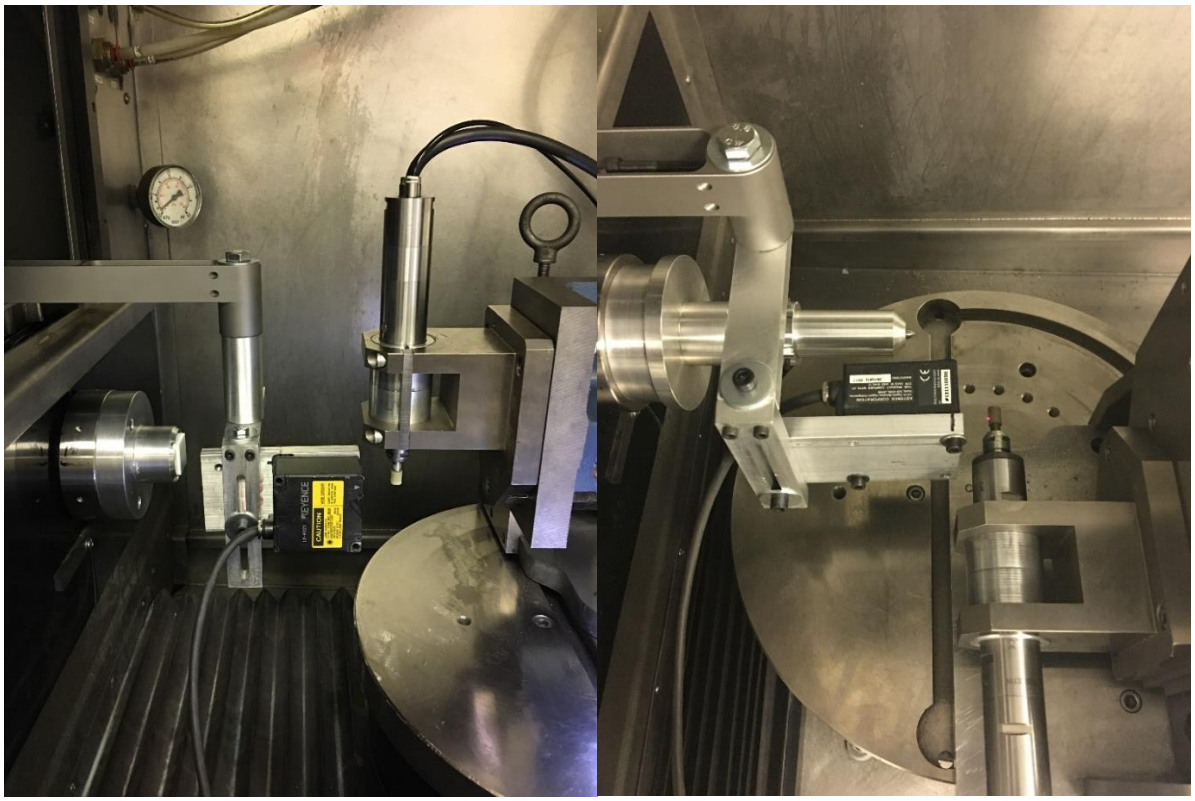

Figure 4-10: Sensor on height adjustable mount positioned adjacent to work piece (left) and dressing nib (right)

For tool setting and alignment and in process monitoring of tool deflection and chatter a 1D measurement is sufficient. However, to use the laser displacement sensor in the cut-measure-compensate process a 2D linear profile must be generated. This can be accomplished with the laser mounted to the machine's X axis. If the laser is traversed across the surface of the grinding wheel at a constant speed the distance between each measurement point can be calculated using the sampling rate through use of the formula shown in Equation 25, allowing the linear profile to be plotted using software such as Microsoft Excel.

$$Distance\ between\ measurements\ (\Delta D) = \frac{Feedrate\ (mm/min)}{60{,}000} \times Sample\ Rate\ (\mu s)$$

Equation 27

4.3.2 USB Microscope

In order to capture images and video of the grinding process in action, a Dinolite AM4113T USB microscope was incorporated into the machine set up. Despite the relatively high cost compared to other USB microscopes of a similar design, this unit was selected for its higher

quality optical performance and the ability to carry out coarse measurements using the specialist software provided. This model has a resolution of 1.3 megapixels and an optical magnification range of 10x to 70x (up to 200x is possible through digital magnification).

The small size and integrated lighting ring allow the Dinolite to be conveniently mounted in several positions on the grinding station. The microscope is mounted using a conventional three finger clamp attached via a boss to a magnetic stand. This provides a secure base which can be easily moved when necessary and allow for adjustment of the height, orientation and angle of the microscope. The mounting system is shown in Figure 4-11.

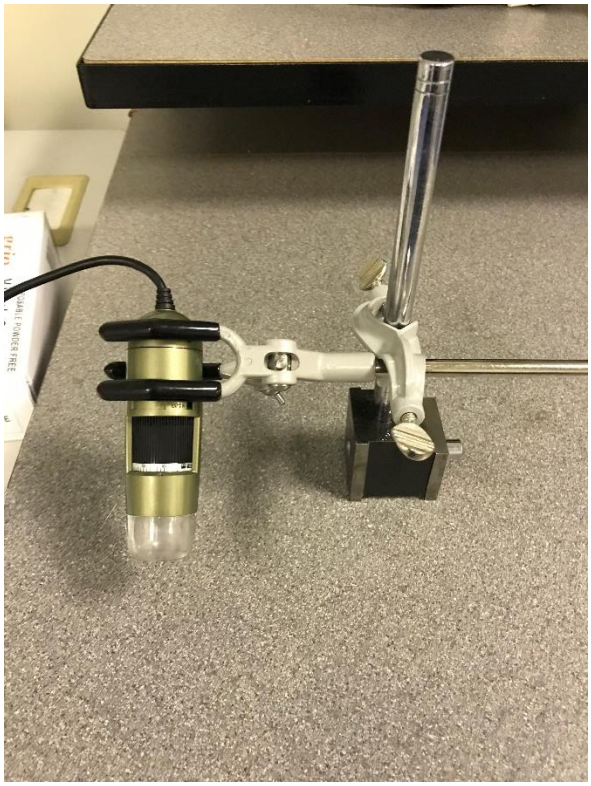

Figure 4-11: Dinolite USB microscope in mounting system

For a given operating distance, focus is controlled by varying the magnification of the microscope. Hence, to achieve accurate measurements the software must be calibrated at the correct magnification each time before use. The software uses a pixel counting method for measurement and consequently the resolution varies depending on the current magnification. In use on the machine, typical resolutions of approximately 5µm were achieved for linear distance measurements. These were considered acceptable for coarse

tool setting. Additionally, the microscope could be used to measure other features such as the angle between the dressing nib and the grinding wheel. These measurements are carried out using reference points on the observed part and as such are not dependent on a linear measurement. Consequently, they have a significantly higher degree of accuracy. In addition to on machine process monitoring the USB microscope provides a quick and convenient means of determining the geometry of the dressing nib and the grinding wheel diameter before and after use reducing the need to remove them from the machine for measurement.

4.3.3 Cost of the Experimental Set Up

A primary goal of this project is the development of a cost effect system which can be retrofitted to a wide range of existing CNC ultra-precision machining systems. The modifications detailed in the chapter consist of a number of new pieces of specialist equipment along with application specific solutions to adapt and integrate them onto the Nanofrom 250 Ultra Grind. **Error! Reference source not found.** gives a breakdown of the costs of the various elements of the system as described and gives an indication of the expected cost of replicating the process on other machines. To generate this breakdown, the cost of each element has been determined based on current prices for new equipment which were accurate at the time of writing. Due to variations in exchange rate, shipping and taxes, exact prices have not been given. Rather, these prices represent a pessimistic estimation of the cost for any potential user. It is likely that costs would be lower, potentially significantly, if users already possess equivalent equipment capable of similar levels of performance.

Area	Component	Price
Nakanishi Grinding Spindle	EM-3060J Motor	£900
	NR-3060S Spindle	£900
	ARG-021E Gearbox	£300
	E3000 Controller	£1500
	EMCD-3000J-3M Cord	£300
Keyence Laser Displacement Sensor	LK-H022 Sensor	£1700
	LK-G5000 Control Unit	£2700
	LK-GD500 Display Panel	£950
Dinolite USB Microscope	AM4113T	£300
Ancillaries and Consumables	Application specific mounting adaptations	£500-1000
	Collets & Tool Holders	£100-150 Each
	Dressing Nibs	£40-100 Each
	Grinding Wheels	£80-200+ each
Total* (*assuming 5 off each consumable)		£12,200 (+ taxes)

Table 4-2: Cost of additional equipment for experimental set up

From **Error! Reference source not found.** It can be seen that an entire, ready-to-use set up could be purchased for approximately £12,000 (+ taxes). When compared to other bolt-on retrofit systems which offer a similar degree of increase in manufacturing capability, this system represents a high degree of value for money. Examples of similar systems which were purchased for use in the same laboratory include a Physik Instrumente Ltd. Hexapod (used for motion control of a micro-polishing head) at approximately £30,000 and a Kinetic Ceramics Fast Tool Servo (to add FTS capability to the Nanoform 250 Ultra Grind) at a cost of approximately £40,000+. At such a low cost, the system described is especially relevant to smaller companies which do not have the capacity for large capital outlay.

4.3.4 The Dressing Process

Conventional single point diamond dressing nibs are used to dress the grinding wheel. These are readily available at low cost and can be supplied with diamonds in a range of carat sizes. These tools consist of a single grain of diamond mounted to a steel shank with a point exposed and sharpened. In some more expensive versions, the diamond grains incorporate multiple sharp points and can be re-set when the exposed point becomes worn and dull. For these experiments the cheaper single use variety of tool were used, However, either type would be suitable for use in this process. The dressing nibs used were mounted

in either a 0.125 inch or a 0.25 inch shank, were sharpened at an angle of 60-65 degrees and had tip radii between 30µm to 40µm. Examples can be seen in Figure 4-12 with a close up image of the tool geometry in Figure 4-13.

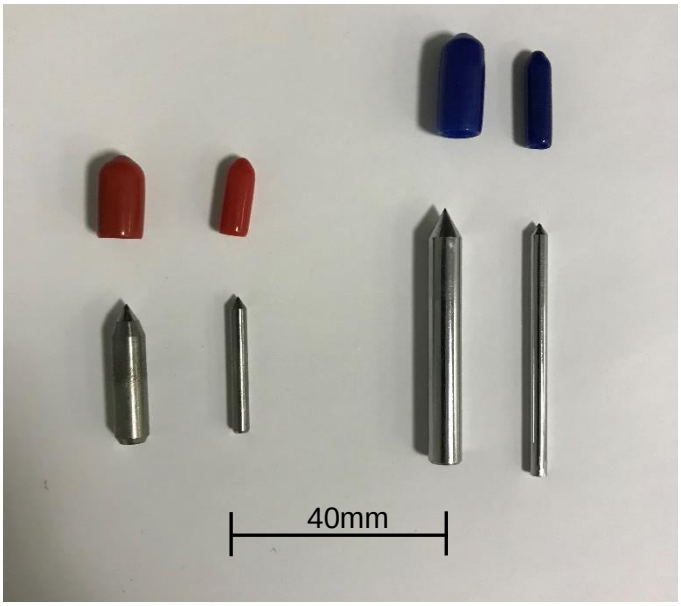

Figure 4-12: Dressing nibs of various sizes

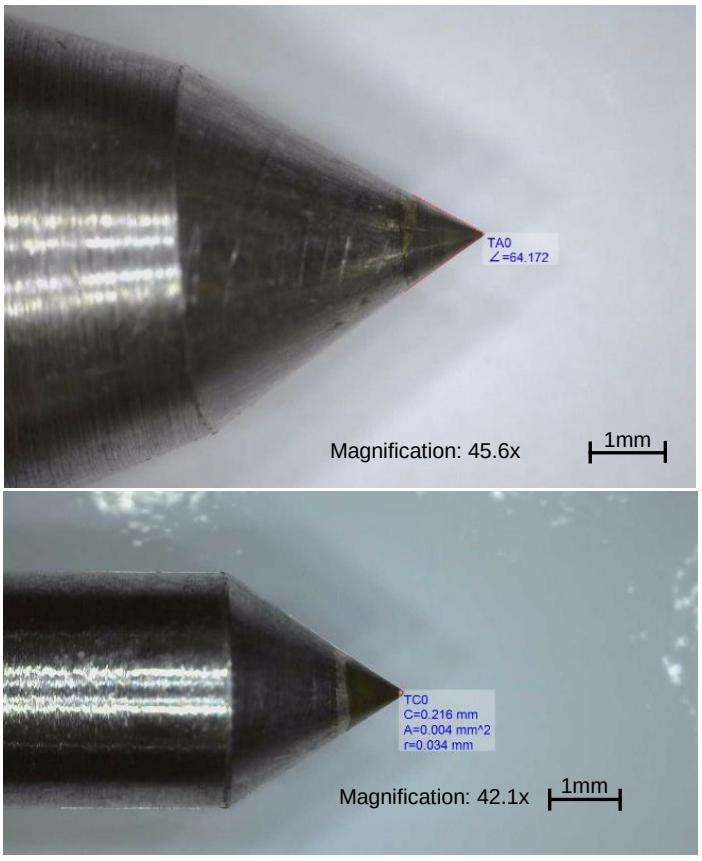

Figure 4-13: Examples of dressing nib geometry taken using the USB microscope

During use, the dressing nib is retained by a specially manufactured tool holder. The tool holder is sized to accept a dressing nib of a particular shank diameter and length and the nib is held in place by a single grub screw. This tool holder is then mounted in an existing workpiece holder and affixed to the machines X axis via the vacuum chuck. This set up is advantageous as it allows for quick tool changes and accurate centring of the dressing tool with the C axis. Coarse centring of the tool can be achieved using the USB microscope, while fine centring is achieved using the machine's finger type integrated gauge head. The same process could be carried out with a conventional finger type Dial Test Indicator (DTI) on machines which are not equipped with a gauge head. The tip of the gauge head or DTI is placed on the body of the dressing nib, ideally as close to the tip as possible, and the whole assembly is slowly rotated to observe the deviation. Periodically moving the tool backwards and forwards along the X axis can prove useful in determining the current high point on the tool. As the assembly is affixed via the vacuum chuck it is possible to adjust its position in very small increments by gently tapping along the base of the workpiece holder with a nylon mallet. The tool should be centred using this method until the deviation between the maximum and minimum height while rotating is less than 1µm. It is important that this deviation is kept as low as possible, as when the nib is rotated during the dressing process any deviation present will be translated onto the surface of the grinding wheel.

The position of the dressing nib along the length of the grinding tool is controlled by the machines X axis while dressing depth is controlled by the Z axis. Tool setting is carried out using the USB microscope. The X axis position can be quickly set with the microscope positioned above the tool as shown in Figure 4-14. The start and end points of the dressing operation are set with the dressing nib between 0.5mm to 1mm beyond the edges of the grinding wheel, this can easily be observed using the microscope. It is important that the start and end points are off the surface of the grinding wheel to allow time for the X axis to accelerate to the correct feedrate.

Figure 4-14: USB microscope positioned for tool setting

The height of the dressing nib relative to the centreline of the grinding wheel is set by adjusting the height of the grinding spindle. This process requires a much greater degree of accuracy than the positioning along the X axis. The USB microscope is repositioned to sit in line with the grinding spindle axis, viewing the grinding wheel end on. With the edge of the grinding wheel in sharp focus the dressing nib can be moved in small increments until the tip is also in focus, ensuring that the tip is in very close proximity to the plane of the face of the grinding wheel. At this point the measurement function on the USB microscope is used to determine the centreline of the grinding wheel and the height of the rotational axis of the dressing nib. Using the calculation steps given in chapter 3 it is possible to determine the appropriate height for the grinding wheel to achieve the correct dressing angle relative to the centreline of the wheel. The height of the grinding wheel is adjusted using the process previously described and the measurement function is used to confirm the correct angle has been achieved. The dressing depth can then be set moving the Z axis forward incrementally until the surface of the grinding wheel is in close proximity to the tip of the dressing nib. It is

beneficial to leave a gap of approximately 10µm to 20µm between the nib and the surface of the grinding wheel when setting the zero depth; this allows for any undulations left by previous grinding to be progressively dressed out. At this point the setup is ready for preliminary dressing and truing.

With both the X and Z axes in their zero (0,0) position the dressing nib can be slowly rotated by the C axis and the grinding spindle activated to rotate at the dressing speed. The Z axis is then moved forward incrementally by the desired dressing depth and the dressing nib traversed across the surface of the grinding wheel at the feedrate necessary to minimise scalloping to an acceptable level. A coolant stream of Clairsol 330™ and air is aimed at the dressing nib to aid the operation and prevent build-up of waste material. It is recommended that Macor® is machined using a water based coolant however this is not possible on the Nanform 250 Ultra Grind which requires oil based coolants to prevent damage to the electrical components inside the machining space. Clairsol 330™ is an odourless kerosene based coolant which is approved for use on the Nanoform 250 Ultra Grind (Leading Solvents, 2013). After the operation the grinding wheel is dried and observed using the USB microscope to determine the state of the surface. Large faults, such as the remnants of previous structured grinding or areas of glazing are readily identified. This process is repeated until the whole surface has been refreshed and is visibly free from defects. The accuracy of dressing can be confirmed using the Laser Displacement Sensor. A flowchart for the truing process is shown in Figure 4-15.

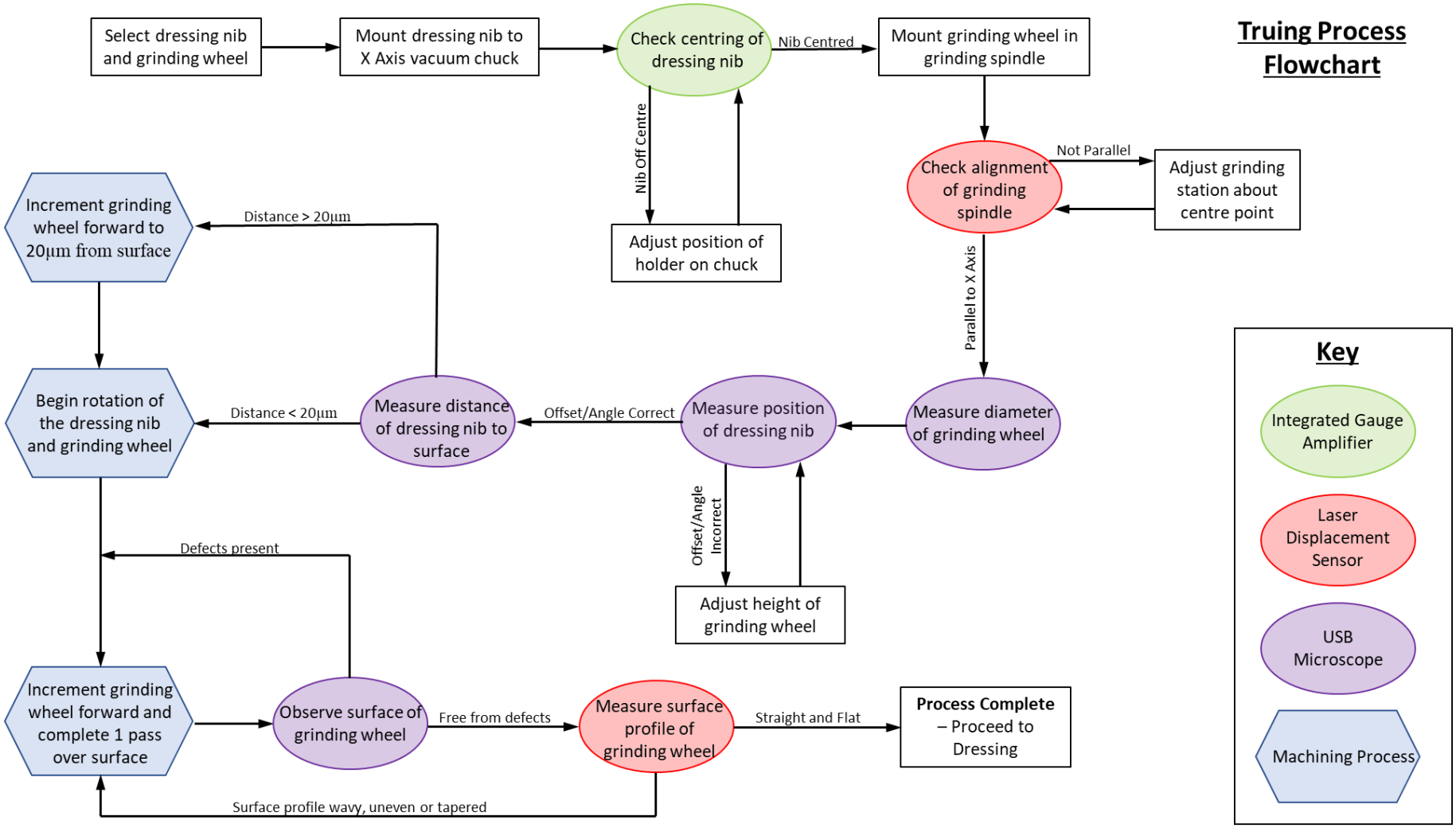

Figure 4-15: Truing process flowchart

The final dressing process, to create the required profile on the grinding wheel, must be carried out with a dressing nib of known geometry. The dressing nib used in the preliminary dressing operation will no longer have the same geometry due to wear and must either be replaced or remeasured, either of which requires removal from the tool holder. After replacing the nib, it is necessary to reset the X axis to zero to achieve the correct dressing depth. To accomplish this the nib is first positioned in the same manner as previously described. Once at a distance of approximately 10µm from the surface of the grinding wheel the Z axis is moved forward in 1µm increments while carefully rotating the grinding wheel by hand, completing at least one full revolution. Using this method, it is possible to feel when the dressing nib has made contact with the grinding wheel at which point the Z axis can be zeroed and the setup is ready for final dressing.

The initial stage of the final dressing process is carried out using the machine's CNC system and consists of setting the start position, dressing depth, profile geometry, feedrates and dwell time (if required). Dressing conditions such as nib rotation, grinding wheel speed and coolant flow are kept as for preliminary dressing. After the initial dressing pass is completed the Laser Displacement Sensor is placed on its mount adjacent to the dressing nib. The grinding tool is then retracted and moved to the measurement position. With the laser spot running along the centreline of the grinding wheel a linear profile measurement is taken. This can be used to assess the accuracy of the dressing process and identify any areas for corrective dressing. This process is termed cut-measure-compensate. Any grooves where the profile or dressing depth deviate from the design parameters can be corrected in a second dressing stage. The necessary corrections are determined and then a new CNC program is created with the level of corrective dressing required. Corrections are usually required to increase the dressing depth to account for tool wear, but it is also possible to correct the profile of the groove by adjusting the tool path. After each corrective dressing stage, the tool is re-measured and further corrections carried out as necessary until the profile meets the design criteria. This process is illustrated in Figure 4-16.

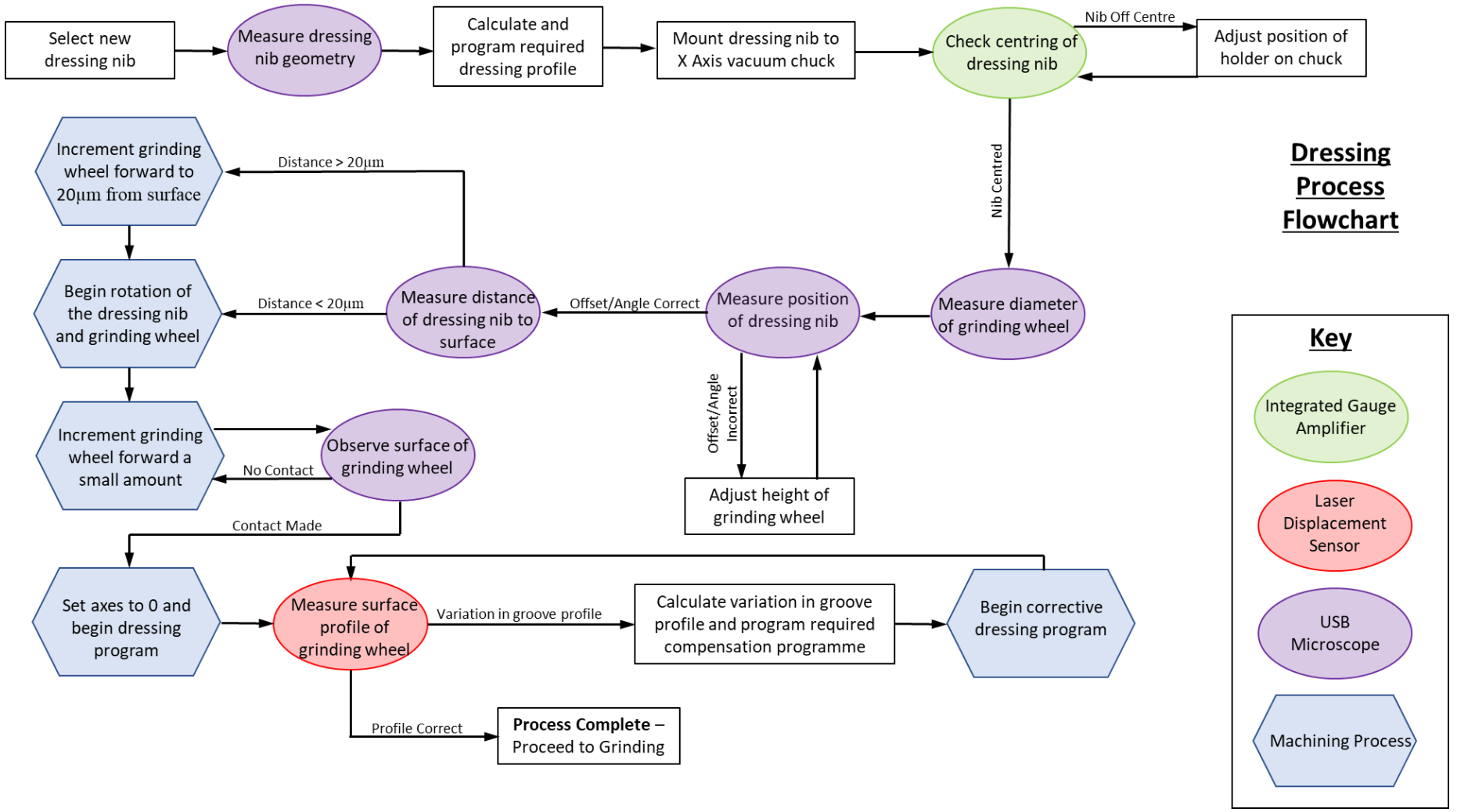

Figure 4-16: Final dressing process flowchart

The grinding process is carried out with the grinding spindle in the vertical orientation. The grinding wheel must be aligned to be parallel to the surface of the workpiece. This is achieved using the gauge strip aligning process previously described. Once the spindle has been aligned with the workpiece the grinding wheel is moved forward incrementally until contact with the workpiece is observed using the USB Microscope. At this point the axes can be zeroed and the first grinding process commenced. Once complete the workpiece can be rotated as required to carry out subsequent grinding passes and complete the machining process. This procedure is detailed as a flowchart in Figure 4-17.

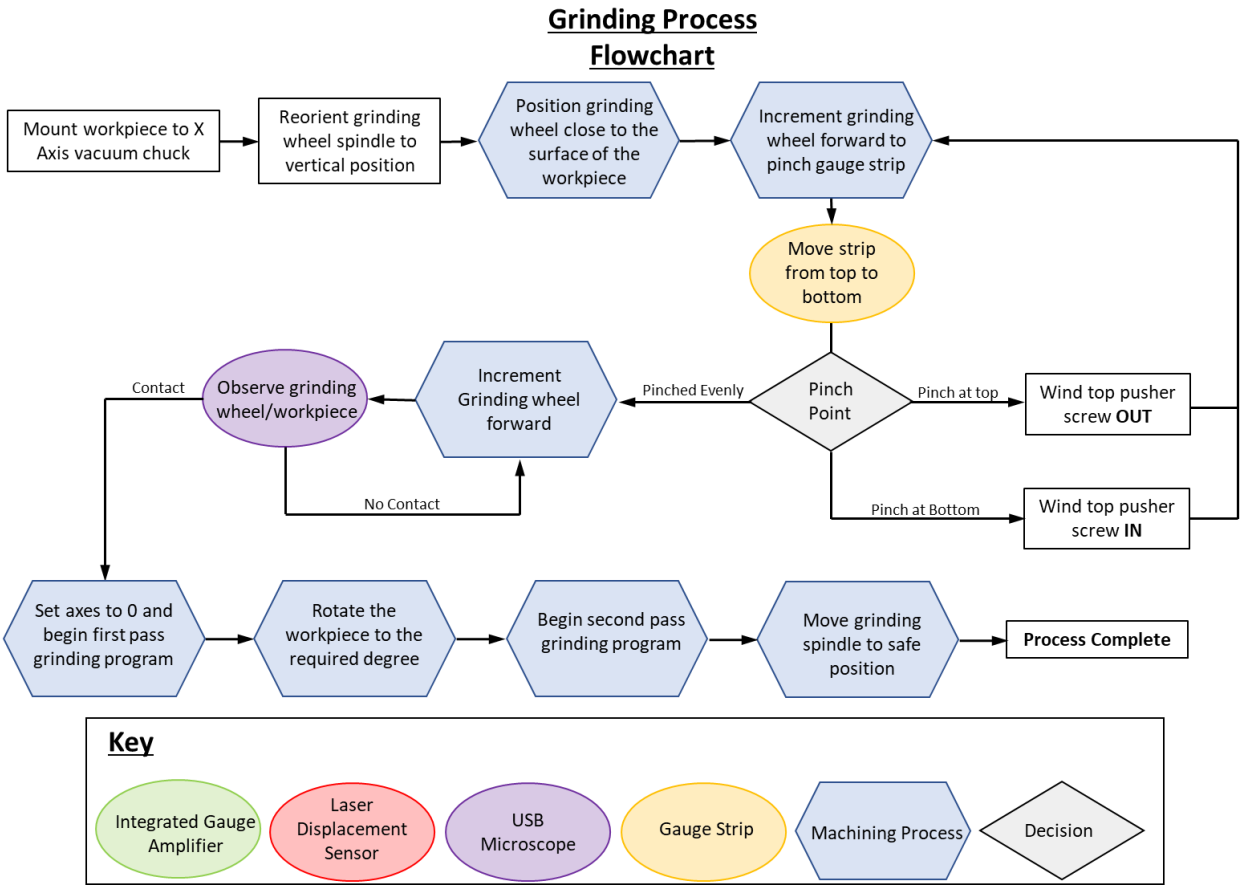

Figure 4-17: Grinding process flowchart

Chapter Five

Structured Grinding

Over the course of the research several different methods of structured grinding have been trialled with all trials carried out on the Precitech Nanoform 250 Ultra-grind. This chapter details the processes and procedures utilised in each trial and provides an analysis of the results obtained. The results from each trial and the challenges encountered formed the basis for continuous development and refinement of the process which resulted in incremental increases in capability. This progression in capability is easily identified when comparing the results of each experiment. The previous chapter detailed the equipment and methodologies used. However, many of these were developed, or refined, as a direct result of the previous trial. As such, the set up utilised and experimental method varied between experiments. For this reason, the process parameters used in each experiment will be given in detail.

5 Structured Grinding

5.1 Single Pass Radial Grooves – Micro Riblets

To determine the accuracy of the dressing process and the fidelity of form generation a trial was carried out using a series of widely spaced grooves orientated radially around the body of the grinding wheel. The full parameters used in this experiment are provided in Table 5-1 with the terminology for each aspect of the profile geometry illustrated in Figure 5-1. The grooves were spaced in 800µm intervals as it was expected that this would be sufficiently far apart that there would be little risk of them interacting and weakening the bonding matrix between the grooves. A second objective of this trial was to determine the performance of the grinding process at the very low spindle speeds and high feedrates necessary to carry out Stępień style helical grinding.

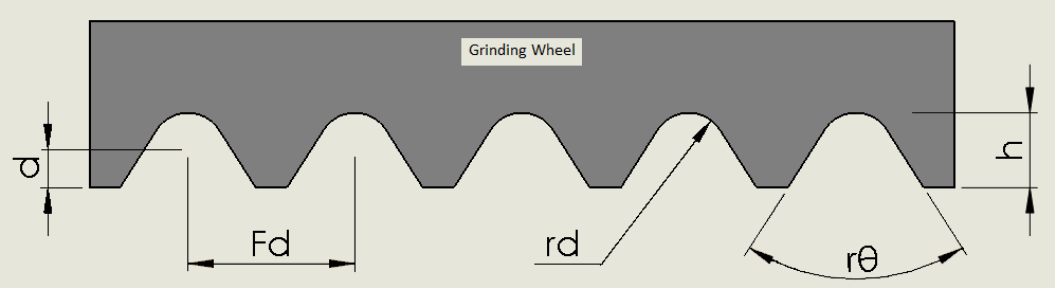

Figure 5-1: Grinding wheel profile geometry

Feature/Parameter	Symbol	Value
Dressing Depth	h	20µm
Groove Pitch	F_d	800µm
Nib Radius	r_d	34µm
Nib Angle	ϑ	64.2 Degrees
Dressing Speed	S_d	500 RPM
Grinding Speed	S_g	2000 RPM
Feedrate	V_w	50 mm/min
Grinding Depth	d	10 µm
Grinding Surface Speed	V_s	0.84 m/s
Grinding Wheel Grit		1200 Grit
Grinding Wheel Bond Type		Resin

Table 5-1: Micro riblet process parameters

For this procedure the Nakanishi EMR-3008-K electric spindle incorporating a 1:4 reduction gearbox was used. A 1200 grit diamond super-abrasive resin bonded grinding wheel with a nominal outer diameter of 8mm and length of 10mm was selected.

The Keyence lased displacement sensor was mounted using two mounting solutions. For tool alignment and dressing the sensor was mounted on a bracket to the machine's C axis using the vacuum chuck. For tool deflection and run out monitoring in process the sensor was mounted directly to the Z axis bed directly behind the wheel. The Dinolite USB microscope was used throughout for tool setting and process monitoring.

5.1.1 Truing and Dressing process – Micro riblets

Before dressing the wheel was trued using a part worn diamond dressing nib so that its surface was parallel to the motion of the workpiece axis. This process was carried out in incremental steps until an entirely fresh surface was visible on the grinding wheel. The dressing and truing operations were carried out at a spindle speed of 500 RPM. While much higher than desirable for dressing the grinding wheel this was the lowest possible speed at which the spindle could be used under load. The dressing process was carried out with the spindle mounted to the Z axis in a horizontal orientation. The dressing nib was mounted in a specially manufactured holder on the X axis of the machine using the vacuum chuck with the C axis locked to prevent rotation. As such, positioning of the dressing nib along the surface of the grinding wheel was controlled by the X axis while truing and dressing depth was controlled by the Z axis.

The dressing operation was carried out using a fresh dressing nib with a tip radius of 34µm. No angle was used between the dresser nib and the grinding wheel during dressing of the grooves and the dressing nib was not rotated. It was understood that this would be detrimental to the lifespan of the dressing tool but as this was the most accurate method of setting the dressing tool to the workpiece surface it was deemed acceptable. Dressing nib centre height setting was achieved using the USB microscope and a small sharp pointer mounted in the spindle collet. The two points were brought into close proximity and then the height of the tool spindle was adjusted until the points were aligned.

At each of the specified groove locations the dressing nib was plunged into the rotating wheel at a speed of 5mm/min to a depth of 20µm with a dwell period of 2 seconds before

being retracted. This process was carried out using the Nanoform's CNC control with the start point being set by the user. This was acceptable as the pattern or grooves did not extend across the whole length of the grinding wheel. The dressing operation was carried out on the lower portion of the wheel with the upper portion left untouched after truing to provide a basis for comparison. Coolant was not used during dressing, but an air stream was directed at the dressing nib to prevent build-up of material. The process was monitored throughout using the USB microscope.

This initial dressing of the grinding wheel was carried out twice. Once to allow the process to be checked and the second time to carry out the procedure. This was necessary as once dressed, the grinding wheel cannot be removed from the grinding spindle without potentially introducing positioning errors. As part of assessing the success of the dressing process, several Scanning Electron Microscope (SEM) images were taken of the grooves. Figure 5-2 shows two adjacent grooves.

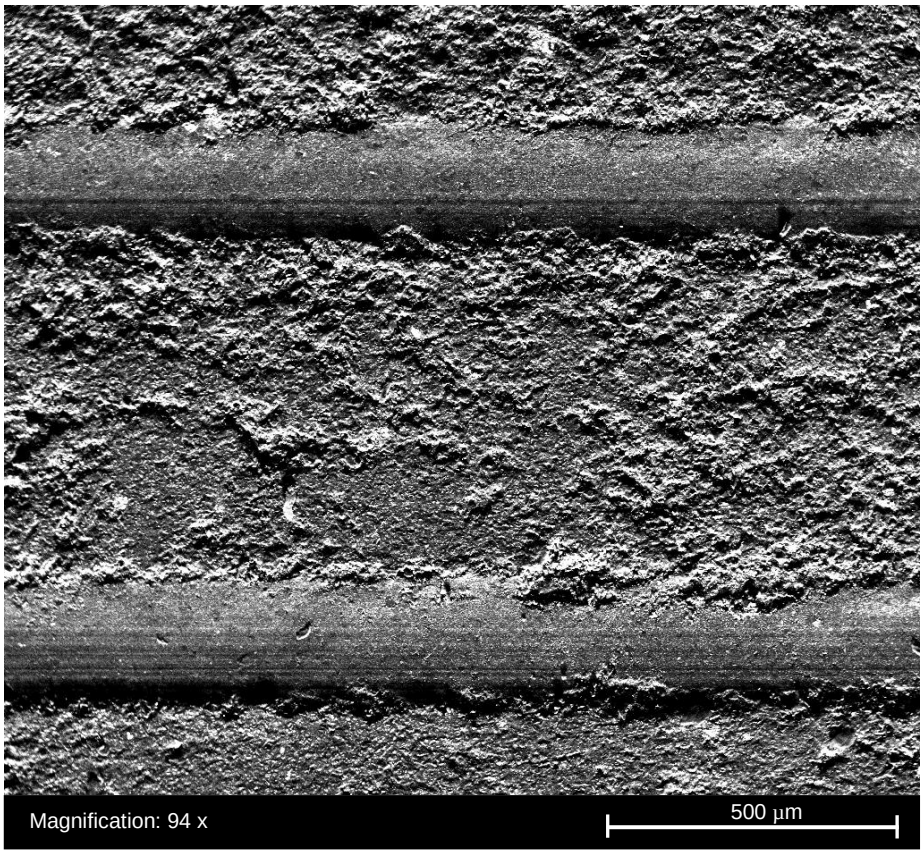

Figure 5-2: SEM Image of adjacent grooves

At this magnification it is difficult to discern individual grains, but it is possible to see that there is a distinct difference between the trued surface which is heavily pitted, and the bottom of the groove which is smooth and flat. Due to the lack of low speed control possible on the grinding spindle used in this experiment, the dressing procedure was carried out at high RPM which is not ideal. This most likely led to the high degree of surface fracture present on the surface of the grinding wheel and the glazing on the bottom of the grooves. Glazing is common when worn nibs are used at high speed. This glazing is particularly evident in Figure 5-3 where individual exposed grains are discernible on the edge of the groove walls but on the bottom of the grooves the grains are fully embedded in the bonding material with no voids or bond cavities present.

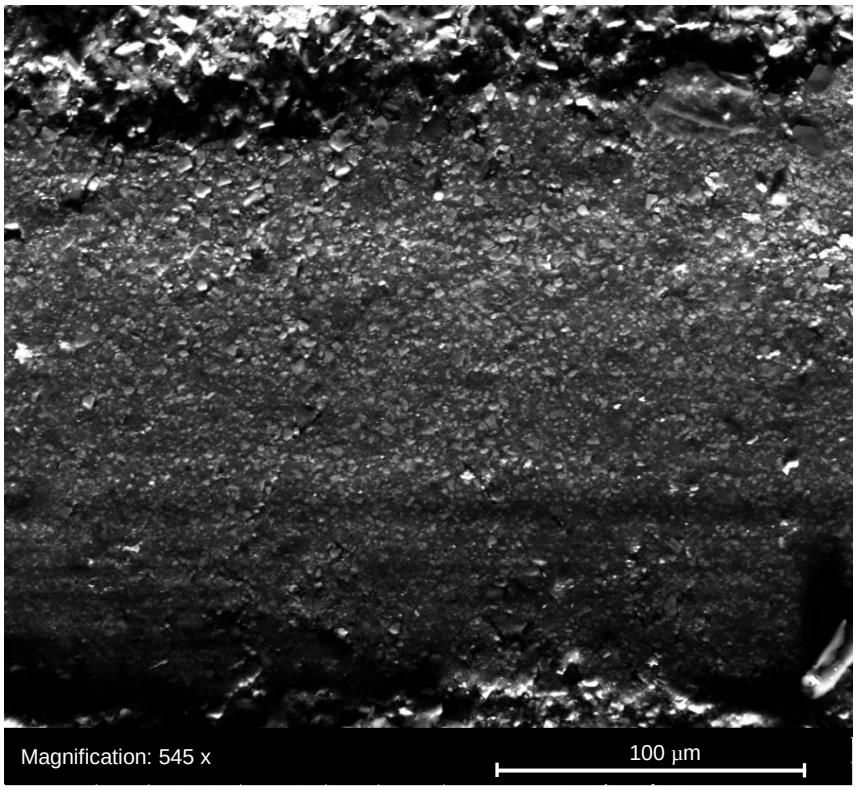

Figure 5-3: SEM Image of glazing on groove bottom

The edges of the dressed groove are indistinct, and several areas of inconsistent material loss can be observed. The mechanism for this material loss is speculated to be material pull

out resulting from material build up on the edge of the blunt dressing nib. This indistinct edge is clearly visible in Figure 5-4.

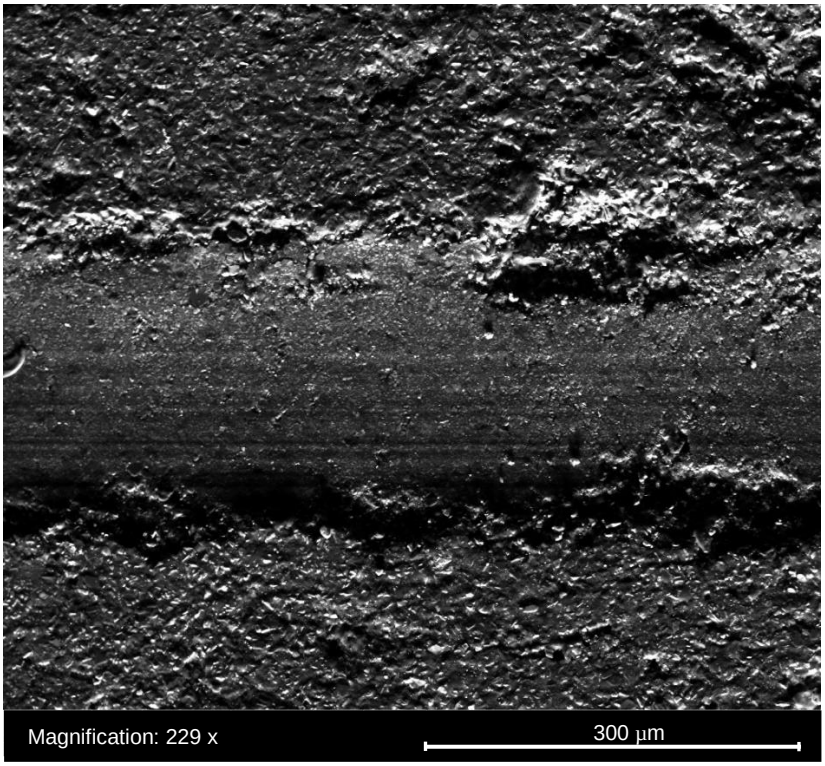

Figure 5-4: SEM Image of groove edge shown material loss

5.1.2 Grinding Process – Micro riblets

Brass was selected as a medium for the first grinding operation due to the ease with which it could be machined in-situ on the Nanoform to present a flat and true surface for the grinding operation. While grinding is not frequently used for machining brass, due to its ductile nature and high machinability, these characteristics were desirable for this experiment. The relatively high depth of cut combined with a high feedrate and slow spindle speed meant the tool and workpiece interaction were significantly different from traditional creep feed grinding, being more similar in many respects to a milling process.

The workpiece was first face turned on the machine to create a flat surface for grinding. The edges of the round bar were then milled away to leave a square profile with straight edges. These edges were broken by gentle hand filing to produce a small chamfer. This was

necessary to ensure that the grinding wheel came into contact with the workpiece in a uniform manner.

Before grinding could take place, it was necessary to move the grinding spindle into a vertical orientation and align it with the workpiece surface. To allow the laser displacement sensor to be positioned behind the grinding wheel to monitor tool runout and deflection it was necessary for the grinding wheel mounting station to be at an angle from perpendicular to the motion of the X axis. While theoretically this would not impede the grinding process, as the grinding station was angled relative to the axis of rotation of the grinding spindle, in practice this made tool alignment significantly more difficult. Figure 5-5 and Figure 5-6 show the grinding wheel in position adjacent to the surface of the workpiece and the complete set up ready for grinding.

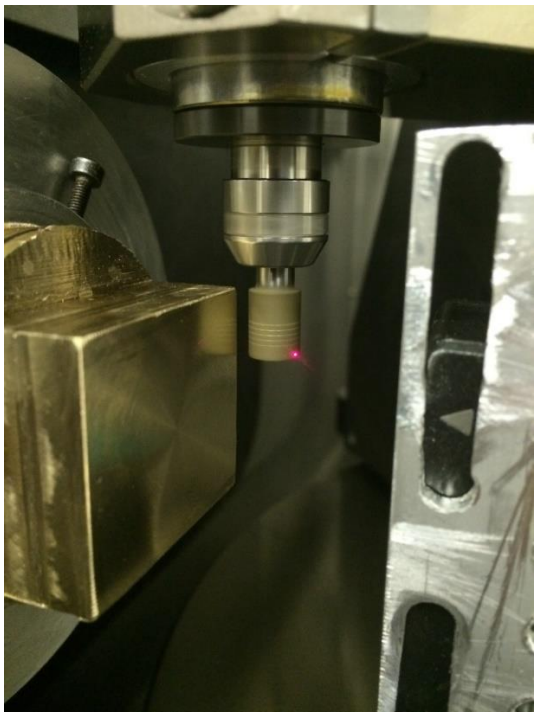

Figure 5-5: Grinding wheel in position with laser positioned to measure tool deflection

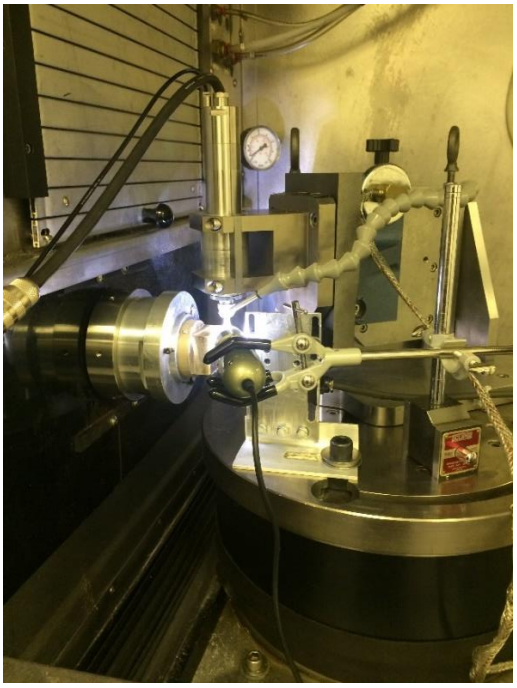

Figure 5-6: Complete setup in position ready for grinding (Grinding wheel and workpiece obscured)

The tool was brought into close proximity to the surface of the workpiece using the USB microscope and then moved forward in increasingly small steps until it made contact with a 50µm thick sheet of plastic gauge strip on the face of the workpiece. At this point the grinding spindle was activated and moved forward incrementally until it contacted the workpiece. It was noted that the lower edge contacted the workpiece first. The grinding wheel was moved forward while running by 18µm in 1µm increments until the whole wheel was in contact with the workpiece. Over the full 10mm length of the grinding wheel this indicated that the setup was 0.1 degrees or 6 Minutes of Angle (MOA) out of alignment. The decision was taken to continue with the experiment as the intention was to grind to the full depth of the groove. Figure 5-7 shows the grinding wheel positioned above the surface of the workpiece before first contact had been made; the profiled grooves are clearly visible on the surface of the grinding wheel.

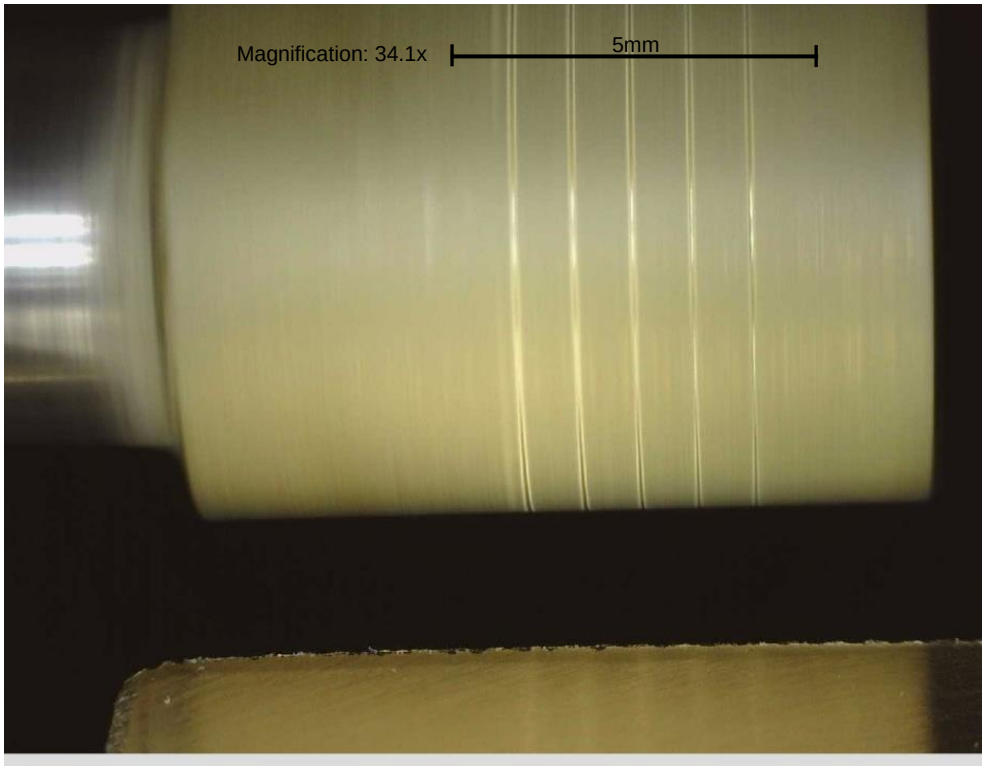

Figure 5-7: Grinding wheel in position with grooves visible

Grinding was carried out at 2000rpm and a feedrate of 50mm/min. Upon completion of the first grinding pass the workpiece was rotated 180 degrees and the procedure was repeated to produce a second ground surface. The fully contacted grinding wheel can be seen in Figure 5-8 with the resultant surface partially visible.

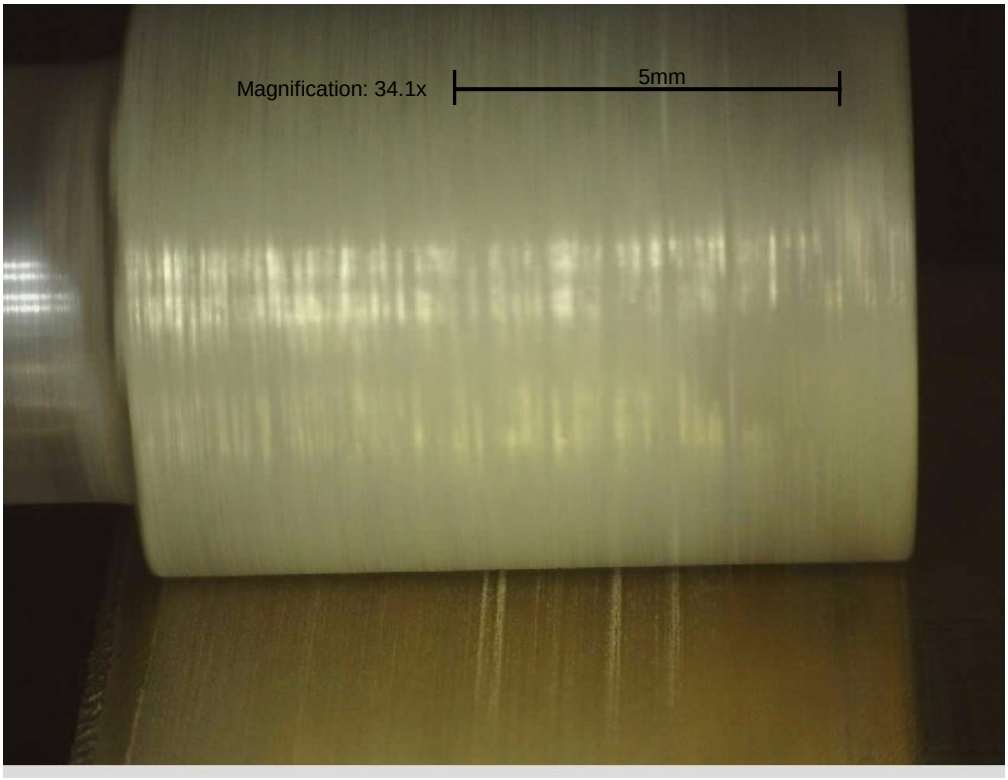

Figure 5-8: Grinding process with resultant surface partially visible

During the first grinding pass the tool deflection was measured close to the tip of the grinding wheel. The rough nature of the grinding wheel surface combined with the tool rotational speed, meant that the resulting measurement would be very noisy, this was acceptable as the measurement noise was low in comparison to the tool deflection being measured. This can be seen in Figure 5-9. Measurement was started as the grinding wheel commenced its path towards the workpiece surface. As the tool makes contact it can be seen that it rapidly deflects and then peaks at approximately 35μm towards the laser displacement sensor as the tool becomes fully engaged. As the tool is passed over the surface of the part the measurement steadily reduces, this is due to the measurement being taken at the grinding wheel surface while the grinding wheel is wearing, effectively reducing its diameter. As the tool disengages from the surface of the part it relaxes back. It is noteworthy that the final position is approximately 2μm back from its original point. Combined with the observation about the grinding wheel wear, this suggests that the tool has been axially displaced in the collet.

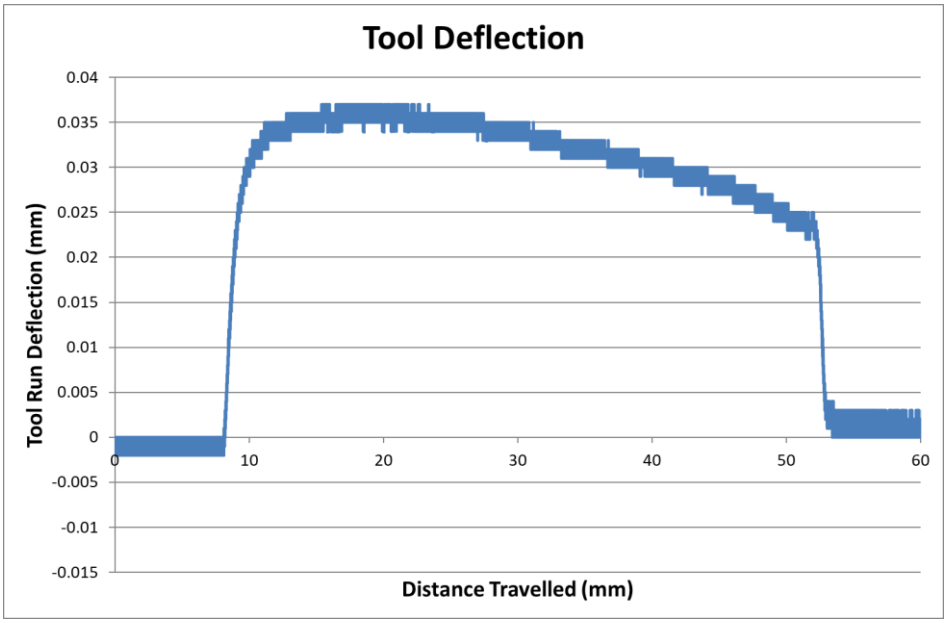

Figure 5-9: Tool deflection measured at grinding wheel tip

5.1.3 Results – Micro riblets

Both grinding passes successfully generated micro riblets along the whole length of the ground surface of the workpiece. The two separate grinding passes are shown in Figure 5-10 and Figure 5-11 (note in Figure 5-10 one riblet is not shown as it was outside the measurement area). The height of the riblet features is only 10µm at its maximum. This is primarily a result of the dresser nib wear. As the same dressing nib was used for preliminary dressing and truing significant wear occurred throughout the process.

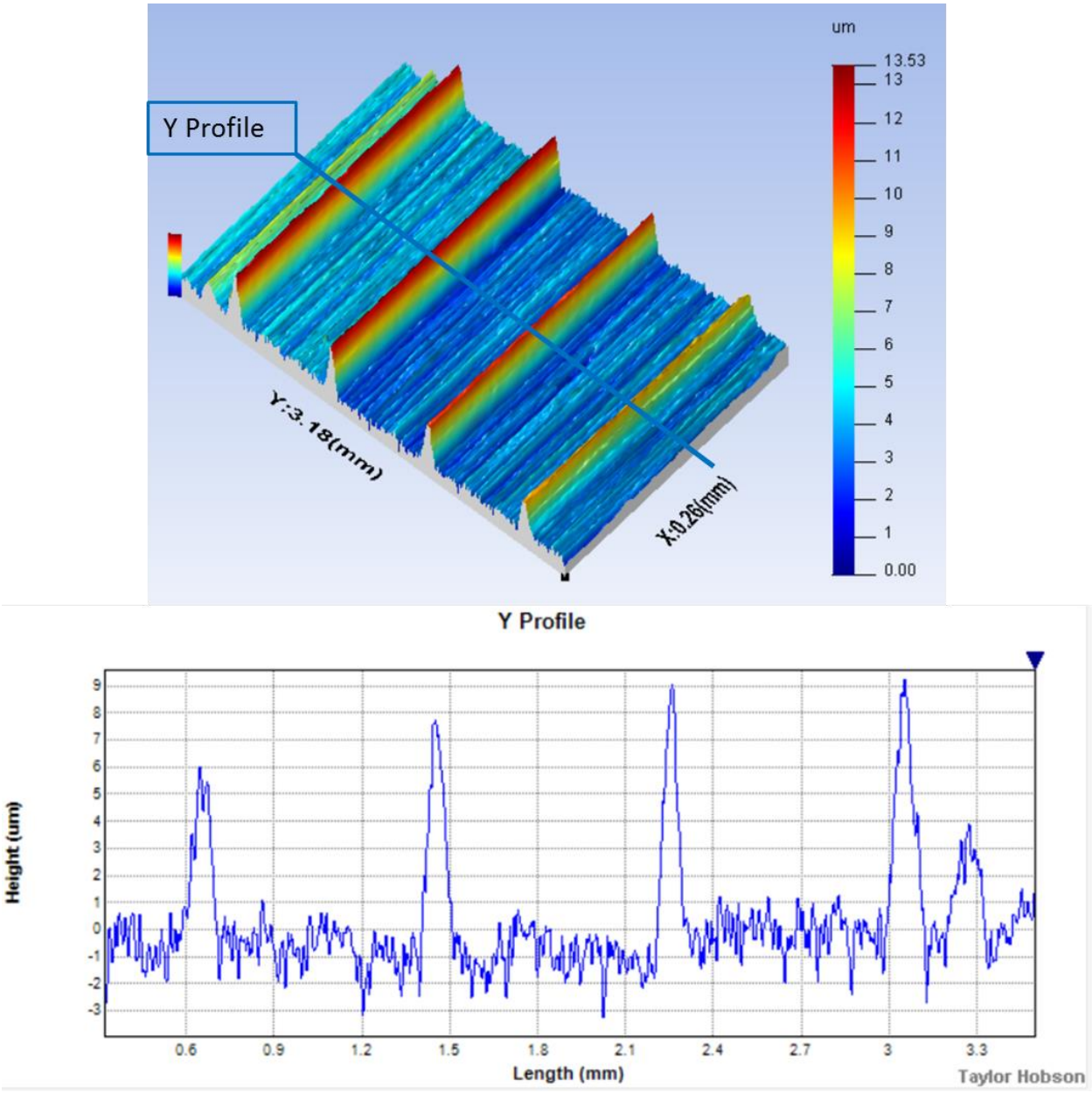

Figure 5-10: First grinding pass

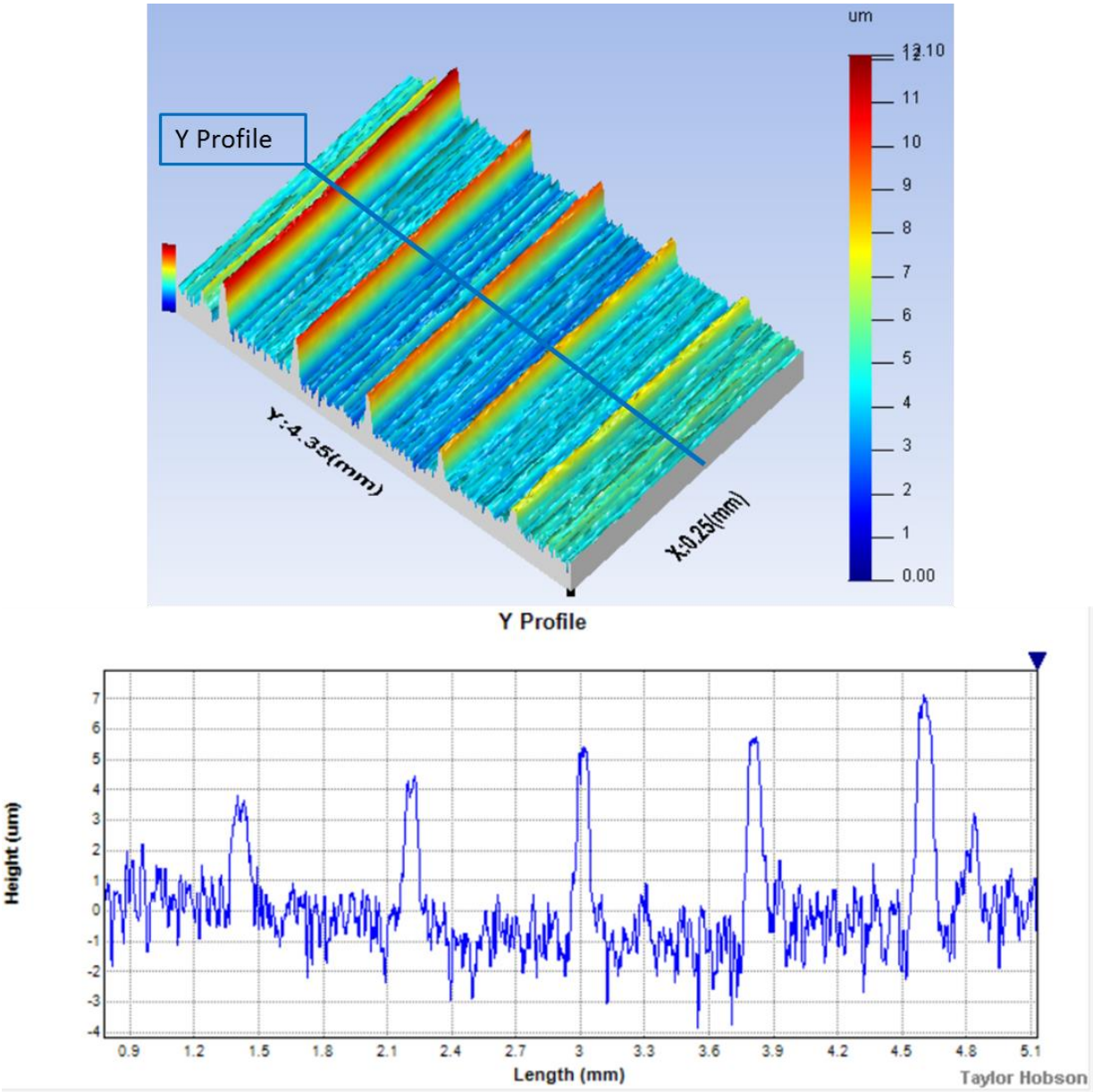

Figure 5-11: Second grinding Pass

Figure 5-12 shows the dressing nib after the profile dressing operation. It can be seen that the tip has been worn completely flat. This wear was not accounted for in the dressing operation causing the grooves to be dressed to a much shallower depth than intended, with a reduction in depth for each consecutive groove. As the profile was dressed to the intended grinding depth, i.e. the whole surface would be active, this resulted in a reduction in the height of the riblets on the resultant surface.

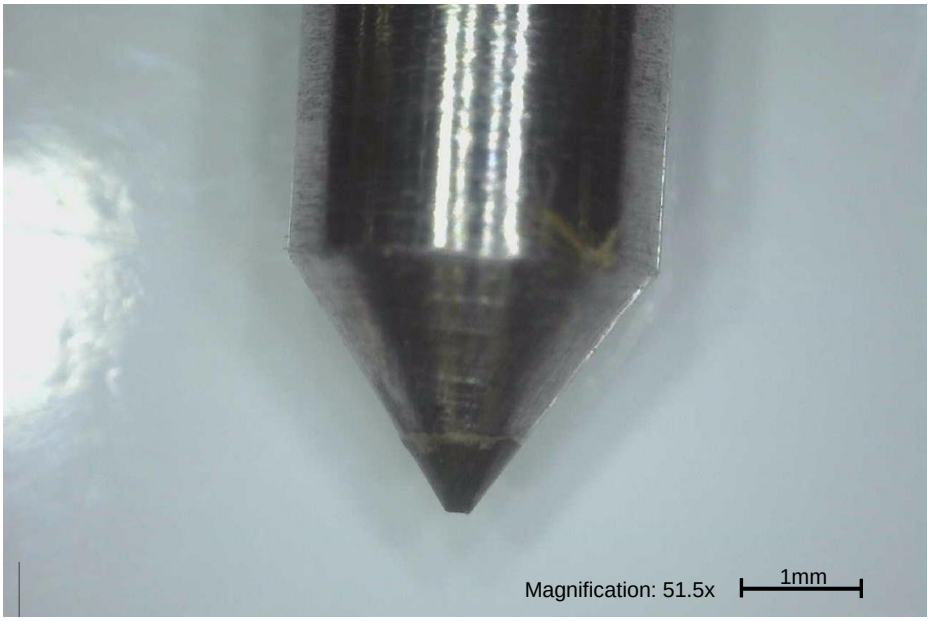

Figure 5-12: Heavily worn dresser nib

Further reduction in the height of the riblets occurred between passes. This effect can be seen by isolating one of the riblets and comparing the profile after the first and second passes. This is shown in Figure 5-13. It can be seen that the height of the riblet has decreased and there has been a marked change in the profile of the riblet. A comparison of the profiles is given in Figure 5-14. Approximately 5µm of height has been lost and the profile is much less well defined with a flatter top and steeper sides. This is a result of grinding wheel wear reducing the depth of the groove and changing the geometry of the groove at the edges and base. This comparison was made at approximately the same point along the cutting path for each ridge. It should be noted that the grinding wheel was constantly wearing throughout the process and at any given point the difference in height would be a function of the degree of wear that had occurred. The rate of grinding wheel wear would also change as the surface profile alters. Hence the difference in height between two matching ridges is a complex interaction of several variables.

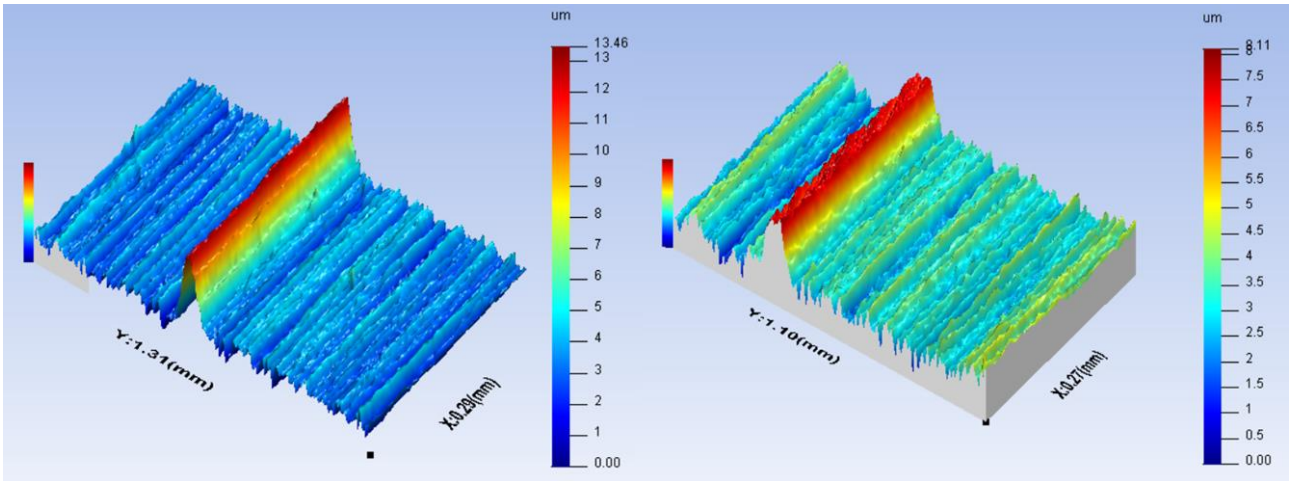

Figure 5-13: Single rib from first pass (left) and second pass (right)

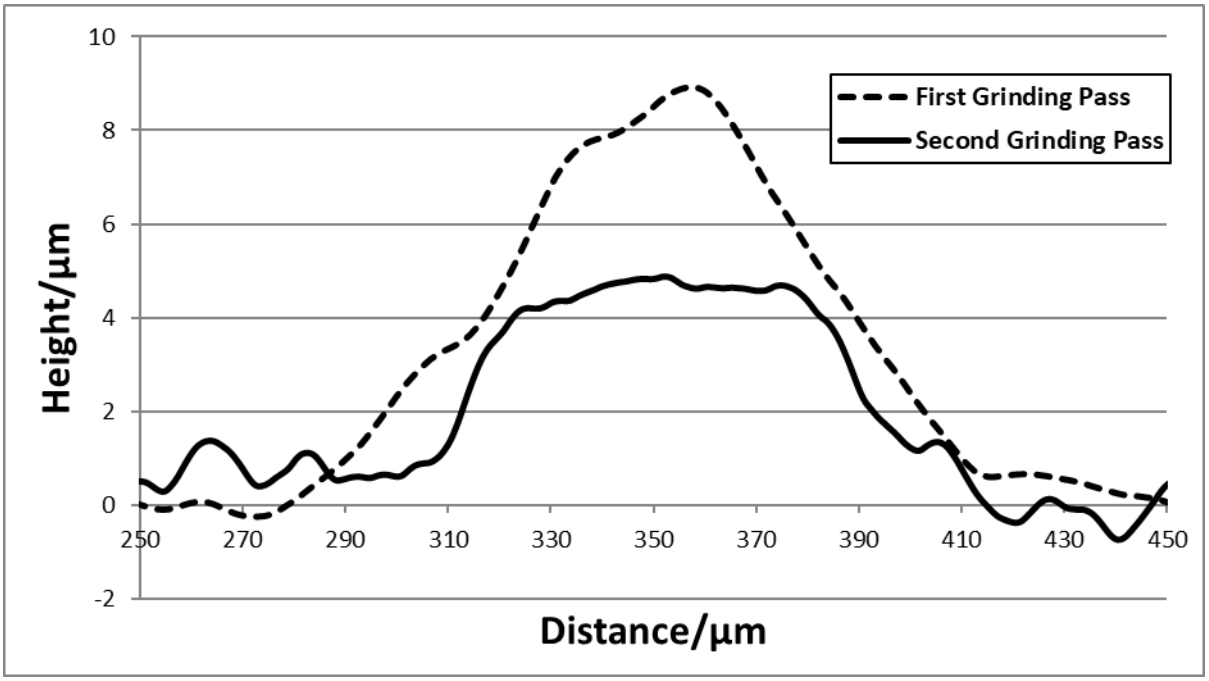

Figure 5-14: Comparison of a single riblet from the first and second grinding passes

This experiment identified two major challenges to the process of selectively grinding surface geometries. Firstly, the rate of dresser nib wear must be accounted for to ensure the desired profile is dressed onto the surface of the grinding wheel. This can be facilitated firstly by introducing an angle between the dressing nib and the grinding wheel and rotating the dressing nib slowly throughout the procedure. These steps will reduce the tendency of the grinding wheel to wear flat and will instead cause the nib to be constantly shaped. In the dressing of conventional grinding wheel an angle of approximately 15 degrees is recommended for this purpose. While this introduces new challenges in tool setting it should

reduce the rate of wear and prevents the tip from wearing completely flat; however, it cannot not eliminate wear completely. Secondly profiles will be dressed to a depth greater than the intended grinding depth. This will mitigate the reduction in grinding depth caused by wear and prevent the profile at the bottom of the groove impacting upon the profile of the resultant features.

5.2 Double Pass Radial Grooves – Micro Patches

Developing on the experiments carried out with micro riblets, the next progression was to use a similar technique with two perpendicular passes intersecting to create micro patches. The purpose of this trial was to investigate a revised dressing process and to carry out the procedure on a material better suited to grinding as a machining process.

Following on from the previous work, the need for a much lower dressing speed was identified. To facilitate this, the modular Nakanishi spindle system described in chapter 4 was purchased and installed adjacent to the Nanoform 250. The spindle was installed in the tool holding clamp and run-out checked using the method previously described. A static run-out of 2µm to 3µm measured at the tool shank was observed, matching the performance of the previous spindle.

Corning Macor® machinable glass ceramic was selected as a workpiece material as it is more representative of the types of brittle materials which would typically be machined by grinding. Macor® exhibits excellent machinability characteristics, has high thermal stability and is capable of holding tight machining tolerances of greater than 0.5µm. Furthermore, optimum machinability is achieved when using superabrasives such as diamond or CBN. When polishing with superabrasive compounds surface finishes of up to Ra 0.013µm are achievable. These properties make it an ideal material for experimentation (Corning, 2012). Further details of the mechanical properties of Macor® can be found in Table 5-2. A 25mm x 25mm workpiece with a thickness of 5mm was mounted to the machine using the vacuum chuck and a specially designed workpiece holder. This setup facilitates accurate and secure positioning whilst also allowing for easy attachment and removal of the part.

Feature/Parameter	Value
Density	2.52 g/cm^3
Porosity	0%
Young's Modulous	66.9 GPa
Poisson's Ratio	0.29
Shear Modulus	25.5 GPa
Knoop Hardness	250 kg/mm^2
Modulus of Rupture	94 MPa
Compressive Strength	345 MPa

Table 5-2: Macor® Ceramic mechanical properties (Corning, 2012)

A summary of the process parameters is given in Table 5-3. A Diagrind 1200 grit diamond resin bonded wheel with a nominal outer diameter of 8mm and a length of 10mm was used in this experiment.

Feature/Parameter	Symbol	Value
Dressing Depth	h	50µm
Groove Pitch	F_d	400µm
Nib Radius	r_d	46µm
Nib Angle	ϑ	65.8 Degrees
Dressing Speed	S_d	62.5 RPM
Nib Rotation	S_n	8 RPM
Dressing Angle	dθ	18.78 Degrees
Grinding Speed	S_g	2000 RPM
Feedrate	V_w	20 mm/min
Grinding Depth	d	10 µm (1st Pass) 20 µm (2nd Pass)
Grinding Surface Speed	V_s	0.78 m/s
Grinding Wheel Grit		1200
Grinding Wheel Bond Type		Resin

Table 5-3: Micro patches process parameters

5.2.1 Truing and Dressing Process – Micro patches

The full parameters for this experiment are given in Table 5-2. Significantly, to address the excessive wear of the dressing nib the offset dressing process was carried out with the nib at a relative angle of approximately 18.8 degrees while the dressing nib was rotated at 8 RPM throughout the dressing process.

A part worn nib was used for preliminary dressing and truing, this was then replaced with a fresh nib for final dressing of the profile geometry. The parameters of the final dressing nib

can be seen in Figure 5-15. Tool setting was accomplished using the USB microscope as can be seen in Figure 5-16 and the dressing nib was centred using the integrated gauge head with the tip on the shank of the dressing tool.

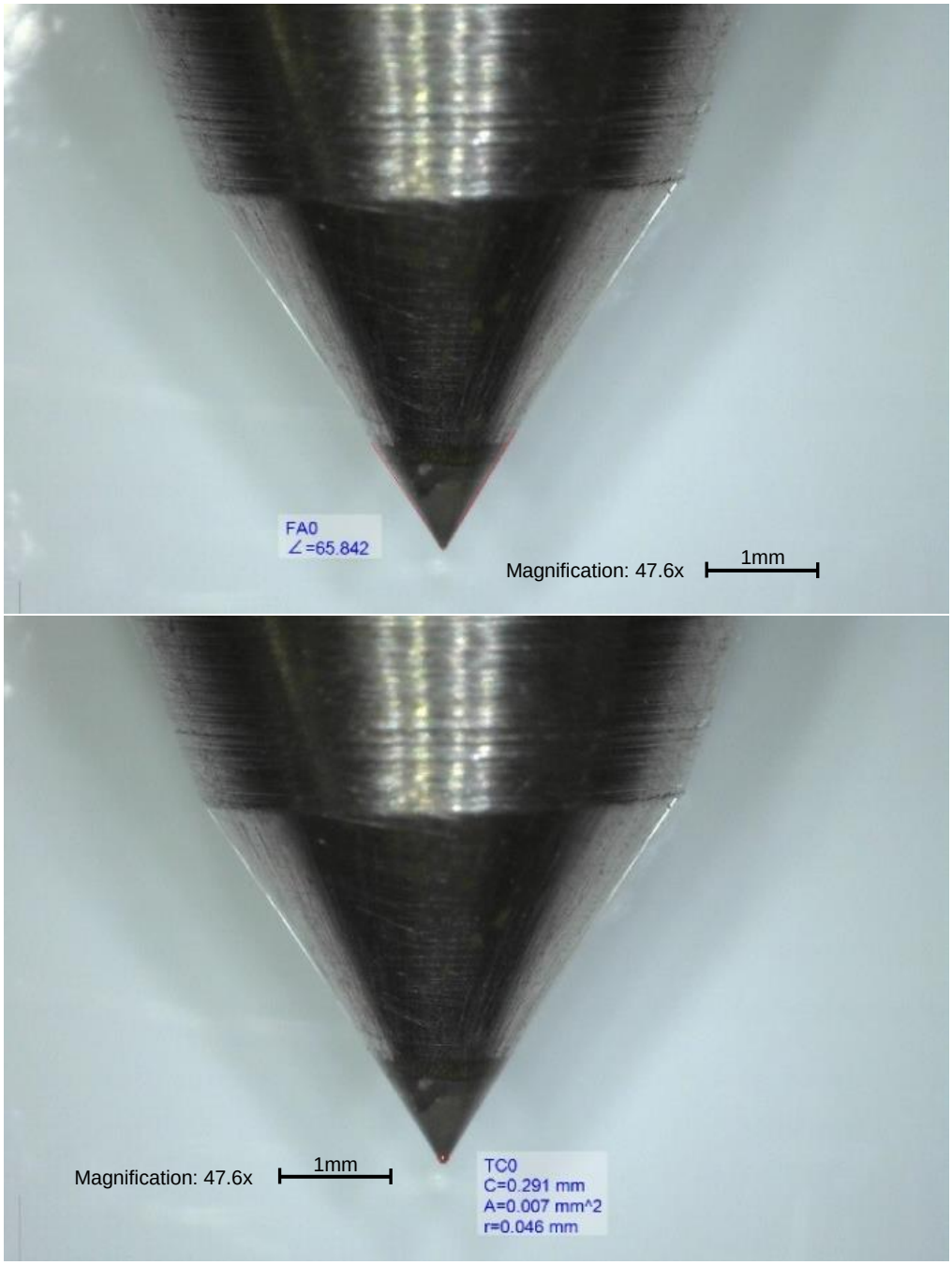

Figure 5-15: Dressing nib angle and tip radius

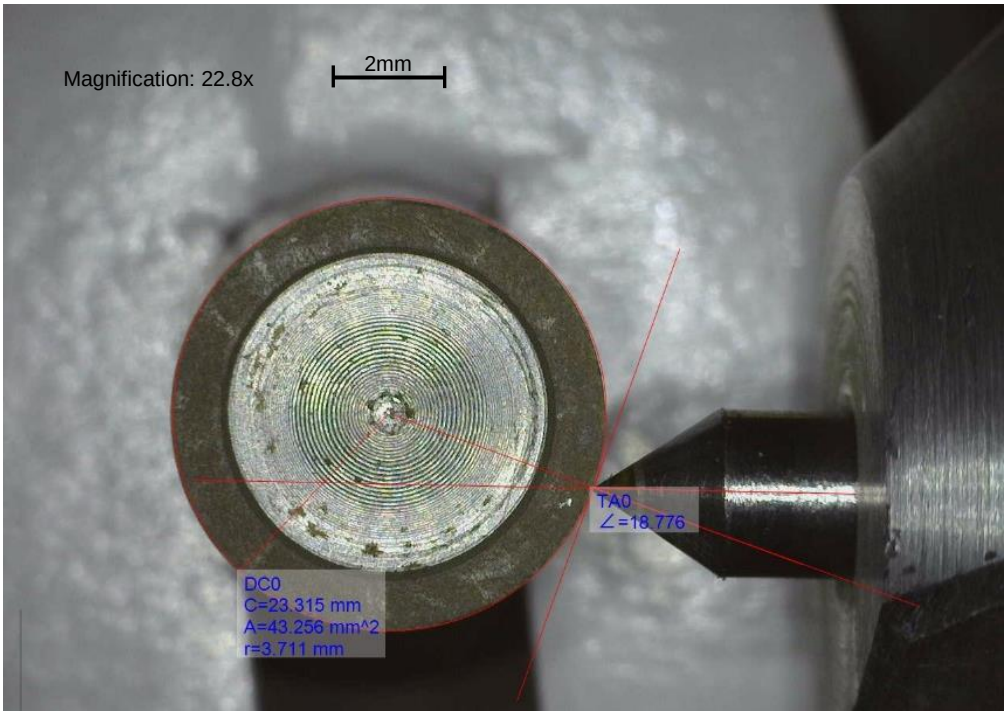

Figure 5-16: Offset Dressing Angle

In an attempt to compensate for the effects of wheel wear when grinding, the profile dressing depth was set at 50µm, significantly greater than the design depth for grinding. From Equations 5 to 9 (chapter 3) the calculated groove width at the surface of the grinding wheel was 115µm. It was observed using the USB microscope that there was some differentiation in the dressing depth of each groove, this can be seen in Figure 5-17 where the bottom most groove is significantly deeper. The effect is more evident in Figure 5-18 however, due to the challenges of focussing accurately on the curved surface of the grinding wheel the measurement shown cannot be considered accurate as the magnification required to generate a sharp focus could not be determined. After dressing the grinding spindle was re-orientated for the grinding process.

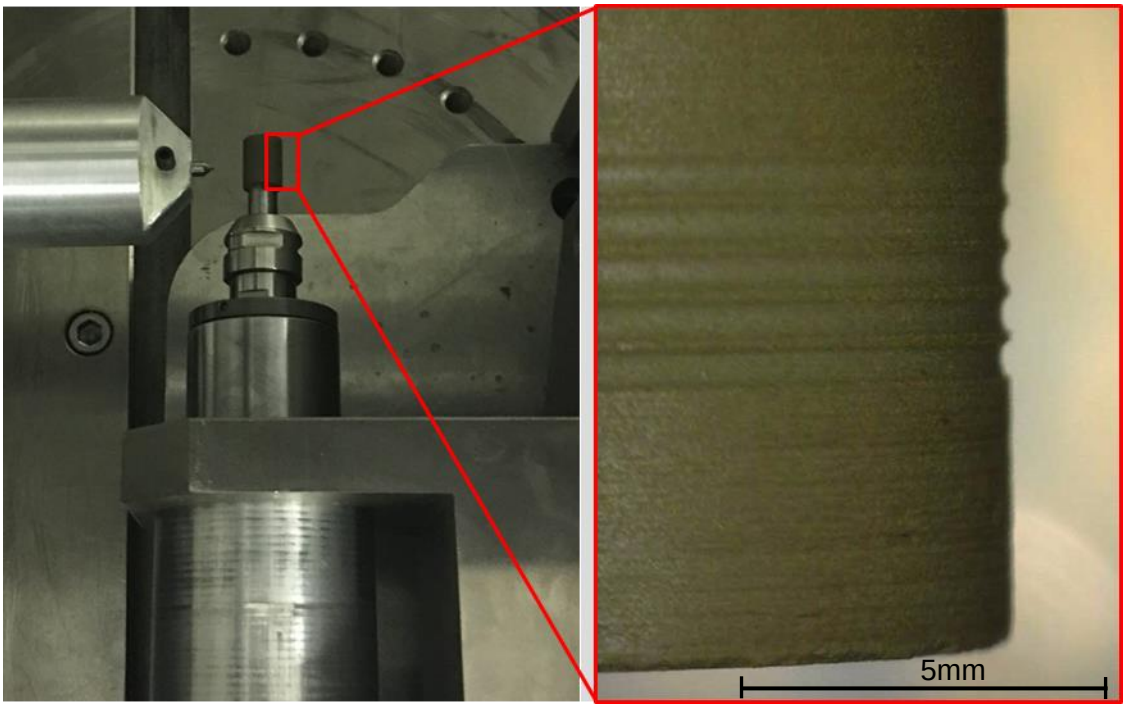

Figure 5-17: Grinding wheel post dressing with visible grooves highlighted

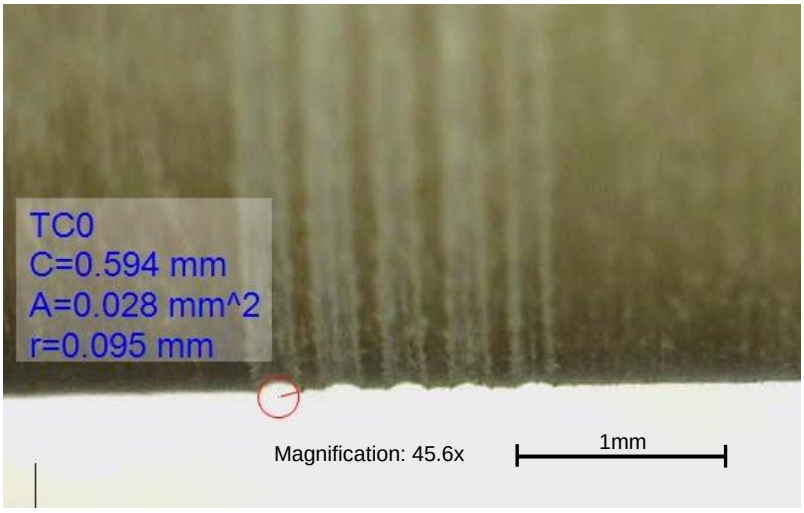

Figure 5-18: Differentiation in dressing depth

5.2.2 Grinding Process – Micro patches

The grinding wheel was aligned with the surface of the workpiece using plastic gauge sheet as described in chapter 4. To assist in alignment the grinding station was positioned perpendicular to the X axis, this ensures that any correction to the angle of the tool is in a plane parallel to the surface of the workpiece. This allows for a significantly simpler and more accurate alignment process but does not leave sufficient space behind the grinding wheel to mount the laser displacement sensor precluding the opportunity for in process

measurement of tool run-out, displacement and chatter. Given that the spindle head has the same performance envelope as the Nakanishi EMR-3008-K used previously, confirmed in earlier measurements, this was considered acceptable.

To accurately set the grinding depth, the grinding wheel was slowly brought forward until it made contact with the workpiece. To aid in identifying the contact point the workpieces was coated in engineer's blue. This created a blue tint to the surface which was removed when the grinding wheel made contact, revealing the white ceramic material beneath. Once the contact point had been established an initial pass at 10µm depth was made to ensure contact was consistent across the whole workpiece surface. Clairsol 330™ coolant mist was used throughout the process to improve the finish of the Macor® ceramic.

After the initial pass to check tool alignment, the depth was increased by a further 10µm to take the total depth to the required 20µm. An additional benefit of bluing the material before grinding was that it was possible to observe the area being ground. This confirmed that a portion of the workpiece corresponding to the grooves on the grinding wheel had not been contacted. Once the grinding had been completed along one side of the workpiece, the grinding wheel was returned to its home position. The workpiece could then be rotated by 90 degrees and the procedure repeated. The second pass is carried out without increasing the grinding depth i.e. a 20µm cut was once again taken along the whole length of the workpiece resulting in the creation of the micro patch pattern where the two grinding passes intersect. Figure 5-19 shows the grinding wheel in position for the second pass; the results of the first pass can clearly be seen as pale blue stripe running laterally from left to right. The workpiece was rotated multiple time to create intersecting ground patches on different corners.

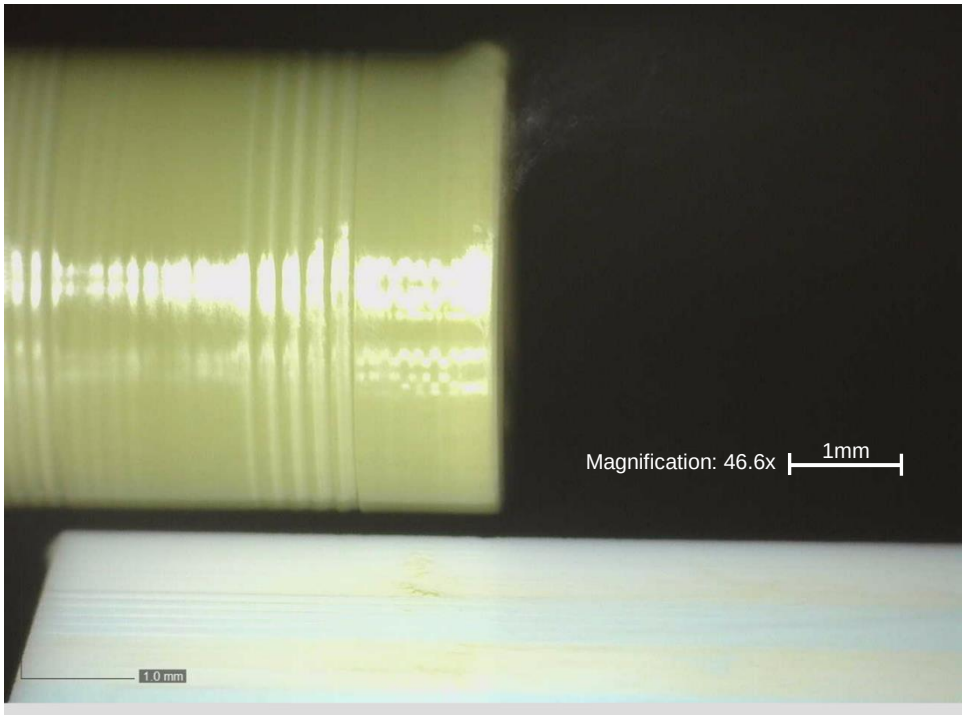

Figure 5-19: Grinding wheel in position for second pass

5.2.3 Results – Micro patches

Following grinding the intersecting zones were individually measured using a Taylor Hobson Talysurf contact profilometer; the results are shown in Figure 5-20 to Figure 5-22. There is a great deal of variation in the geometry both of the individual patches within a zone and between the zones themselves. The average height of features within a zone is relatively consistent, ranging from 16.6µm to 18.4µm. However, there was a great deal of variation between individual patches. For example, in Zone 1 a minimum height of 7µm and a maximum height of 27µm are observed. This variation is attributed primarily to misalignment between the grinding wheel and the surface of the part causing grinding to be carried out at an angle. This may have been exacerbated by any taper present in the workpiece which would cause the tool angle to alter as the workpiece was rotated for successive grinding passes.

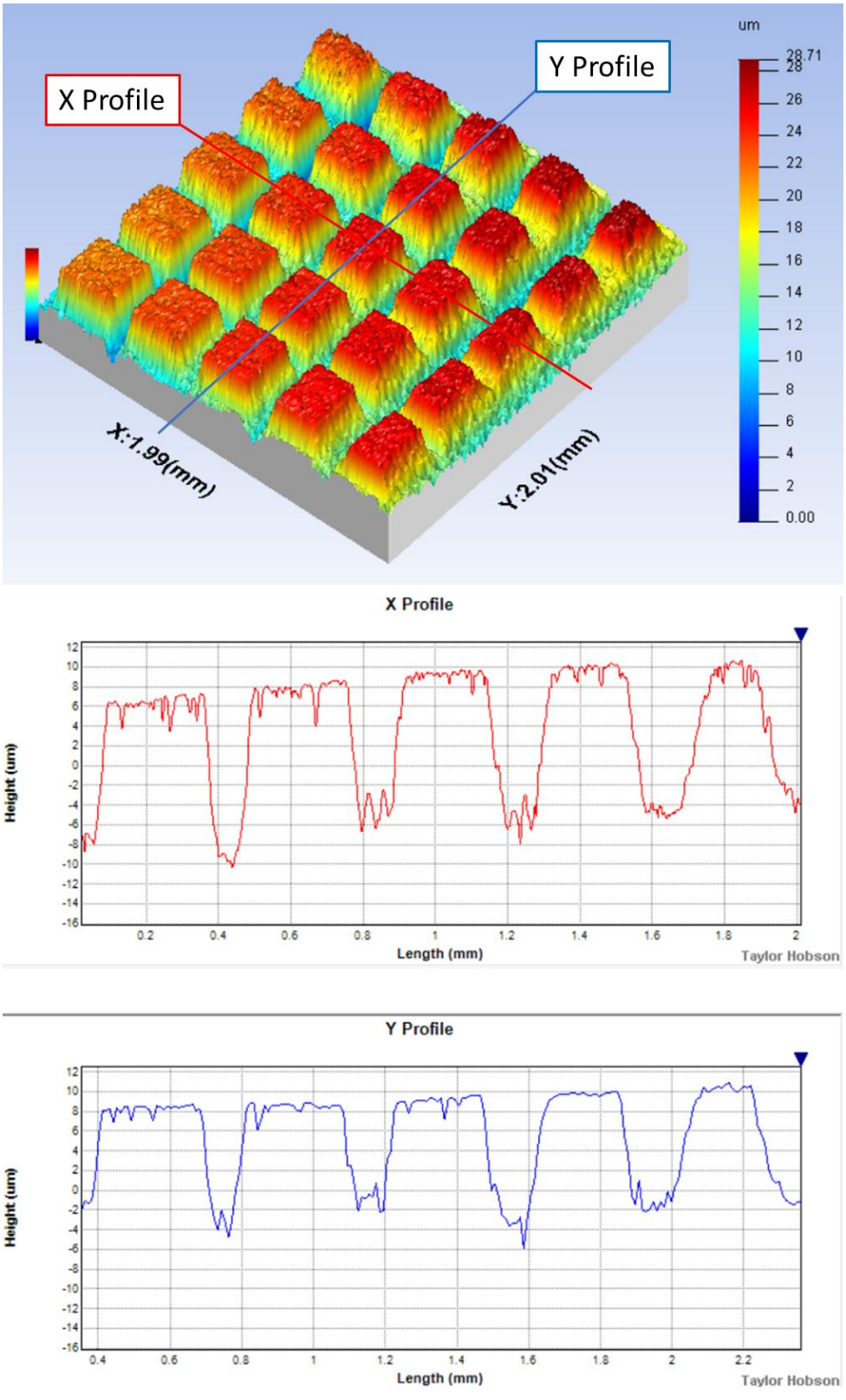

Figure 5-20: Zone 1 profile (average height 16.6µm)

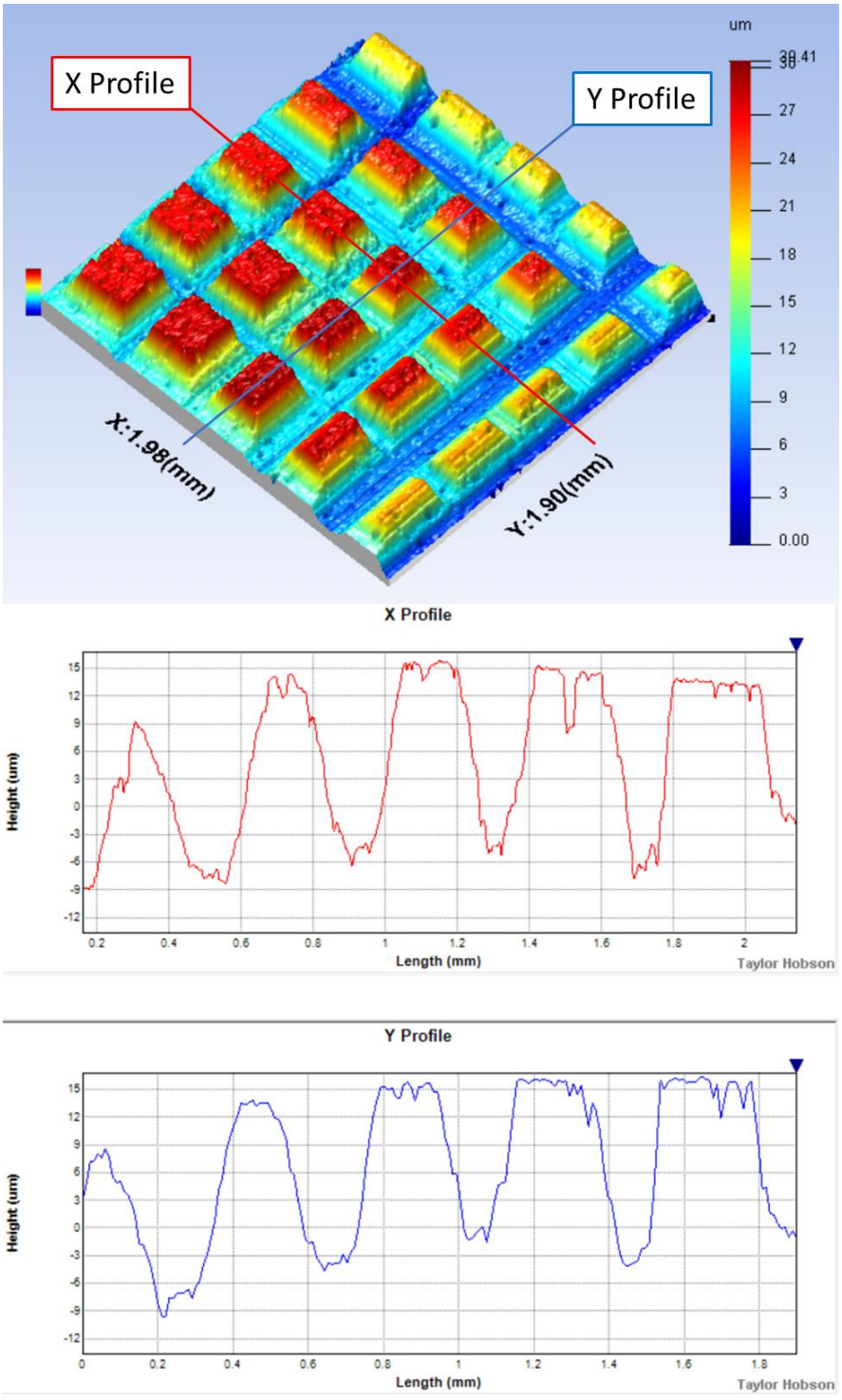

Figure 5-21: Zone 2 profile (average height 18.4µm)

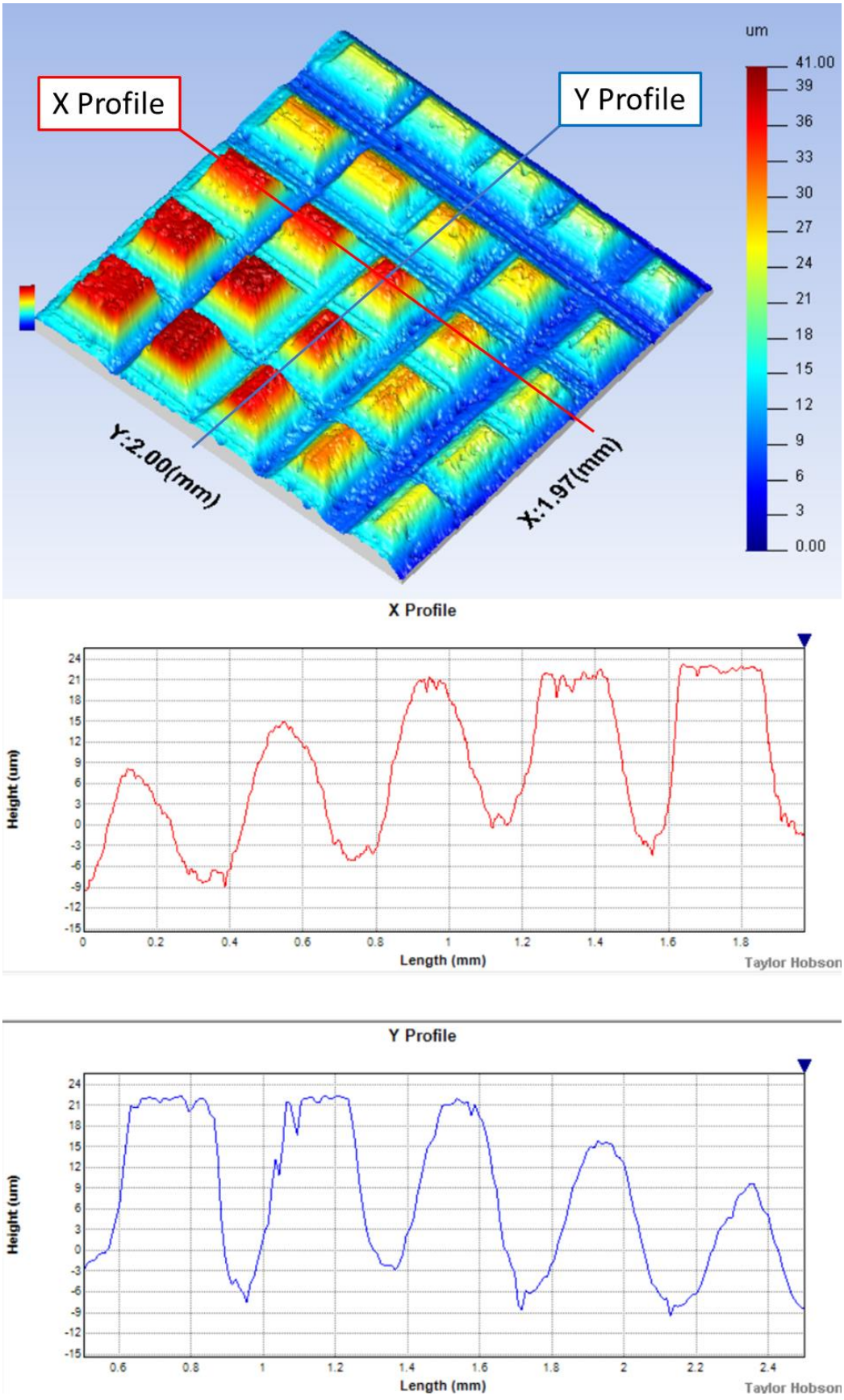

Figure 5-22: Zone 3 profile (average height 18.2µm)

There are two sources of variation in the geometry of the individual patches. Firstly, the dressing depth for each groove decreased with wear of the dressing nib and secondly wear of the tool wheel decreasing the effective radius of the grinding wheel. In combination these two factors explain the gradually decreasing height and changing profile of the patches. The design width of the side of the patches calculated using Equation 9 (chapter 3) is 114µm however the achieved side lengths for each zone are as follows:

- Zone 1 – max 334µm, min 201µm
- Zone 2 – Max 292µm, min 181µm
- Zone 3 – Max 291µm, Min 148 µm

The initial difference between the maximum and minimum values can be attributed to the dresser tip wear causing variation in the dressing depth and consequently a change in the profile of the groove. This can be seen in the way that when a groove intersects with itself the resultant feature has consistent side lengths but when a groove intersects with a different groove the lengths of perpendicular sides are varied. There is also clear trend towards a reduction in both maximum and minimum side lengths between successive grinding passes. This is caused by the erosion of the grinding wheel surface. The profile of the groove at the surface of the grinding is essentially similar to the base of a trapezium. As the material wears away the height of the trapezoid decreases causing the base length to similarly decrease. This effect also explains the gradually increasing amount of ground surface between patches with successive grinding passes as a greater area of grinding wheel surface becomes active.

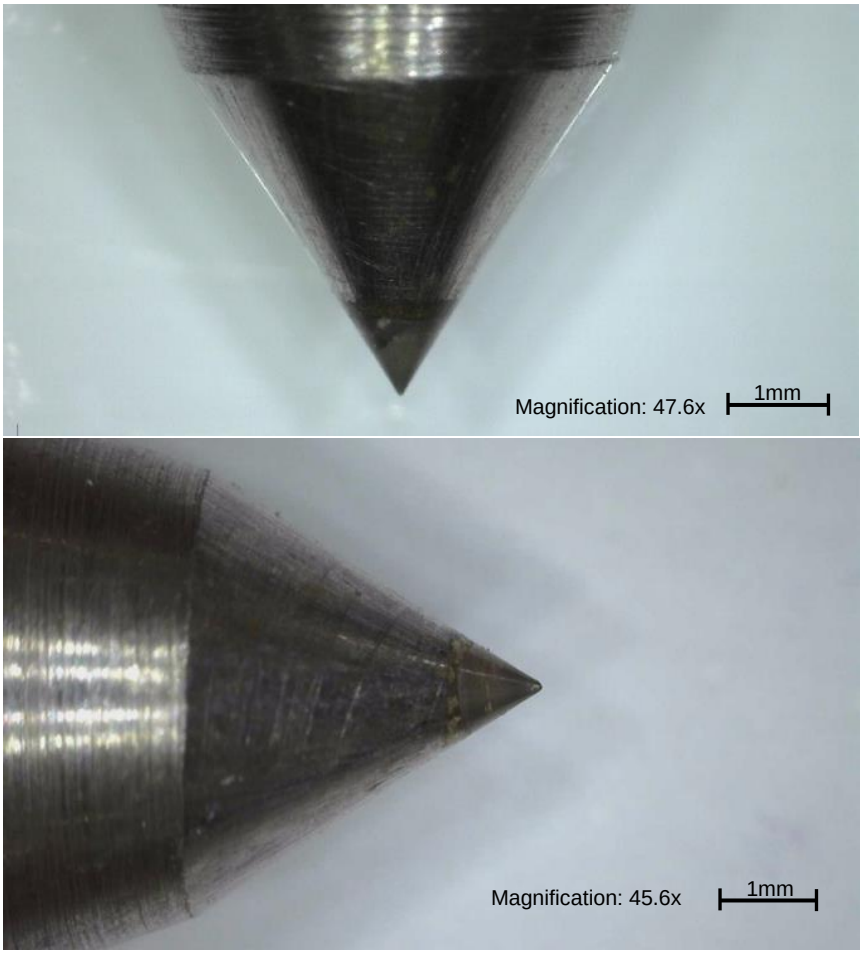

Figure 5-23: Dressing nib before (top) and after (bottom) profile dressing

The nib used in the dressing of the profiles was examined before and after the dressing process. As can be seen in Figure 5-23 the dressing nib experienced significantly less wear as a result of the offset rotating dressing process. The tip radius increased from 46µm to 102µm but did not wear flat and maintained a radiused profile.

5.3 Laser Compensated Double Pass Radial Grooves - Micro Patches

Previous grinding trial have identified several potential sources of error in the dressing and grinding operations and also several potential remedial actions. The aim of this manufacturing trial was to draw on these findings in an effort to replicate and improve upon the results of micro patch grinding that has previously been demonstrated. This has primarily been achieved through the adoption of a cut-measure-compensate dressing programme. This process is facilitated by the design of a mounting solution for the laser displacement sensor which allows it to mount to the X axis of the Nanoform 250 without the need to

remove the dressing nib. Additionally, a new dressing strategy was used incorporating a groove widening step to produce deeper and more consistent groove geometry which in turn allows for the grinding of feature with higher aspect ratios.

5.3.1 Dresser Nib Wear

To compensate for errors in dressing caused by wear of the dressing nib, an investigation into the rate and mechanism of nib wear was undertaken to develop a compensation strategy. To conduct the investigation a preliminary dressing and truing operation was carried out on a fresh 1200 grit resin bonded diamond grinding wheel. The results of this preliminary operation were measured using the laser displacement sensor mounted to the X axis of the Nanoform 250. The laser displacement sensor was positioned using an arm and height adjustable mounting bracket designed to allow the sensor to be positioned adjacent to the dressing nib without requiring its removal. The results of the preliminary dressing and truing can be seen in Figure 5-24. There is significant deviation from the nominal centreline, indicated by the dashed blue line, with the maximum and minimum points being ±11µm. This was as expected due to the stochastic distribution of the abrasive grains which will typically range in size from 3µm to 9µm. The measurement also confirmed that the grinding wheel was dressed true and parallel to the axis of motion.

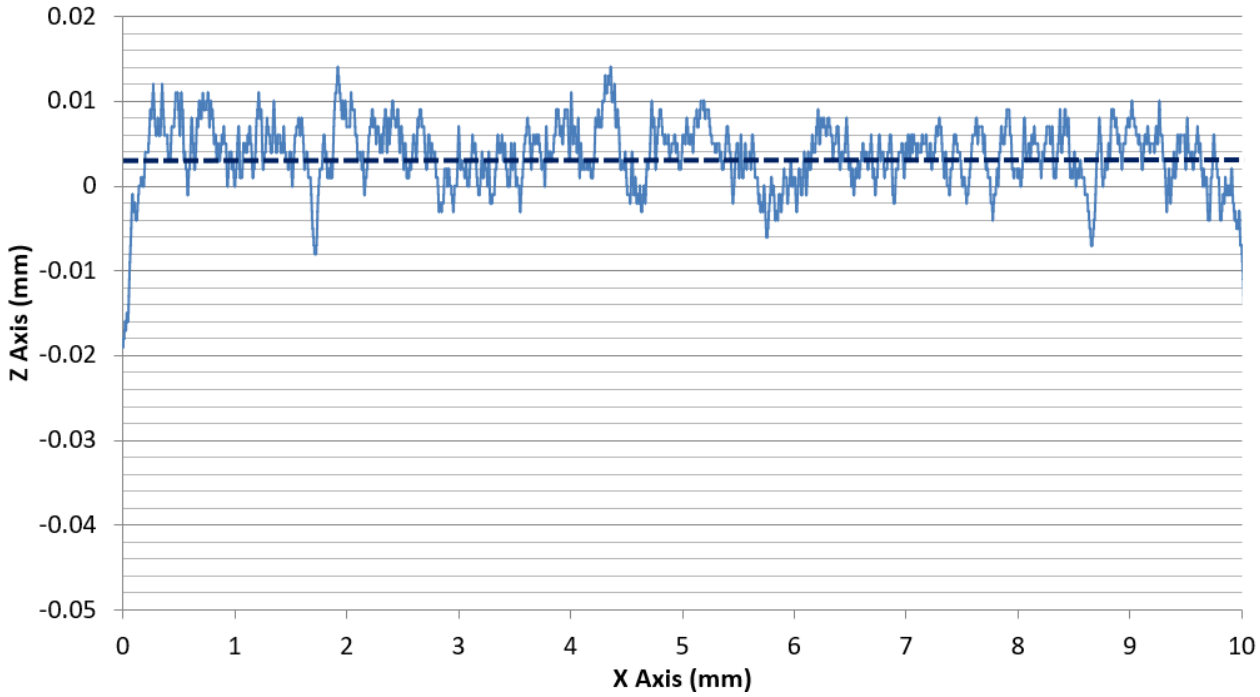

Figure 5-24: Preliminary dressing and truing

Following the preliminary dressing operation, the worn nib was replaced with a fresh nib which was re-centred and zeroed against the grinding wheel. To ensure accuracy the finger of the integrated gauge head was placed as close to the tip as possible and the procedure monitored by the USB microscope. The nib was centred to a run-out of within 1µm. A series of 16 concentric radial grooves spaced in 0.5mm intervals were then dressed along the length of the grinding wheel to a nominal depth of 50µm. The offset dressing process was used with a relative angle of 13.4 degrees between the grinding wheel and nib. The dressing nib was rotated at 5 RPM and coolant was used throughout the process. The dressed grinding wheel is shown in Figure 5-25.

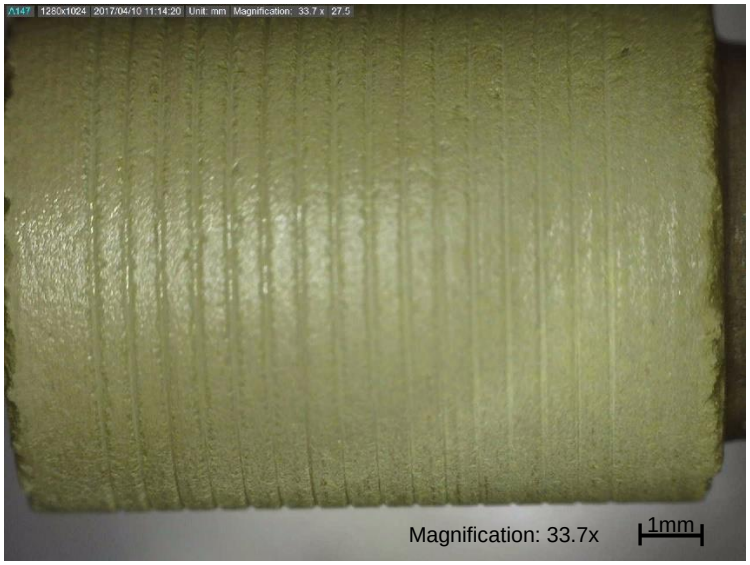

Figure 5-25: Grinding wheel dressed with 16 radial grooves

The grooves were dressed using a CNC programme with an infeed rate of 6mm/min and held for a dwell period of 1.5s on reaching the bottom of the groove. For a 50µm groove this results in a dressing time of 2s per groove. With the grinding wheel rotating at its lowest speed for dressing, 62.5 RPM, the wheel completed 2.08 revolutions before the dressing nib was withdrawn, guaranteeing that the groove is fully dressed. To calculate the distance covered by the dressing nib it was necessary to have a more accurate value than the nominal design specification for the diameter of the grinding wheel. The radius of the wheel was measured, using the USB Microscope, at 3.907mm, hence, for each groove the dressing nib travelled 51.15mm over the surface of the wheel and over all 16 grooves the dressing nib travelled 818.37mm.

Following the profile dressing pass the grinding wheel was once again measured using the laser displacement sensor; the results of this measurement are shown in Figure 5-26. The dashed blue line represents the nominal height of the surface of the wheel and the dashed red line indicates the progressively decreasing dressing depth from right to left. The Y axis of the graph is scaled to highlight the differential heights of the grooves. The first point of note is that the base of the deepest groove is 57µm below the nominal surface, 7µm deeper than the desired dressing depth. This is likely caused by the stochastic distribution of abrasive particles, as previously discussed, affecting the setting of the zero depth by contact the fresh

nib to the surface of the wheel. It is unlikely that contact will be made exactly at the nominal zero. Therefore, if contact is made at a relatively high or low point on the wheel, for example on top of an exposed grain or at a point where a whole grain has been dressed away, the dressing depth will be offset from the nominal zero by an equivalent amount. This represents a fundamental limit to the accuracy of tool setting that can be achieved using this contact method.

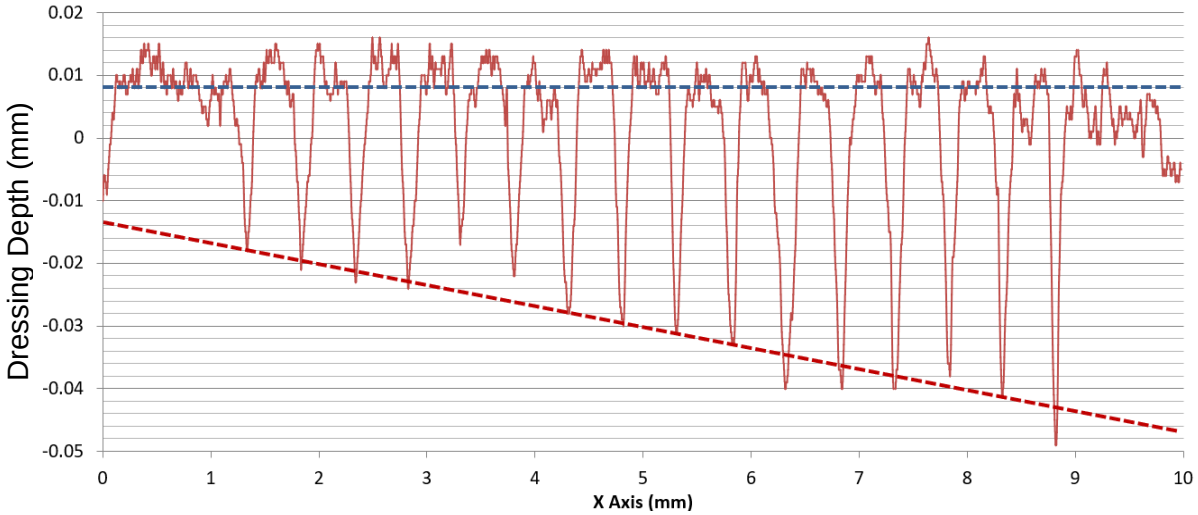

Figure 5-26: Dressed profile showing progressive wear

The dressing depth of the grooves progressively decreased from 57µm to 26µm for a total reduction of 31µm. This suggests a reduction of 1µm in depth for every 26.4mm of distance travelled across the surface of the grinding wheel. It can be seen that the reduction in height is not a constant slow erosion of the dressing nib; rather, the reduction in depth occurs in stages. This effect is illustrated in Figure 5-23. The green lines indicate the number of grooves dressed before a major change in the dressing depth. There is some degree of variability, likely caused by the distribution of abrasive particles. There are two observations pertinent to compensating for dresser nib wear. The first is that there is a relatively large change between sets of grooves at different depths. The reduction has occurred in steps of approximately 10µm. This is likely due to brittle failure of the diamond tip with chips flaking off as the tool is weakened throughout the dressing process. The second observation is that

the amount of dressing carried out before a step change in the dressing depth, is not consistent.

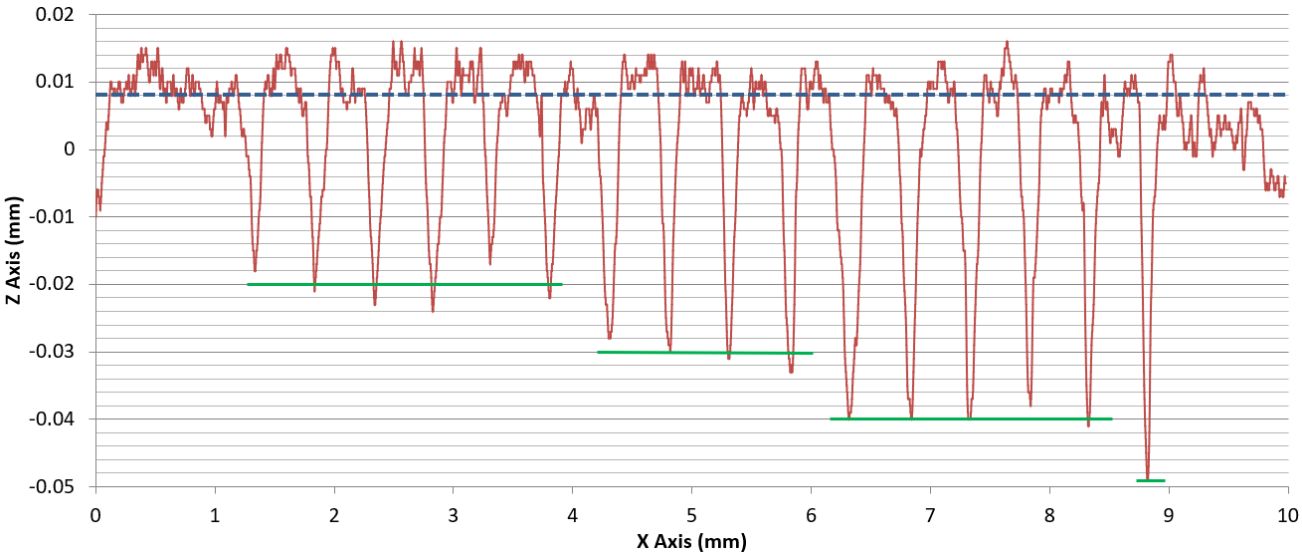

Figure 5-27: Stages of dressing depth reduction

The findings of this investigation have several implications for compensation for dresser nib wear. Firstly, it is not possible to compensate for wear in a single profiling cut by progressively increasing the dressing depth based on surface distance travelled. As the dresser nib wear occurs in stages, this would result in grooves dressed either too deep or too shallow as the compensation rate attempts to average out the nib wear. Secondly, as the point at which the nib wear occurs through brittle fracture is not consistent or predictable, it is necessary to measure the grinding wheel after the dressing operation to identify the areas which require corrective dressing. Finally, brittle fracture results in a change in the geometry of the dressing nib. There appears to be a trend for the rate of wear, i.e. the rate at which chips fracture off, to decrease as the tip becomes more worn. This is logical due to the fact that as chips flake off the effective radius of the tool increases, consequently reducing the stress concentration at the tip. This suggests that the use of a slightly worn dressing nib may result in a more consistent dressing of the profile geometry and require less correction. Images of the dressing nib before and after use can be seen in Figure 5-28. The wear of the tip can clearly be seen, and the radius increased from approximately 20µm to 49µm over the course of the procedure, corresponding to the decrease in dressing depth. It is notable that

the tip retains a radius profile, albeit imperfect, which is an improvement over perpendicular dressing where the tip is worn flat.

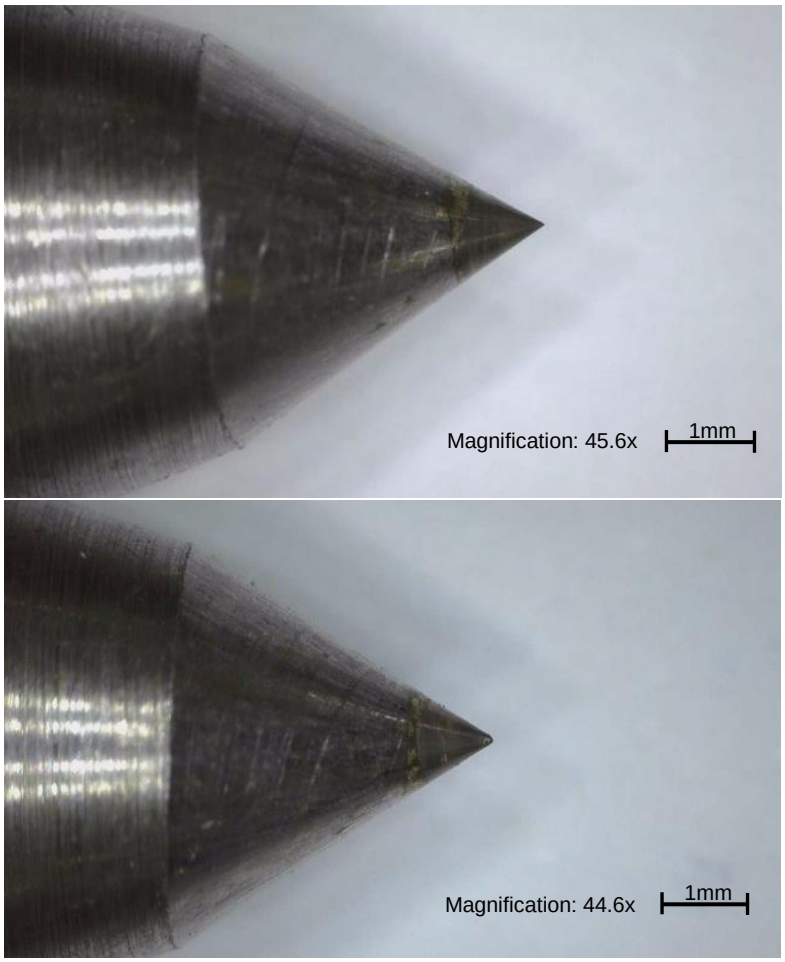

Figure 5-28: Dressing nib before (top) and after (bottom) dressing

5.3.2 Cut-Measure-Compensate Dressing and Grinding

A 1200 grit diamond resin bonded grinding wheel with a nominal diameter of 8mm and 10mm length was first dressed and trued using the procedure previously demonstrated and then measured with the laser displacement sensor. To investigate the effect of tip wear on the dressing process two profiles were dressed onto the surface of the grinding wheel. The first profile was dressed using a part worn nib while the second profile was dressed under the same conditions with a fresh, unused nib. The offset dressing procedure previously described and the parameter for the dressing and grinding operations are given in Table 5-4.

Feature/Parameter	Symbol	Value
Grinding Wheel Radius	R	3.945mm
Dressing Depth	h	70µm
Groove Pitch	F_d	400µm
Nib Radius	r_d	Part Worn Nib – 41µm New Unused Nib - 21µm
Nib Angle	ϑ	Part Worn Nib – 65.02 Degrees New Unused Nib – 64.19 Degrees
Dressing Speed	S_d	62.5 RPM
Nib Rotation	S_n	5 RPM
Dressing Angle	dθ	13.4 Degrees
Groove Enlargement	G	50µm
Grinding Speed	S_g	2000 RPM
Feedrate	V_w	20 mm/min
Grinding Depth	d	10 µm (1st Pass) 40 µm (2nd Pass)
Grinding Surface Speed	V_s	0.83 m/s
Grinding Wheel Grit		1200
Grinding Wheel Bond Type		Resin

Table 5-4: Laser Compensated Dressing process parameters

To ensure consistency, the initial dressing process for each profile was carried out using the same CNC program. An image of the plot of the tool path is shown in Figure 5-29 with the plunge, groove enlargement and retraction steps clearly visible. This CNC program was modified as required for each of the corrective dressing operations. Corrective dressing was carried out in stages so as not to overcompensate and induce further errors.

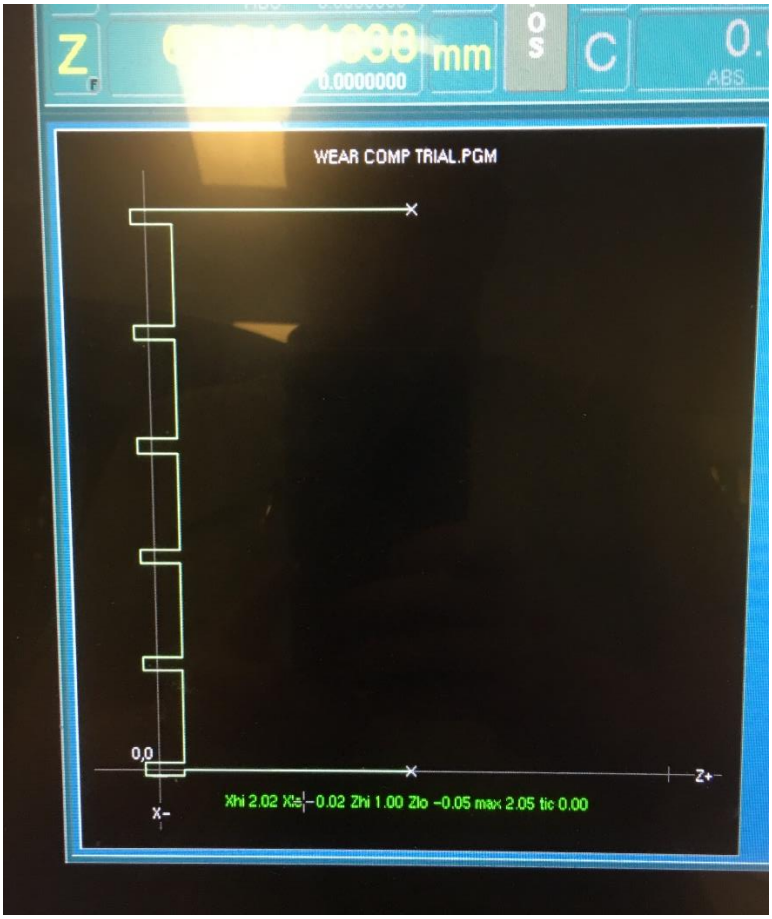

Figure 5-29: CNC program plot

After each dressing operation the profile of the groove set was measured with the laser displacement sensor. An example of the resultant profile from the initial dressing of grooves using a part worn tool is shown in Figure 5-30. The nominal surface level of the grinding wheel is shown as a red dashed line. It can be seen that there is a difference of approximately 10µm between the first and deepest groove and the final groove. Measured at the nominal centre point of the groove the depths ranged from 57µm to 70µm with the average depth being 63.5µm.

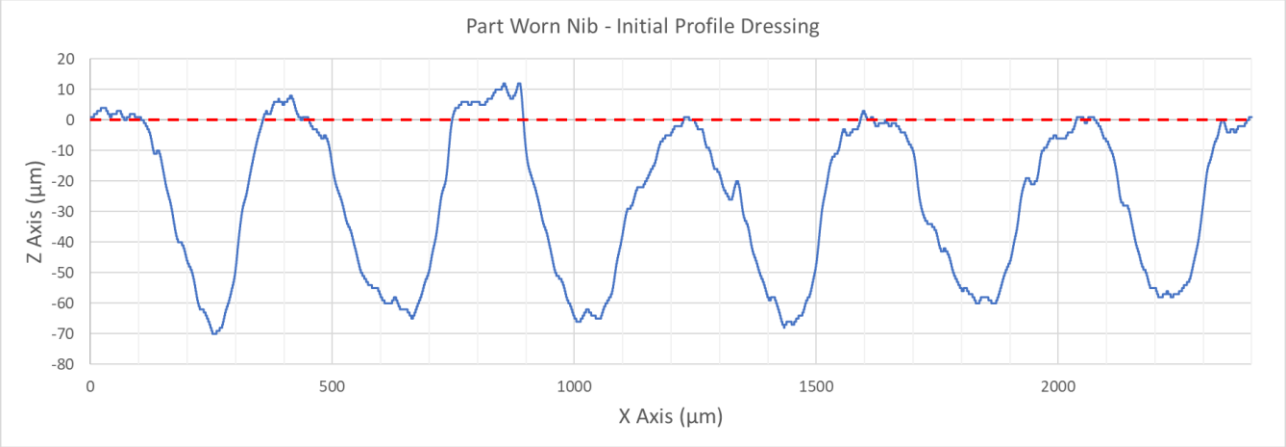

Figure 5-30: Part worn nib, initial profile dressing

A corrective dressing operation was carried out on all grooves with the depth for each groove increased as necessary. No change was made to the groove enlargement stage. However, redressing over the same tool path did yield an improvement in the consistency of the profile of the grooves. The results of the corrective dressing operation are shown in Figure 5-31. Due to the stochastic distribution of particles and the brittle failure of the bond material it is impossible to generate a completely smooth profile. However, as the bottom of the groove would be inactive during the grinding process it wasn't deemed necessary to correct for any deviation that wouldn't contact the surface of workpiece. Measured from the nominal centre of the groove, the average groove depth was increased to 69.6µm with a range of 5µm between the maximum and minimum values.

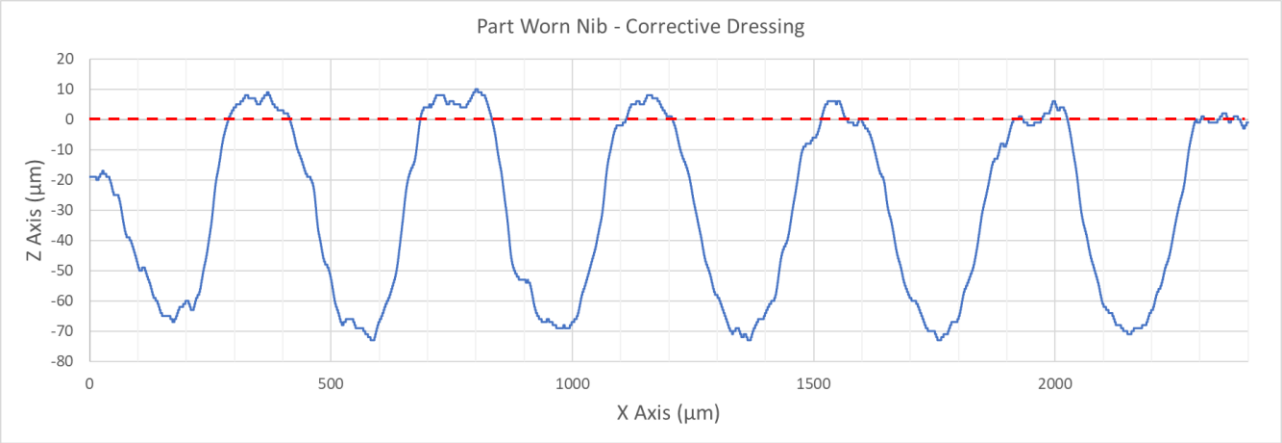

Figure 5-31: Part worn nib, corrective dressing

After successfully dressing the first set of grooves the part worn nib was replaced with a fresh, unused, nib which was re-centred, and the tool zero height was set using the

procedures previously described. The machine X axis zero was reset on a different portion of the grinding and the procedure was repeated as before. The results of the initial dressing operation can be seen in Figure 5-32. As predicted, there was greater variability with the new tip as due to the significantly smaller tip radius it was more prone to brittle fracture and wear. While the first groove dressed did approach the design parameter at 66µm deep, the remaining groove were widely varied with a range of 32µm between the deepest and shallowest grooves and an average groove depth of 49.5µm.

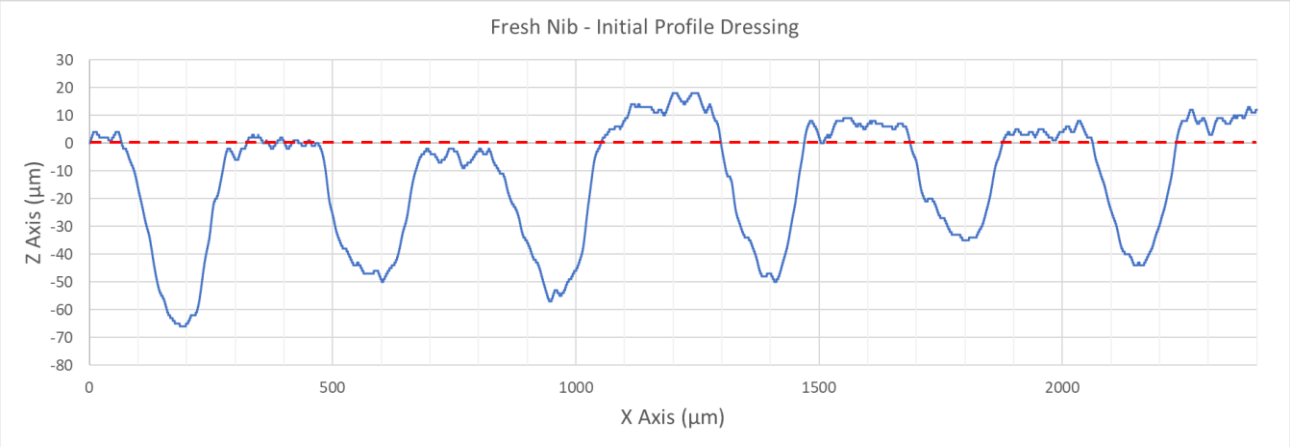

Figure 5-32: Fresh nib, initial dressing

Due to the high degree of variability and the amount of additional material to be removed, the corrective dressing operation was carried out in two stages. The first stage reduced the variability to 16µm and increased the average dressing depth to 63.2µm while the second operation further improved to consistency and resulted in an average dressing depth of 71.3µm. As before, the groove enlargement stage was not altered but repeating the same tool path improved the consistency of the profile of the grooves. The result of the 2nd and final corrective dressing operation is shown in Figure 5-33.

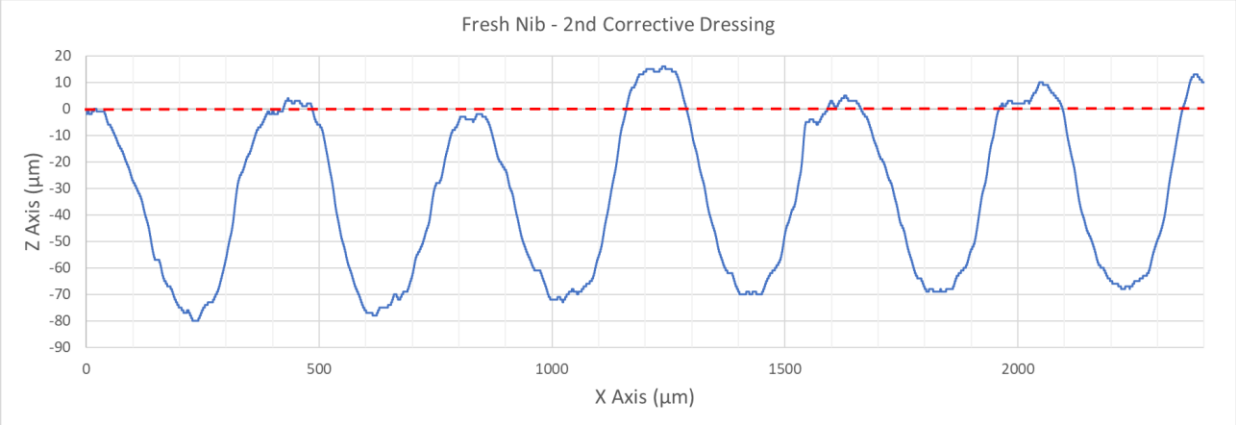

Figure 5-33: Fresh nib, final corrective dressing

The geometry was calculated from Equations 5 to 9 (chapter 3). The original profile geometry would alter slightly when the dressing operation was deepened to account for tool wear with the groove width becoming slightly larger. The groove widths for each groove set were calculated as follows:

- Part worn nib original profile – 184µm
- Part worn nib corrected profile – 197µm
- Fresh nib original profile – 161µm
- Fresh nib corrected profile – 186µm

The degree of change between the original and corrected profiled for the fresh nib was greater as the depth had to be more significantly increased to account for the additional tip wear. This further supports the use of part worn nib where possible to provide greater control over the profile of the grooves. The actual groove widths of the dressed profiles were significantly larger than calculated at:

- Part worn nib average – 274µm
- Fresh nib average - 258µm

This implies that an additional 35-40µm of material had been removed from each side of the groove. The mechanism for this increase in width is not fully understood but it is speculated that this is caused by brittle fracture of the bond material at the edge of the groove. It can be

seen that as the groove approaches the nominal zero line at the surface of the grinding wheel there is a tendency for the profile to deviate from the straight line which would be expected at the dressing tool/grinding wheel interface suggesting that the material has not been actively removed through a deterministic process but instead has broken away more randomly.

Once the dressing operations were completed the grinding wheel was reoriented into the vertical position and aligned for the grinding operation. With the exception of grinding depth, which was increased to 40µm, the same grinding conditions and workpiece material as previously used for the production of micro patches were used to provide a basis for comparison. As before, an initial pass of 10µm was made to confirm full tool engagement before the grinding was completed at the full depth. The workpiece was rotated through 90 degrees for the second pass. Figure 5-34 shows the grinding wheel positioned above the surface of the workpiece and the two sets of radial grooves are visible and clearly defined.

Figure 5-34: Grinding wheel positioned above workpiece

5.3.3 Results – Laser compensated dressing

The whole area of the ground surface was measured using the Talysurf® contact profilometer and the results are shown in Figure 5-35. The different zones of micro patches were distinct and easily identified. Each zone has been numbered to aid analysis. It is speculated that there was some degree of taper present in the workpiece when attached to the vacuum chuck as there is a gradual decrease in the height of the ground features which cannot be attributed to wheel wear. Linear striations can be observed on the fully ground portion of the surface. This is expected as the feed direction matched the rotation of the wheel and the motion was completely lateral, with no vertical component. The striations match the paths of the abrasive grains. There is some waviness to the profile which suggests that surface of the grinding wheel was not completely flat throughout the whole process. This waviness is most noticeable in the fully ground area suggesting the unprofiled portion of the grinding wheel did not wear evenly in use.

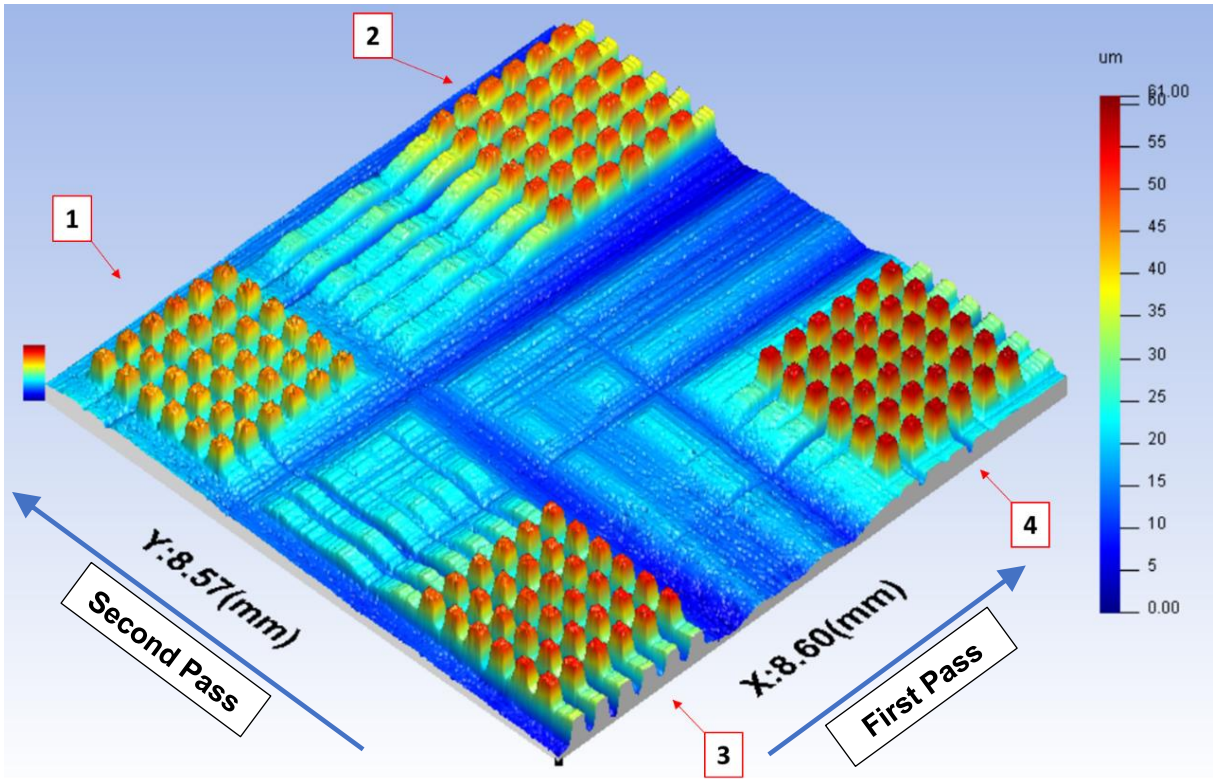

Figure 5-35: Complete ground area indicating different patches and direction of grinding passes

Figure 5-36 through to Figure 5-39 show measurements of the individual zones. In general, it can be observed that the micro patches have well defined edges and the patches in each zone have a consistent height. The four zones were created by the intersecting paths of the different groove sets on the wheel and thus the patches in each zone have different geometry. If the groove widths of the different groove sets are referred to as (a) for the part worn nib and (b) for the new nib then the patches in each zone would have side lengths as follows: Zone 1 (b,b), Zone 2 (a,b), Zone 3 (b,a) and Zone 4 (a,a).

Using equations 7 and 9 from chapter 3, at a grinding depth of 40μm, the calculated width of the top of the micro patch features would be 129μm for the grooves dressed with the part worn nib and 101μm for the grooves dressed with the new nib. By measuring the profile of one micro patch from zone 3, which has sides produced by both sets of grooves, the actual values are 200μm and 181μm respectively. This increase in size corresponds well to the increase in the groove width that was measured previously at 35μm to 40μm per side. By carrying out a similar measurement on a patch in zone 2 it can be seen that the widths have increased to 211μm and 190μm, this suggests a further loss of material resulting from tool wear.

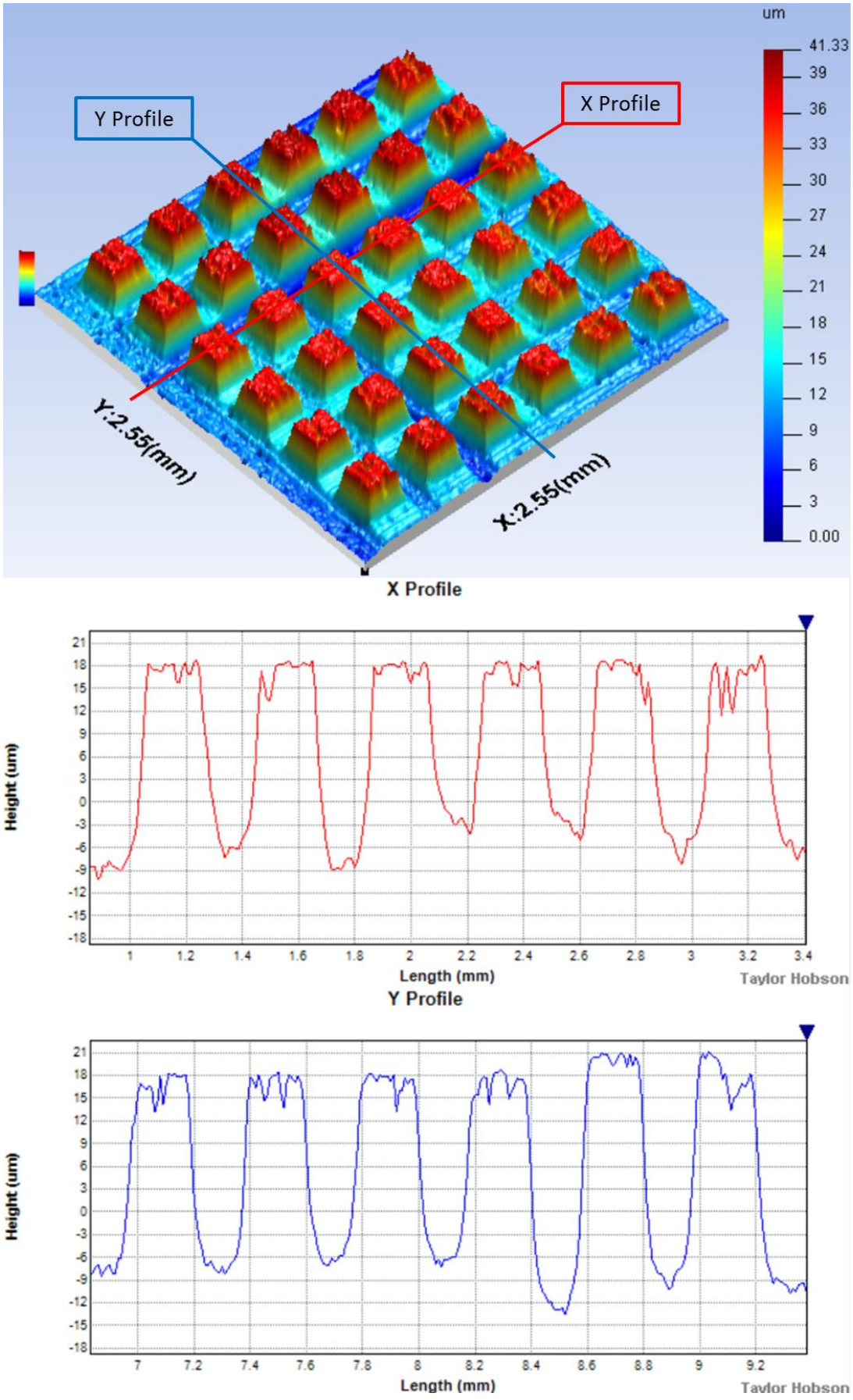

Figure 5-36: Zone 1 Profile (average height 24.6µm)

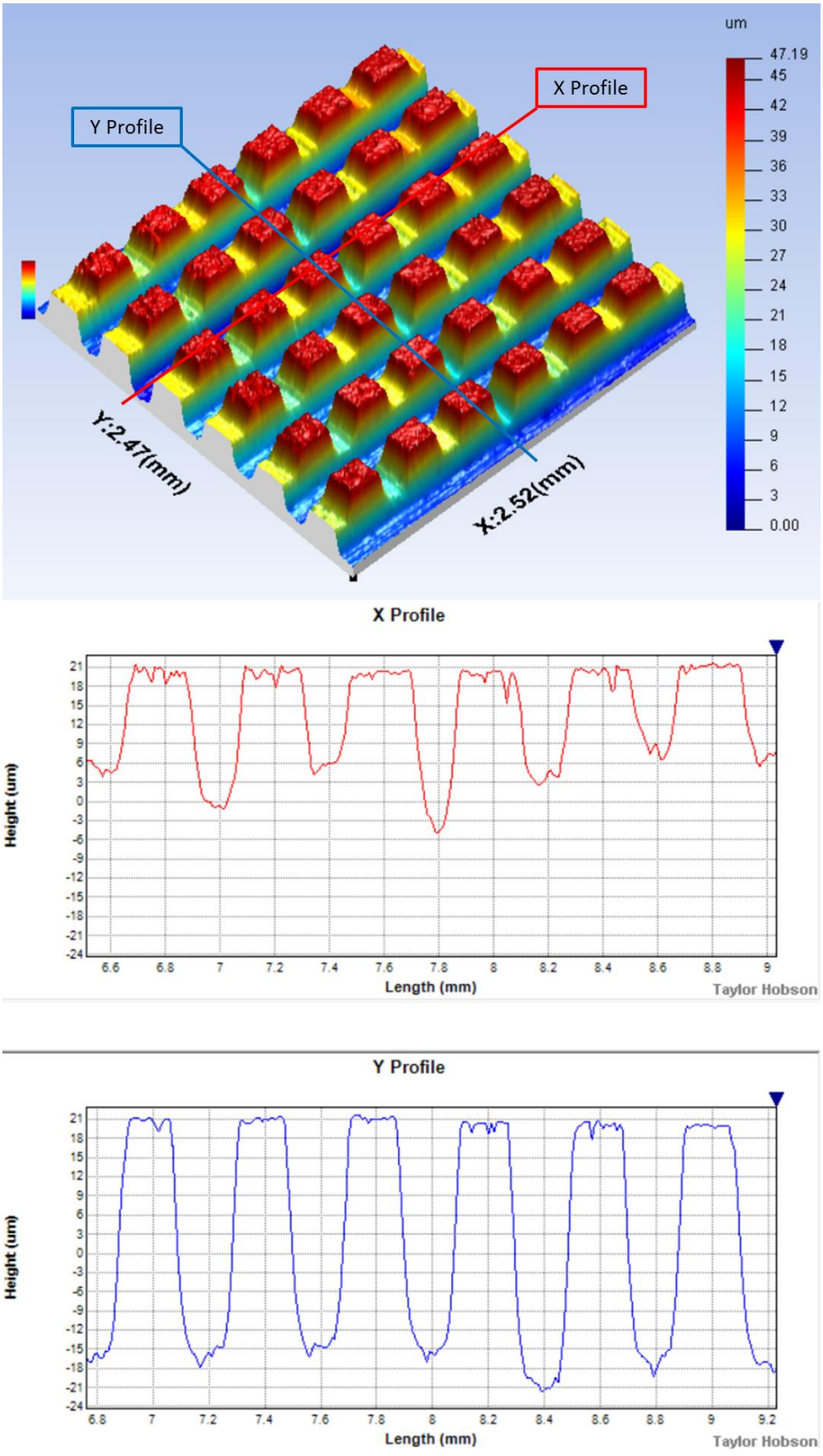

Figure 5-37: Zone 2 Profile (average height 37.1µm)

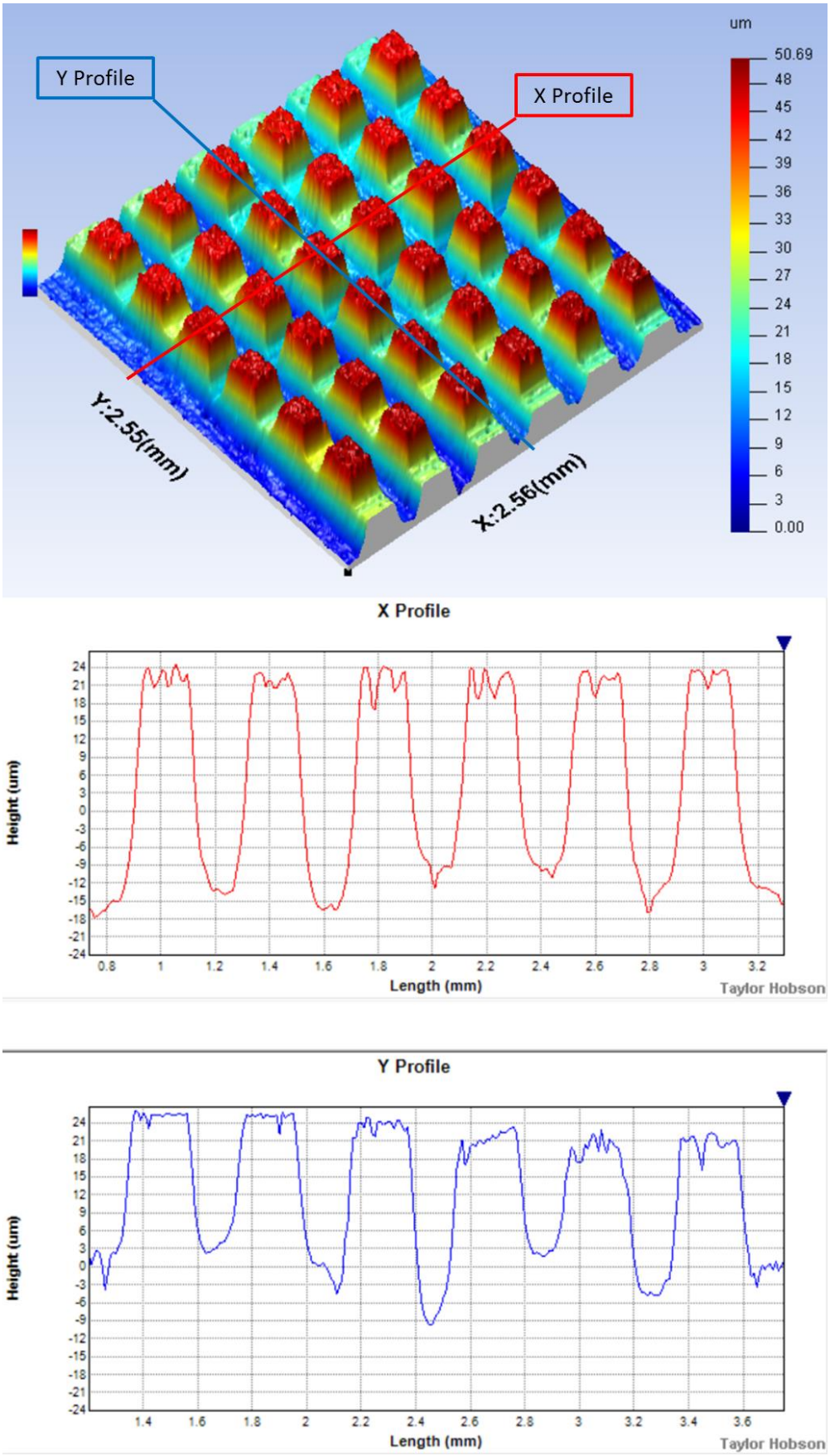

Figure 5-38: Zone 3 Profile (average height 38.3µm)

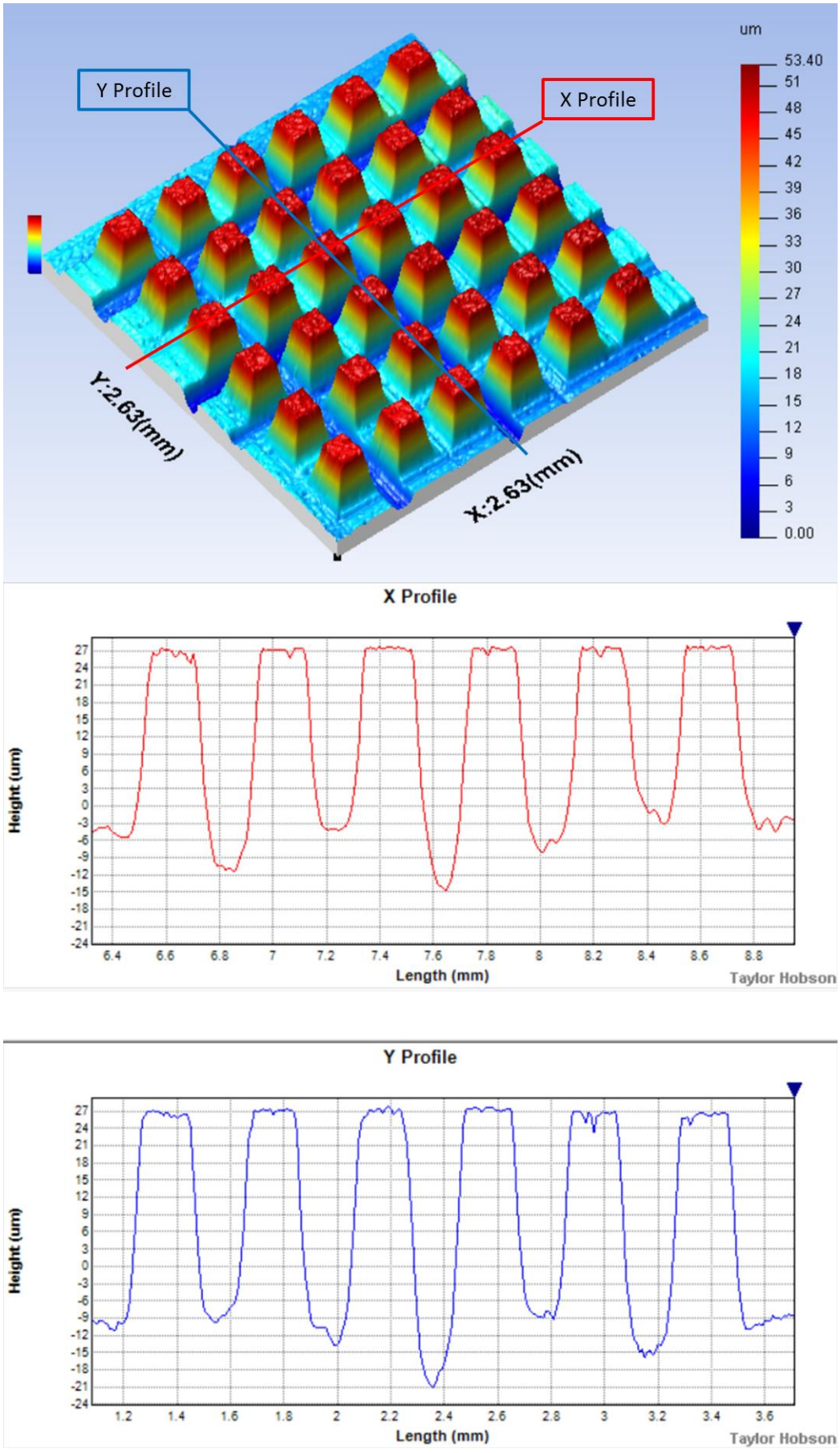

Figure 5-39: Zone 4 Profile (average height 39.3µm)

In zones 2 and 3 shown in Figure 5-37 and Figure 5-38 respectively, it can be seen that there is a significant difference in the height of features when measured along the X and Y axes with an average difference of approximately 15µm. The mechanism for this difference is most likely a combination of grinding wheel wear and taper on the workpiece surface. Figure 5-40 and Figure 5-41 show the grooves sets as measured after grinding. The average depth of the grooves has been reduced to 57.25µm suggesting that the diameter of the grinding wheel has been reduced by approximately 13µm.

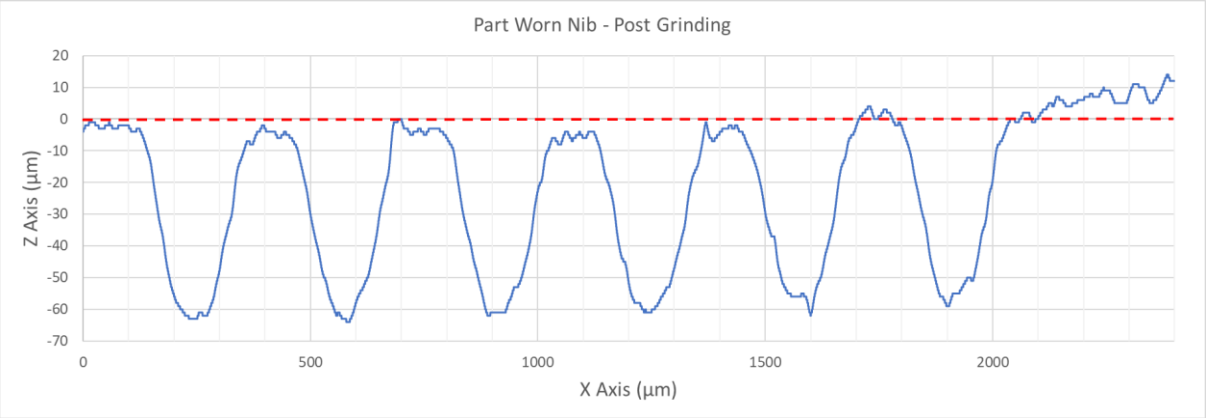

Figure 5-40: Part worn nib groove set after grinding

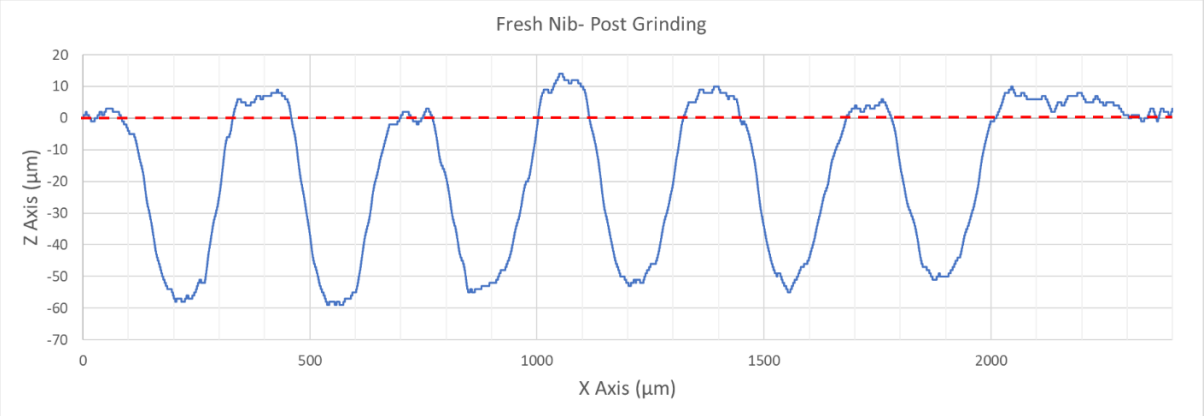

Figure 5-41: Fresh nib groove set after grinding

To assess the taper present in the workpiece, the part was measured using the integrated gauge amplifier with the part mounted in the vacuum chuck. Measurement was taken on the back face of the part so that an unground flat surface could be measured. As only a small portion of the total workpiece area had been ground, and non over the vacuum holes, it was possible to create a good seal and retain the workpiece. The measurement was carried out

along the paths as indicated in Figure 5-42. It is important to remember that as this is the back of the workpiece, the part is inverted and rotated relative to the original grinding tool paths.

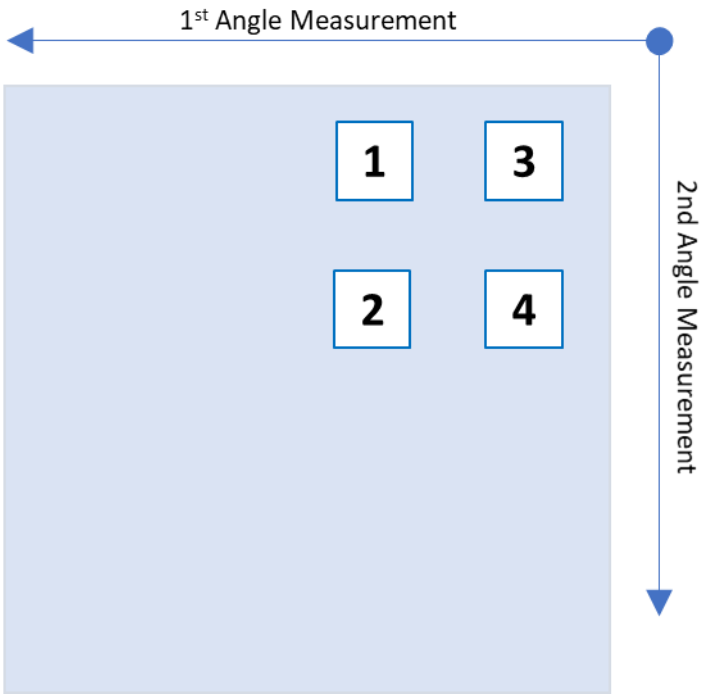

Figure 5-42: Workpiece taper measurement of back face of workpiece

Using this method, the taper along the 1st Angle Measurement was measured at 2μm over a 10mm distance, yielding a taper angle of 0.0115 degrees. Along the 2nd Angle Measurement, the measurement was 9.4μm over a 10mm distance which corresponds to a taper angle of 0.0539 degrees. There is a total distance between the centres of each feature array of 5600μm. With the taper values calculated this would lead to an expected difference in height of 1.12μm along the first grinding pass and 5.27μm along the second grinding pass. Between zone 3 and 4 there is a difference of the average height of the feature of 1μm. This corresponds very well to the calculated value and as there has been little interaction between the grinding wheel and the workpiece at this point it is likely that the difference can mostly be attributed to this taper. Between zones 3 and 1 there is a difference in height of 13.7μm. This is significantly greater than the value of 5.27μm which can be accounted for purely by taper. However, at this point the grinding wheel has travelled significantly further

and wear will be a greater factor. Coupled with the fact that tool alignment was carried in the initial orientation, an added source of error has been identified. It would be beneficial to develop and incorporate a facing operation into the process to eliminate this source of error. However, this presents a challenge as to maintain the accuracy of the dressed tool in the collet, it cannot be removed. Hence the facing operation must be carried out in a difference tool in a separate grinding spindle.

The Cut-Measure-Compensate dressing strategy has shown a significantly improved capability to dress repeatable profile geometry onto the surface of a grinding wheel which then shows a high degree of fidelity of transfer onto the ground surface. This enables deeper grinding and the generation of surface profiles with higher aspect ratio geometries.

5.4 Stępień type Helical Grinding

An attempt to replicate the Stępień type helical grinding process using the techniques developed was made using a 1200 grit diamond metallic bonded grinding wheel with a nominal outer diameter of 8mm and a length of 10mm. Because the Stępień process produces surface patterns by controlling the ratio of the workpiece feed with the surface speed of the grinding wheel and using an interrupted cut, it was necessary to deviate significantly from the established parameters. A part worn dressing nib with a nib radius of 108μm was selected as for this process larger nibs allow a greater groove pitch to be used. Secondly, the true diameter of the grinding wheel was measured at 8.608mm. These two parameters were used, along with equations 10 to 24, detailed in Chapter 3, to determine a dressing and grinding solution which would yield a nominal surface with the profile geometry described in Table 5-5. A groove depth of 4μm was the maximum that could realistically be achieved while maintaining a flat, unground bearing segment at the top of the rib profile. A simulation of the nominal profile generated using the Microsoft Excel spreadsheet tool developed to model Stępień type helical grinding is shown in Figure 5-43.

Feature	Symbol	Value
Groove Pitch	L	500 µm
Groove Bottom Length	b	96.14 µm
Groove Depth	d	4 µm
Groove Side curve length	l_c	185.51 µm
Groove Total Length	l	467.17 µm
Length of Bearing Segment	l_b	32.83 µm

Table 5-5: Nominal rib profile geometry

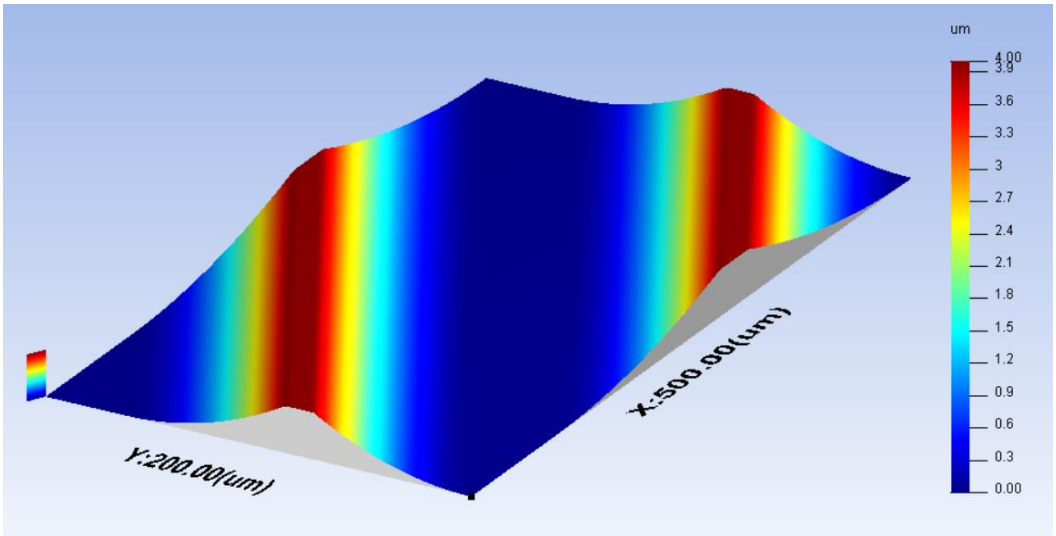

Figure 5-43: Nominal designed surface profile

To achieve the required groove pitch, the grinding wheel surface speed and workpiece feedrate must be matched. This required a very slow spindle RPM along with a fast feedrate. Feedrate on the Nanoform 250 Ultra Grind is limited to 400mm/min during machining operations which limited the maximum speed of the grinding wheel to 800RPM. The wheel was initially trued flat using the process previously described. Final Dressing was then carried out to a depth of 10µm and, with a dressing speed of 62.5 RPM, the dressing nib was passed over the surface a at a constant rate of 7mm/min to achieve the required groove pitch. **Error! Reference source not found.** gives full details of the dressing and grinding parameters while ***Figure*** 5-44 shows the dressing nib positioned close to the surface of the

grinding wheel before dressing commenced. ***Figure*** 5-45 shows a still image of the grinding wheel taken from the video monitoring of the process and the close spaced helical grooves are clearly visible.

Feature/Parameter	Symbol	Value
Grinding Wheel Radius	R	4.304 mm
Dressing Depth	h	10 μm
Groove Pitch	F_d	112 μm
Nib Radius	r_d	108 μm
Dressing Speed	S_d	62.5 RPM
Nib Rotation	S_n	5 RPM
Dressing Angle	dθ	13.7 Degrees
Grinding Speed	S_g	800 RPM
Feedrate	V_w	400 mm/min
Grinding Depth	d	4μm
Grinding Surface Speed	V_s	0.36 m/s
Grinding Wheel Grit		1200
Grinding Wheel Bond Type		Metallic

Table 5-6: Stępień type helical grinding parameters

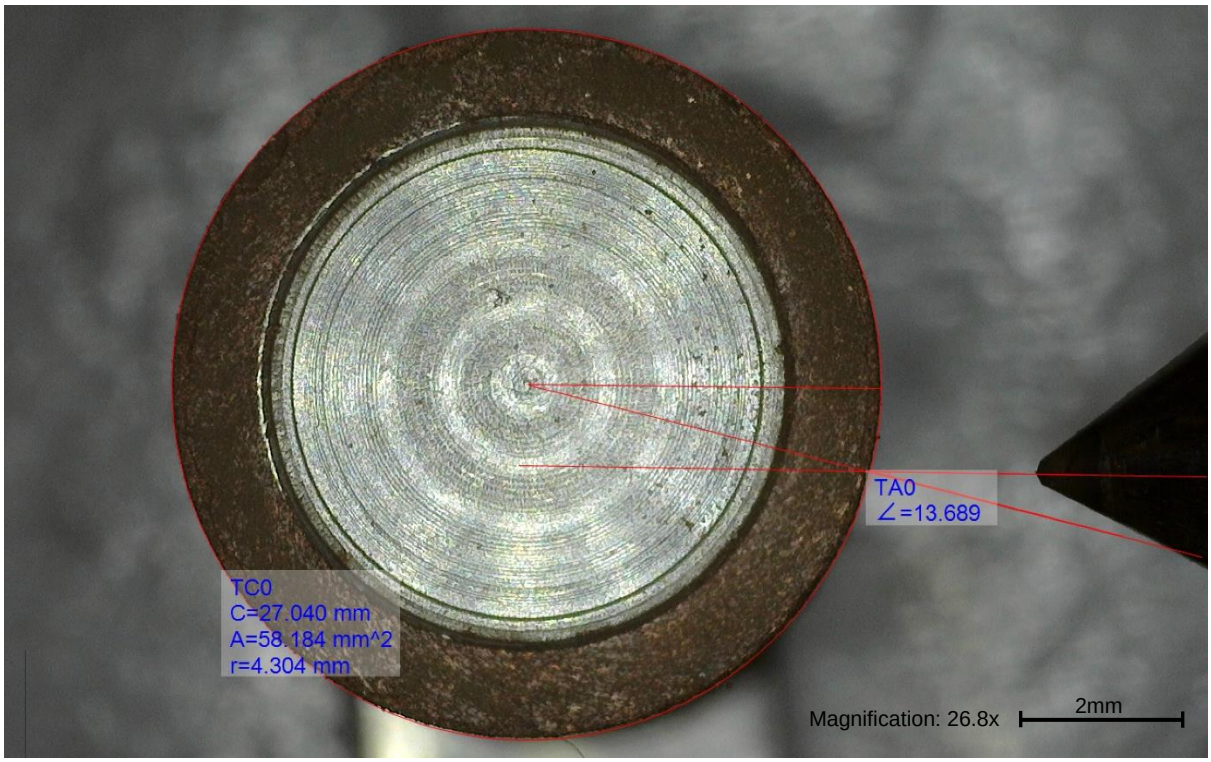

Figure 5-44: Dressing nib positioned to measure offset angle

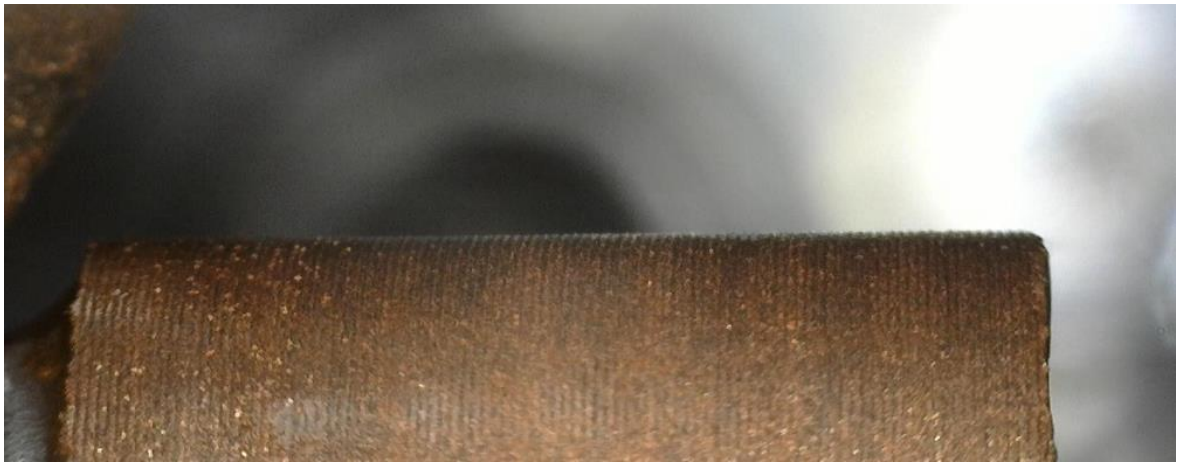

Figure 5-45: Grinding wheel after dressing with close spaced helical grooves visible

Following the dressing procedure, the surface of the grinding wheel was measured using the laser displacement sensor as previously described. It was noted that the originally flat and true profile of the grinding wheel had been altered significantly with a high degree of waviness induced. Figure 5-46 shows the measured profile with a nominal base line at the dashed red line. The peaks of the grooves can be seen to be regularly spaced but their height above the nominal base line varies considerably. The two high peaks at approximately 1.9mm and 8.7mm along the surface of the grinding wheel were likely the result of material removed during dressing and remaining on the surface. Before measurement the surface of the part was cleaned with an air duster and a cleaning spray but to avoid damage to the grooves the wheel was not wiped and therefore it is likely that some detritus remained. It is speculated that the waviness was partly induced as a result of the continuous feeding of the dressing nib over the surface at a relatively high feed rate combined with rotation of the dressing nib to maintain a radiused edge. This issue was further exacerbated by the very low dressing depth of the grooves when compared to previous experiments. As the dressed groove is, in effect, one continuous feature, it was not possible to carry out a corrective dressing operation as the exact start point of the feature could not be determined accurately nor the motion of the dressing nib effectively synchronised with the rotation of the grinding spindle.

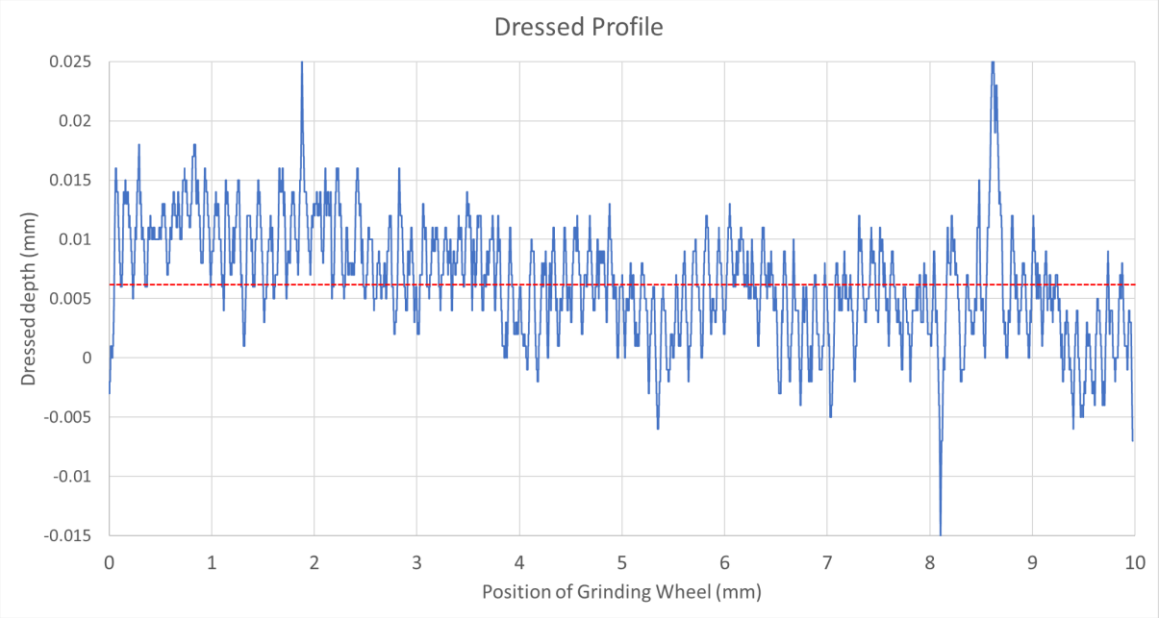

Figure 5-46: Wheel surface measured after dressing

To attempt to assess the accuracy of the dressing process, a 1mm area of the grinding wheel was assessed separately and the pitch of grooves measured. To accomplish this the peak between each groove valley was estimated using the slope of the grooves as a guide. It was not possible to definitively identify the mid-point as the groove profiles were inconsistent. These measurements can be seen in Figure 5-47. Over seven identifiable features the pitch ranged from a minimum of 103μm to a maximum of 118μm with an average distance of 109.9μm. Given the challenges in accurately placing the centre of each feature this is very close to the design pitch of 112μm. the dressing depth was also difficult to assess in a meaningful fashion as it is very close to the maximum grain size of 9μm in a 1200 grit wheel.

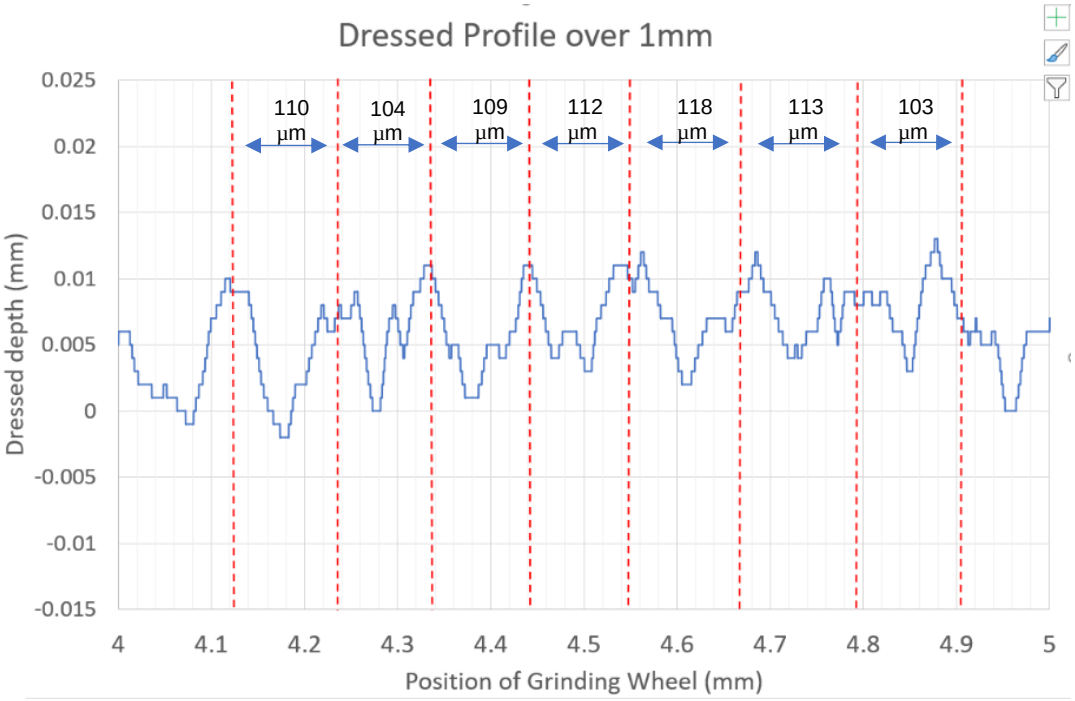

Figure 5-47: 1mm portion of grinding wheel surface with peak positions highlighted

Successful feature replication was unlikely across the whole width of the grinding wheel due to the waviness in the wheel surface. However, as the groove pitch had been accurately created and the helical profile was evident it was decided to carry out a grinding operation to examine if any portion of the grinding wheel accurately replicated a profile onto the workpiece surface. As it was not possible to use the regular method of touching off against the workpiece to set the zero depth, the laser displacement sensor was used to determine an accurate position for the edge of the grinding wheel, relative to the surface of workpiece. Given the wavy nature of the surface of the grinding wheel this could only be estimated. A spot at approximately 5mm along the edge of the grinding wheel was chosen as this was very close to the nominal baseline that had been calculated for the wheel. The grinding was carried out in a single pass at the desired depth of 4µm across the whole width of the workpiece. The first 5mm of the grinding area were measured using the Taylor Hobson Talysurf contact profilometer and an example of the results is shown in Figure 5-48. This is a typical measurement of the whole surface and it can be seen that no profiled features are present and that the surface has a very poor surface finish and straightness. This is undoubtedly a result of the unfavourable grinding speed and feedrate.

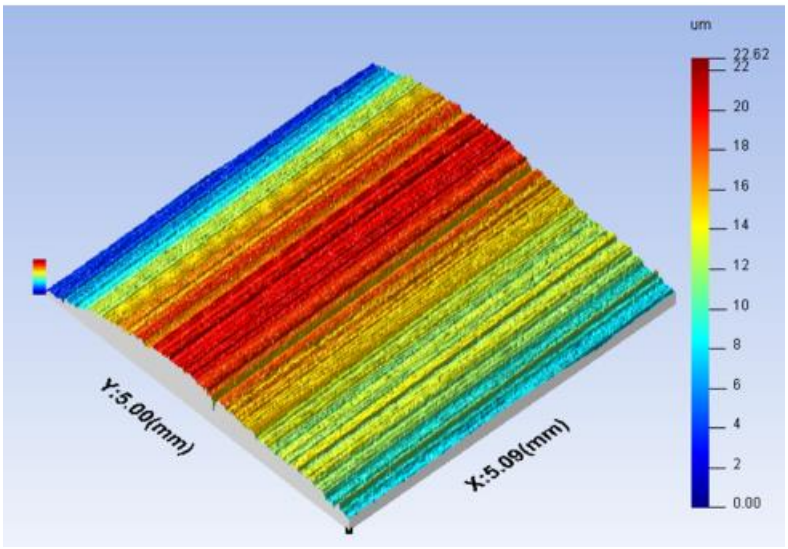

Figure 5-48: Example of ground surface

A sample area has been shown in Figure 5-49 To further highlight that the surface of the part in no way matches the nominal design profile. Linear striations are present along the whole length of the ground area. These were not designed features and are a result of individual grains passing over the workpiece surface.

From all the evidence gathered in this experiment it can be concluded that the process which has been developed and demonstrated successfully in the creation of radial grooves, is not suitable for the production of Stępień type helical grooves. Challenges in the positioning and motion control of the dressing process make it difficult to accurately dress the required geometry onto the surface of the grinding wheel.

Furthermore, adapting the Stępień process for use in the production of high aspect ratio micro scale surface features is likely to prove impossible with the grinding wheels currently available. The grinding depths which can be achieved are approximately the same size, or smaller than the abrasive grains present in the grinding wheel. It is also the case that, to achieve a usable feature pitch, the required ratio between the workpiece feedrate and grinding wheel surface speed leads to conditions that will cause significant damage to the grinding wheel and exacerbate wheel wear to an unmanageable rate.

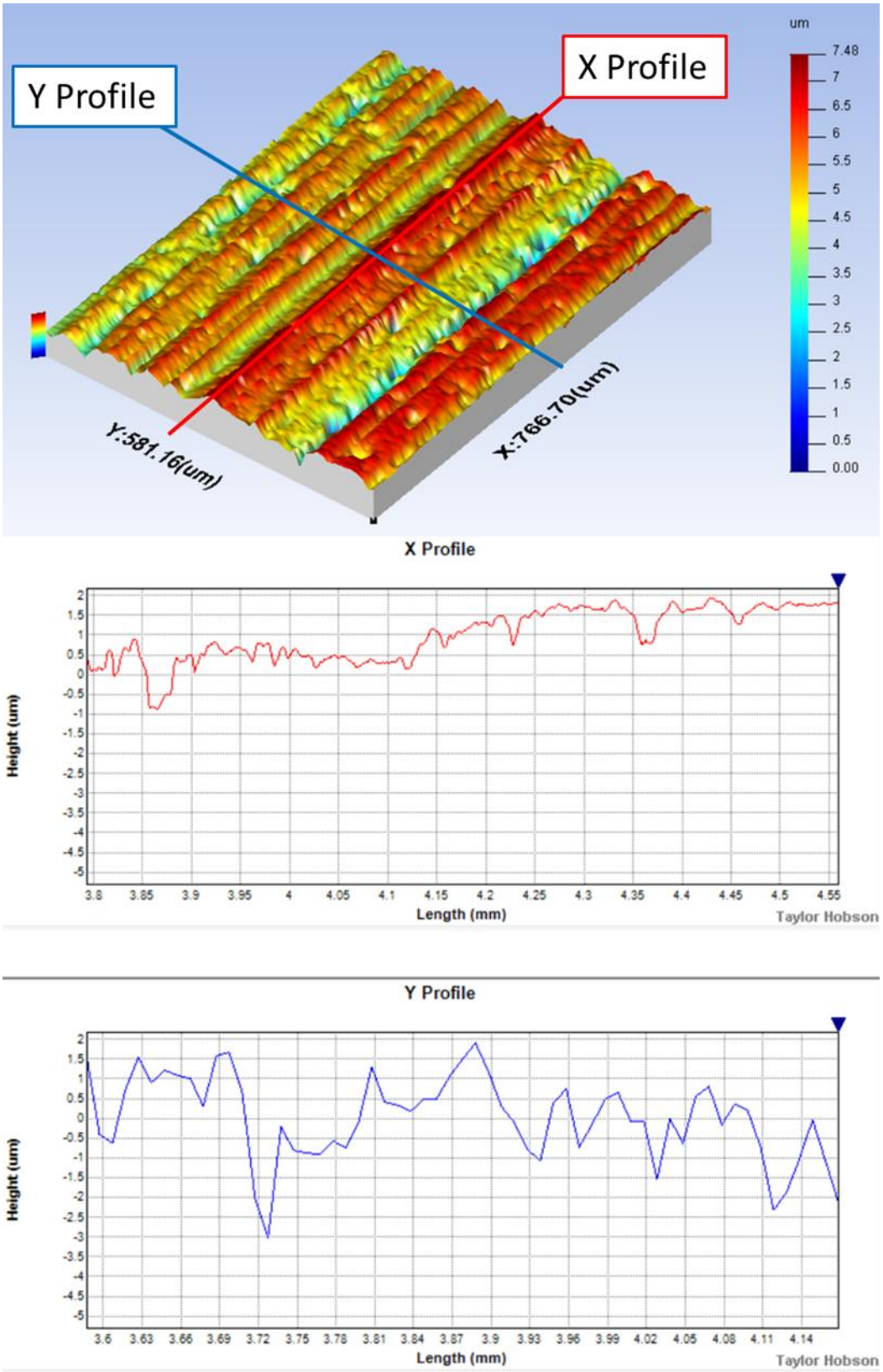

Figure 5-49: Sample area showing profile measurements

Chapter Six

Discussion and Conclusions

The following chapter presents a critical discussion of the major elements of this work and the findings of the various experimental procedures that have been carried out. The discussion evaluates the level of success and also the limitations of the work and draws comparisons with other structured grinding techniques. The chapter ends with a summary of the outcome of the project.

6 Discussion and Conclusions

6.1 Level of success of grinding surface structures

The technique developed has been used to successfully grind micro-scale features onto the surface of parts to depths of between 5µm and 50µm. Two types of feature have been produced, linear micro riblets and square micro patches of varying side length. Though not demonstrated due to time constraints, other profiles could be created using this technique by varying the profile dressed on the wheel, for instance to produce saw tooth ridges, or by varying the angle between grinding passes to create rhomboid patches. The technique has been used to produce an array of features over an area in a single machining process, rather than by machining each feature individually. This represents an improvement over conventional direct machining processes and demonstrates the potential for improvements in processing times. While only small arrays were produced in the trials, these could be significantly expanded by carrying out the dressing process over a wider area. Ultimately the limiting factor for the size of the array is the length of the grinding wheel. The minimum spacing of features is limited by the geometry of the profile and the strength of the bonding matrix of the grinding wheel. There must be sufficient material between the grooves to retain abrasive grains and to resist wear.

Over the course of the experiments several improvements were made to improve the accuracy of the dressing and grinding processes. Rotating offset dressing, dressing with a slowly rotating nib positioned off line from the centre of the grinding wheel to provide an equivalent angle of approximately 15 degrees, significantly decreased the wear rate of the dressing nib. This maintains a more consistent profile allowing it to be used accurately for longer periods. Some degree of tip wear is inevitable; integration of the laser displacement sensor into the dressing process allows for the errors which result from tool wear to be corrected in a way referred to as cut-measure-compensate. The diamond tip of the dressing wheel is eroded through a brittle fracture wear mechanism. For this reason, the wear does not proceed in a slow progressive way, rather a chip will occasionally flake away from the tip

changing the profile and reducing the dressing depth. Thus, it is not possible to use progressively deeper cuts based on time, as the point at which wear occurs cannot be known in advance. Determining the geometry of the resultant groove dressed into the surface of the grinding wheel presents several challenges. It is possible to accurately control the depth and width of the base of the groove and compensate for any loss of errors caused by dresser nib wear by using the laser displacement sensor to measure the linear profile of the grinding wheel to determine which grooves have not been fully dressed and to carry out a corrective dressing operation. Controlling the geometry of the sides of the grooves has proven more challenging. Excess material is usually removed from the sides of the groove through brittle fracture of the bond material causing the groove width at the surface of the wheel to be greater than predicted. Further research into the mechanism and rate of material removal through computer simulation may yield a method of more accurately predicting the geometry of the sides of the groove but at present the only method of generating the required geometry is to undersize the grooves and progressively widen them until they reach the desired design width. While time consuming and requiring several corrective operations, this is possible through use of the Cut-Measure-Compensate dressing technique. It should be noted that the rate of dresser nib wear decreases over time as the nib is used. This is because as the nib wears its profile becomes broader and more resilient to flaking. Where possible it is preferable to use as broad a dresser nib as possible to improve accuracy of the dressing process.

The process developed is comparable to the process described by Denkena, et al. (2010) for the production of riblet structures by profile grinding. This process used specialised diamond profile rollers to create the required geometry on the surface of a macro-scale grinding wheel. These specially profiled wheels have been successfully used in the production of riblets; these resemble the riblets described in chapter 5. When comparing the two processes, the use of a profile roller has several advantages. Firstly, the roller can be used to profile multiple grooves in one operation rather than by dressing them individually and

secondly the accuracy of the form of the profile roller can be confirmed in advance. This means that there is no need to measure each individual groove on the grinding wheel and carry out a second corrective step to ensure accuracy. However, single point dressing does offer some advantages. The diamond profile rollers must be specially manufactured in advance and the profile, once determined, cannot be changed. Single point dressing is much more adaptable and a single, low cost, dressing nib can be used to dress a wide variety of profiles. Denkena, et al. (2010). experienced similar issues with regards to wheel wear and the minimum feature size that could be dressed onto the grinding wheel. These issues are fundamental to grinding wheels and discussed in more depth below. While the two processes are capable of producing similar results, they differ in their suitability for different applications. Due to the use of macro-scale grinding wheels, the Denkena process is well suited for the production of surface structures over large parts with concurrently large surface areas. The use of specialised grinding machines and diamond profile rollers mean the process is best suited to high volume manufacture of parts where parameters are not frequently changed. In comparison, the process developed in this thesis is much lower cost and more adaptable. The technique can be adapted for use on a wide range of machinery and the profile of the grinding wheel can be changed as and when required. However, the use of ultra-precision grinding wheels with smaller dimensions limits the surface area that can be machined in a single operation.

Attempting to replicate the structured grinding processes described by Stępień (2011) and Oliveira, et al. (2010) on a micro-scale has proven significantly more challenging. These techniques rely on profiles shaped in such a way as to interrupt the grinding cut and as such the velocity ratio between the surface speed of the grinding wheel and the feedrate of the workpiece is critical to the texture generated. Additionally, these processes are carried out with macro-scale grinding wheels with diameters of least 250mm while grinding to depths of up to 25µm. The textures produced by these techniques cover large surface areas with a very low aspect ratio between the length of the features and their height. There are a

number of difficulties in attempting to scale down these processes for use with ultra-precision grinding wheels, typically 3-12mm diameter, while maintaining a grinding depth useful for the production of surface structures. Theoretical calculations, using the methods set out in chapter three, have been used to determine what kinds of surface profile can be generated and the concurrent grinding wheel profile. To achieve a groove pitch, effectively the linear distance between features, that could be considered a surface structure requires the use of prohibitively low grinding speeds and concurrently high feedrates. These are not conducive to good conditions for grinding and exacerbate wheel wear. The dresser feed pitch required to dress the profile on the grinding wheel is also typically small, in the region of 50-200µm. Consequently, there is only a small amount of grinding material active, further increasing the rate of wheel wear.

Dressing depth is a key component of Stępień type helical grooves. To generate the geometry required to grind features to a depth of up to 5µm requires dressing depths in the region of 10µm to 15µm. This is within the range of the noise on the surface of a grinding wheel which results from the stochastic distribution of abrasive particles. Furthermore, it is approximately the same size as the largest abrasive grains that may be present in the available grinding wheels. Attempts to produce suitable helical grooves on ultra-precision grinding wheels have had very limited success. It is possible to achieve the correct feed pitch, but the resultant surface of the grinding wheel is too noisy to identify any features. Additionally, the high dressing rate necessary to achieve the correct feed pitch at the minimum rotational speed of the Nakanishi spindle induces undesirable feature such as waviness onto the surface of a previously trued grinding wheel. These large amplitude features are often greater than the design grinding depth, making accurate tool setting impossible. Further experimentation with a variety of wheel diameters, grain sizes and alternative dressing techniques is necessary to determine if interrupted grinding can be used successfully at this scale. Experiments have thus far concentrated on interrupted grinding using single, continuous helical grooves rather than the variety of profiles described by

Oliveira, et al (2010). This is primarily due to the lack of suitable equipment to oscillate the dressing nib in synchronisation with the grinding wheel spindle. In this technique, the pitch of the features along the axis of the grinding wheel, and the profiles required to generate them, are independent of the rotational speed of the grinding wheel. For this reason, they may be better suited for use with the micro-scale grinding techniques developed in this project.

6.2 Limitations of Nanoform 250 Ultra Grind

The Precitech Nanoform 250 Ultra Grind used throughout this project is representative of the type of ultra-precision machining centre that may be commonly found in industry. Over the course of the work the machine experienced a number of technical difficulties requiring significant downtime and maintenance. However, despite this it has proven a viable platform for the process of machining surface structures using ultra-precision abrasive machining. Having two linear axis and single rotary axis this specification represents the most basic type of machining centre available. More advanced machines, especially those which incorporate three linear axes, would have significantly increased capability. The third linear axis would enable the grinding wheel to be dressed in the same orientation that it will be used for grinding. This would be a significant improvement, as it would remove the primary source of errors induced by tool alignment. Additional axes also present an opportunity to significantly decrease the processing time as the dressing, measuring, compensating and grinding operations could be carried out in sequence without the need to change the machine set up between each operation. This would be essential for automation of the process and for large volume manufacture.

The Nanoform 250 control systems were used to control the movement of the linear and rotary axes and to provide coolant and air flow but the grinding spindle, laser displacement sensor and USB microscope were each controlled by a separate system. As well as requiring numerous cables to be routed into the machine, this was inconvenient as it was necessary to operate several systems at once. To improve efficiency, it would be beneficial to have all systems integrated into the main CNC controls. This would not only reduce

processing times but also reduce the opportunities for operator error as measurements for tool setting and dressing compensation would not have to be entered manually.

6.3 Limitations of conventional grinding wheels

There are many types of ultra-precision grinding wheels which could potentially be suitable for use with these techniques. The choice of abrasive and bonding matrix would ideally be optimised for the workpiece while the basic geometry of the grinding wheel such as the length and diameter can be selected based on the specific application. The grinding wheels used for the machining trials detailed in this thesis were chosen from the limited selection available as originally supplied with the machine for conventional ultra-precision grinding. This type of super-abrasive grinding wheel is readily available at a relatively low cost, as low as £80 for off-the-shelf parts rising to approximately £200 for custom wheels with specified dimensions, and as such is compatible with the original goal of developing a cost-effective system. Furthermore, the fact that these grinding wheels can be re-dressed and re-used a number of times provides additional cost savings.

There are two factors of grinding wheel technology which limit the performance which can be achieved. The size of the abrasive grains available is a considerable challenge. Smaller grains are better suited to the accurate dressing of geometries onto the wheel; this is because the larger the grain size, the greater the potential for grains located at the edge of a feature to be dislodged leaving an irregular profile. A second advantage of smaller grains is that the cavities in the bonding matrix between grains, essential for carrying coolant and the removal of swarf, are similarly small, further enhancing the fidelity of profile transfer. However, there is a compromise in that for a given bond material, as the grain size decreases so too does the strength of the bond between grains. Up to a point, decreasing grain size will enable smaller, sharper features to be produced on the surface of the grinding wheel. However, beyond this point, a smaller grains size will result in a wheel less able to maintain the integrity of smaller features and more susceptible to wear. The second factor limiting the performance of the grinding wheels is the rate of wheel wear. To maintain

adequate material removal performance, it is necessary that blunted grains are capable of being discarded to reveal the fresh, sharp grains beneath. However, this presents a significant challenge to maintaining a consistent profile across the surface of the grinding wheel. Radial grooves with very steep, approaching vertical, sides can mitigate this to some extent as the wear rate is predictable, but these are difficult, if not impossible to create using conventional single point dressing. Other dressing techniques such as laser dressing may be more successful in generating the desired geometry, but they are not widely available and incur significant equipment costs.

6.4 Limitations of the technique

The techniques developed are capable of producing a wide array of different surface structures which incorporate regular geometric patterns. However, due to the limitations in grinding wheel technology previously discussed and because grinding is a rotary process, there is a limit to the potential geometries of individual structures which can be achieved. There must be sufficient material between features on the grinding wheel for the bonding matrix to provide a solid foundation for the active abrasive grains otherwise there will be excessive wheel wear. For this reason, it is impossible to create features with vary small radii or place grooves very close together. This limits the minimum spacing between structures on the resultant ground surface and the shape of the profiles which can be achieved.

Currently the technique can only fully be applied to parts with a flat surface as it is necessary to re-orientate the tool with the workpiece for the further machining passes. Single pass machining, for features such as micro riblets, can be carried out on external curved surfaces and internal curved surfaces for which the radius is greater than that of the grinding wheel being used.

6.5 Conclusions

This project has focussed on the development of a system for the manufacture of micro-scale functional surface structures using ultra-precision abrasive machining. The technique developed is based around a structured grinding process incorporating specialised wheel geometry. This technique has successfully demonstrated the capability to produce arrays of surface structures on parts with flat surfaces. These surfaces have wide ranging potential applications from drag reduction to improved cooling and lubrication. Several authors have previously demonstrated the use of grinding as a means of producing surface textures and structures. The novelty of this work lies in the development of a method to replicate these techniques on smaller ultra-precision grinding wheels in a cost effective and highly adaptable way and in the development of a technique for in-situ dressing of specialised profiles on ultra-precision grinding wheels.

The system developed is capable of being retrofitted to any ultra-precision CNC machining centre equipped with at least two linear axes and a workpiece axis, while the additional tooling required to add this capability to the machine has low capital costs. This makes the process suitable for a wide range of manufacturing companies and particularly attractive to companies which do not have a large amount of resources available for capital investment but still seek to incorporate functional surface structures onto their products. There are two principle pieces of equipment which must be purchased to enable the use of this technique. The first is a grinding spindle, preferably electronically driven, which is capable of operating at very low speeds with a high degree of speed control; this allows the grinding wheel to be accurately dressed and used without the need to remove it from the collet. The second piece of equipment required is a laser displacement sensor, or other non-contact 1D distance measurement system, which is used for accurate tool setting and to allow for a cut-measure-compensate dressing strategy. Mounting systems are also required to affix these items to the machine and provide means of adjustment for tool angle and height; these will be unique to each set up. The grinding wheels and dressing nibs used are also low cost and can be

considered consumable items. The total cost of implementing this technique onto an existing CNC ultra-precision machining centre would be in the region of £10,000-£15,000, As such the goal of creating a cost effective system has been achieved.

There is significant scope for the process to be optimised. At present the different pieces of equipment are not integrated into a single control system. This makes the process impossible to fully automate, reducing efficiency and increasing processing times. Additionally, the lack of a third linear axis on the Precitech Nanoform 250 Ultra Grind machining centre resulted in a need to physically remove and reposition the grinding spindle between the dressing and grinding operations. This further increased the processing time and resulted in an additional source of error in tool alignment. These challenges are primarily due to the fact that, as a research project, the equipment available was limited and the ideal specification unknown until sufficient experimentation had been undertaken. These issues would be resolved in a productionised system and are discussed further in chapter seven.

Further experimentation into the dressing of different wheel profiles and of different grinding strategies is needed to determine the ultimate capability of the technique and the variety of structures that can be generated by this method. Supplementing this with additional research into the use of advanced dressing techniques such as laser dressing or the use of highly specialised grinding wheels may yield further improvements in performance, although this would incur significantly increased costs.

Chapter Seven

Future Work

The technique developed in this thesis has successfully demonstrated the capability to use an ultra-precision grinding process for the production of structured surfaces in a cost effective system which can be retrofitted to an existing CNC machine. However, there are many areas in which this work could be developed. This chapter presents a brief discussion of areas which may prove fruitful for further investigation, these can broadly be separated into three areas. Firstly, further testing should be carried out to investigate the influence of the various parameter and determine the repeatability of the technique. Secondly, refinement of the existing technique through the use of new dressing and grinding strategies. The final area of investigation focusses on enhancing the technique through the use of technologies such as advanced dressing methods or specialised grinding wheels, that were not available over the course of this research. Ultimately the aim is to develop a system that would be beneficial and attractive to manufacturing companies by allowing a cost effective means to improve manufacturing capability.

7 Future Work

Several potentially valuable areas for future research have been identified throughout the project. These focus on two distinct areas; further refinement of the technique developed to improve performance and enhancing capability through the adoption of equipment and technology not available during the course of this research.

Throughout the course of the work several parameters have been identified which must be accurately controlled for the process to be successful. These include the dressing depth, nib offset angle and rotation speed and grinding depth and speed. Additionally, variables in the equipment available such as the dressing nib angle, tip radius and grinding wheel bond material are not controlled as part of the process but will influence the outcome of the procedure. Further experimentation into the effect of variation into these parameters would be of great benefit in optimising the process and giving confidence in the robustness and repeatability of the procedure.

Additionally, as the dressing nib is mounted in the vacuum chuck on the X axis, it was not possible to face off the workpiece in preparation for grinding without removing the dressed grinding wheel. This would potentially lead to induced positioning errors. The workpieces used had very low degrees of taper however this was still sufficient to cause variability in the ground surface. Developing a method to face off and flatten the workpiece prior to grinding would substantially increase the accuracy of the process, especially when machining over large surface areas.

Only a small range of potential geometries have been produced in the experiments detailed in this thesis. To fully assess the performance of the procedure it would be highly desirable to try a larger range of wheel geometries and grinding strategies. Variables such as depth, profile and spacing of the grooves would be ideal for investigation while varying the direction and number of grinding passes provides another route to creating different surface profiles. Additionally, further research into methods of successfully generating and using more

complex geometries such as helical grooves would be beneficial to increase the range of profiles which can be generated using this method.

While conventional ultra-precision grinding wheels can be used for the processes described it would be advantageous if wheels with smaller grain sizes or specially formed geometries were available. Wheels with smaller grains would allow more accurate dressing and potentially improve the surface finish on the faces of the generated structures. Additionally, newer more experimental super-abrasives such as UcBN, may be particularly well suited to this procedure due to the exceptionally small grain sizes available and favourable wear characteristics.

Advanced dressing techniques such as laser dressing, laser assisted dressing or piezo-electric oscillation of single point diamond dressing nibs present an opportunity to both improve the accuracy of the dressing process and allow the generation of new profiles. While these techniques incur significant additional equipment costs, this may be acceptable if they are capable of commensurately better performance. In process dressing, using techniques such as Electrolytic In-process Dressing (ELID), would also be a potentially valuable avenue for investigation as the ability to maintain a consistent grinding wheel profile while it is in use would increase the accuracy of the grinding process and extend the usable lifespan of the wheel.

The technique developed is currently very labour intensive, requiring the equipment on the machine to be changed between each stage of the process. Replicating the technique on a more capable machine, particularly one with a minimum of three linear axes and a rotary axis for the workpiece, would allow the majority of the process to be automated. This would be beneficial as it would likely yield an increase in the accuracy of the dressing and grinding process. It would also reduce the level of operator skill required. While this area of research might not be considered the most academically challenging, it is the most necessary for the process to become suitable for adoption by industry.

Appendix 1: Publications List

Work completed within this thesis was presented at various conferences, with the details as follows:

"Development of ultra-precision abrasive machining of functional structured surfaces". Christian Young, Liam Blunt, Zavid Mohamed, Zhen Tong. Conference proceedings and Poster presentation at European Society for Precision Engineering and Nanotechnology (eu**spen**) 16th International Conference & Exhibition, Nottingham 2016

"Development of an ultra-precision grinding technique for the production of structured micro-patches on ceramics and tool steel". Christian Young, Liam Blunt, Zhen Tong. Conference proceedings and Oral presentation at European Society for Precision Engineering and Nanotechnology (eu**spen**) 17th International Conference & Exhibition, Hannover 2017

Bibliography

Abbott, S. J., & Gaskell, P. H. (2007). Mass production of bio-inspired structured surfaces. *Proceedings of the Institution of Mechanical Engineers, Part C: Journal of Mechanical Engineering Science*, 1181-1191.

Aspinwall, D. K., Soo, S. L., Curtis, D. T., & Mantle, A. L. (2007). Profiled Superabrasive Grinding Wheels for the Machining of a Nickel Based Superalloy. *Annals of the CIRP, 56*, 335-338.

Bhushan, B. (2012). Bioinspired Structured Surfaces. *Langmuir*, 1698-1714.

Bifano, T., Krishnamoorthy, R., Fawcett, H., & Welch, E. (1999). Fixed-Load Electrolytic Dressing With Bronze Bonded Grinding Wheels. *Transactions of the ASME*, 20-27.

Blas Romero, A. d., Pfaffinger, M., Mitteramskogler, G., Schwentenwein, M., Jellinek, C., Homa, J., . . . Stampfl, J. (2017). Lithography-based additive manufacture of ceramic biodevices with design-controlled surface topographies. *International Journal of Advanced Manufacturing Technology, 88*, 1547-1555.

Blunt, L., & Jiang, X. (2003). *Advanced Techniques for Assessment Surface Topography.* (L. Blunt, & X. Jiang, Eds.) Kogan Page Science.

Brinksmeier, E., Heinzel, C., & Wittmann, M. (1999). Friction, Cooling and Lubrication in Grinding. *CIRP Annals - Manufacturing Technology*, 581-598.

Brinksmeier, E., Mutlugunes, F. K., Aurich, J. C., Shore, p., & Ohmori, h. (2010). Ultra-precision Grinding. *CIRP Annals - Manufacturing Technology*, 652-671.

Brinksmeier, E., Riemer, O., & Gessenharter, A. (2006). Finishing of structured surfaces by abrasive polishing. *Precision Engineering, 30*, 325-336.

Bruzzone, A. A., Costa, H. L., Lonardo, P. M., & Lucca, D. A. (2008). Advances in engineered surfaces for functional performance. *CIRP Annals - Manufacturing Technology, 57*, 750-769.

Buskens, P., Burghoorn, M., Mourad, M. C., & Vroon, Z. (2016). Antireflective Coatings for Glass and Transparent Polymers. *Langmuir, 32*, 6781-6793.

Chapman, G. (2004). *Ultra-precision Machining Systems; an Enabling Technology for Perfect Surfaces.* Moore Nanotechnology Systems LLC.

Chapman, G. (2016, September 26). *Moore Nanotechnology Systems.* Retrieved from http://www.nanotechsys.com/images/PDFs/UltraPrecisionMachingSystem.PDF

Chen, X., & Brian Rowe, W. (1996). Analysis and simulation of the grinding process. Part I: Generation of the grinding wheel surface. *International Journal of Machine Tools Manufacture, 36*, 871-882.

Chen, X., Brian Rowe, W., Mills, B., & Allanson, D. R. (1998). Analysis and simullation of the grinding process. Part IV: effects of wheel wear. *international Journal of Machine Tools Manufacture, 38*(1), 41-49.

Corning. (2012). MACOR: Machinable Glass Ceramic for Industrial Applications. France: Corning.

Curtis, D. T., Soo, S. L., Aspinwall, D. K., & Sage, C. (2009). Electrochemical superabrasive machining of a nickel-based aeroengine alloy using mounted grinding points. *Manufacturing Technology, 58*, 173-176.

Davies, M. A., Evans, C. J., Patterson, S. R., Vohra, R., & Bergner, B. C. (2003). Application of precision diamond machining to the manufacture of micro-photonics components. *Proc. of SPIE: Lithographic and Micromachining Techniques for Optical Component Fabrication II* (pp. 94-108). Bellingham: SPIE.

De Chiffre, L., Kunzmann, H., Peggs, G. N., & Lucca, D. A. (2003). Surfaces in Precision Engineering, microengineering and Nanotechnology. *CIRP Annals - Manufacturing Technology, 52*(2), 561-577.

Dean, B., & Bhushan, B. (2010). Shark-skin surfaces for fluid-drag reduction in turbulent flow: a review. *Philosophical Transactions of the Royal Society A*, 4775-4806.

Denkena, B., De Leon, L., & Wang, B. (2009). Grinding of microstructured functional surfaces: a novel strategy for dressing of microprofiles. *Production Engineering*, 41-48.

Denkena, B., Grove, T., & Gottsching, T. (2015). Grinding with patterned grinding wheels. *CIRP Journal of Manufacturing Science and Technology*, 12-21.

Denkena, B., Grove, T., & Göttsching, T. (2018). Grinding tool design for the manufacturing of UHC-steel. *International Journal of Advanced Manufacturing Technology, 95*, 267-275.

Denkena, B., Grove, T., & Suntharakumaran, V. (2018). Porous metal bonds increase the resource efficiency for profile grinding. *Procedia CIRP. 69*, pp. 265-270. Copenhagen: Elsevier.

Denkena, B., Kohler, J., & Wang, B. (2010). Manufacturing of functional riblet structures by profile grinding. *CIRP Journal of Manufacturing Science and Technology*, 14-26.

Derkx, J. M., Hoogstrate, A. M., Saurwalt, J. J., & Karpuschewski, B. (2008). Form crush dressing of diamond grinding wheels. *CIRP Annals - Manufacturing Technology*, 349-352.

Extrand, C. W., Moon, S. I., Hall, P., & Schmidt, D. (2007). Superwetting of Structured Surfaces. *Langmuir, 23*, 8882-8890.

Favret, E. A., & Nestor, F. O. (2009). *Functional Properties of Bio-inspired Surfaces.* World Scientific Publishing Co. Plc. Ltd.

Feng, R., Zhao, W., Wu, X., & Xue, Q. (2012). Ratchet composite thin film for low-temperature self-propelled Leidenfrost droplet. *Journal of Colloid and Interface Science, 367*, 450-454.

Gao, N., Yan, Y., Chen, X., & Mee, D. J. (2012). Nanoparticle-Induced Morphology and Hydrophilicity of Structured Surfaces. *Langmuir, 28*, 12256-12265.

Garcia-Mayoral, R., & Jimenez, J. (2011). Drag Reduction by Riblets. *Philosophical Transactions of the Royal Society A*, 1412-1427.

Grounds, A., Still, R., & Takashina, K. (2012). Enhanced Droplet Control by Transition Boiling. *Scientific Reports, 2*, 720.

Hernandez-Castellano, P. M., Benitez-Vega, A. N., Diaz-Padilla, N., Ortega-Garcia, F., Socorro-Perdomo, P., Marrero-Aleman, M. D., & Salguero, J. (2017). Design and manufacture of structured surfaces by electroforming. *Procedia Manufacturing, 13*, 402-409.

Hisler, V., Vonna, L., Le Houerou, V., Knopf, S., Gauthier, C., Nardin, M., & Haidara, H. (2014). Model Experimental Study of Scale Invariant Wetting Behaviors in Cassie-Baxter and Wenzel Regimes. *Langmuir, 30*, 9378-9383.

Ishida, Y. (2015). Super long life mirror grinding using ultrafine-crystalline cBN abrasive Grit. *Euspen 15th International Conference & Exhibition*, (pp. 39-40).

Itoh, N., & Ohmori, H. (1996). Grinding Characteristics of Hard and Brittle Materials by Fine Grain Lapping Wheels with ELID. *Journal of Materials Processing Technology, 62*, 315-320.

Jackson, M. J. (2004). Fracture dominated wear of sharp abrasive grains and grinding wheels. *Procedings of the Institution of Mechanical Engineers Part J - Engineering Tribology*, 225-235.

Keyence. (2010). LK-G5000 Series - User's Manual. Japan.

Khan, G. S., Sarepaka, R. G., Chattopadhyay, K. D., Jain, P. K., & Narasimham, V. M. (2003). Effects of tool feed rate in single point diamond turning of aluminium-6061 alloy. *Indian Journal of Engineering & Materials Sciences*, 123-130.

Khangar, A., Dahotre, N. B., Jackson, M. J., & Robinson, G. M. (2006). Laser Dressing of Alumina Grinding Wheels. *Journal of Materials Engineering and Performance*, 178-181.

Kirsch, B., Bohley, M., Arrabiyeh, P. A., & Aurich, J. C. (2017). Application of Ultra-Small Micro Grinding and Micro Milling Tools: Possibilities and Limitations. *Micromachines, 8*(261), 1-18.

Klocke, F., & Linke, B. (2008). Mechanisms in the generation of grinding wheels topography by dressing. *Production Engineering Research and Development*, 157-163.

Leading Solvents. (2013). Odourless Kerosene Safety Data Sheet. Yorkshire, England: Leading Solvents.

Lee, W.-K., Jung, W.-B., Rhee, D., Hu, J., Lee, Y.-A. L., Jacobsen, C., . . . Odom, T. W. (2018). Monolithic Polymer Nanoridges with Programmable Wetting Transitions. *Advanced Materials*, 1-7. doi:10.1002/adma.201706657

Li, C. L., Peng, Y., Chen, D. L., & Pan, T. L. (2018). Theoretical investigation of vertical elliptic vibration-assisted grinding (EVAG) technology. *International Journal of Advanced Manufacturing technology, 94*, 2315-2324.

Li, H. N., & Axinte, D. (2018). On the inverse design of discontinuous abrasive surface to lower friction induced temperature in grinding: an example of engineered abrasive tools. *International Journal of Machine Tools and Manufacture, 132*, 50-63.

Lihua, L., Ziqiang, Z., Yingchun , L., & Longjiang, Z. (2010). Calculation and analysis for stiffness of the thrust aerostatic bearing of ultra-precision machine tools. *Proc. SPIE 7655, 5th International Symposium on Advanced Optical Manufacturing and Testing Technologies: Advanced Optical Manufacturing Technologies* (p. 765507). SPIE.

Liu, Y., Gong, S., Li, J., & Cao, J. (2017). Effects of dressed wheel topography on patterned surface textures and grinding force. *International Journal of Advanced Manufacturing Technology, 93*, 1751-1760.

Liu, Y., Zhao, W., Zhou, T., Liu, X., & Wang, X. (2017). Microgroove machining on crystalline nickel phosphide plating by single-point diamond cutting. *International Journal of Advanced Manufacturing Technology, 91*, 477-484.

Marinov, V. (2010). *Manufacturing Technology.* Eastern Mediteranian University.

Mueller, S., Wirtz, C., Trauth, D., Mattfeld, P., & Klocke, F. (2018). Material removal mechanisms in grinding of two-phase brittle materials. *International Journal of Advanced manufacturing Technology, 95*, 287-298.

Mummery, L. (1992). *Surface Texture Analysis The Handbook.* Hommelwerke Gmbh.

Nadolny, K., & Kaplonek, W. (2012). Design of a device for precision shaping of grinding wheel macro- and micro-geometry. *Journal of Central South University*, 135-143.

Nakanishi Inc. (2015). E4000 Series Catalogue.

Ohmori, H., Takahashi, I., & Bandyopadhyay, B. P. (1996). Ultra-precision grinding of structural ceramics by electrolytic in-process dressing (ELID) grinding. *Journal of Materials Processing Technology, 57*, 272-277.

Ok, T. J., Lopez-Ona, E., Nikitopoulos, D. E., Wong, H., & Sunggook , P. (2011). Propulsion of droplets on micro- and sub-micron ratchet surfaces in the Leidenfrost temperature regime. *Microfluid Nanofluid, 10*, 1045-1054.

Oliveira, J. F., Bottene, A. C., & Franca, T. V. (2010). A novel dressing technique for texturing of ground surfaces. *CIRP Annals - Manufacturing Technology*, 361-364.

Oliveira, J. F., Silva, E. J., Guo, C., & Hashimoto, F. (2009). Industrial challenges in grinding. *CIRP Annals - Manufacturing Technology*, 663-680.

Picard, Y. N., Adams, D. P., Vasile, M. J., & Ritchey, M. B. (2003). Focussed ion beam-shaped microtools for ultra-precision machining of cylindrical components. *Precision Engineering, 27*, 59-69.

Pratap, T., & Patra, K. (2018). Micro ball-end milling - An emerging manufacturing technology for micro-feature patterns. *International Journal of Advanced Manufacturing Technology, 94*, 2821-2845.

Precitech . (2007). Nanoform 250 Ultra Installation & Maintenance Manual P869.

Precitech. (2009). Installation and Operation Manual M17931/A. *Precitech Grinder Systems - Supplementary Manual*.

Precitech. (2014). Nanoform 250 Ultra Grind Precision Diamond Turning Lathe - Data Sheet. New Hampshire, USA: Precitech Inc.

Raguin, D. H., & Morris, M. G. (1993, March 1). Antireflection structured surfaces for the infrared spectral region. *Applied Optics, 32*(7), 1154-1167.

Ruotao, F., Wenjie, Z., Xuedong, W., & Qunji, X. (2012). Ratchet composite thin film for low-temperature self-propelled Leidenfrost Droplet. *Journal of Colloid and Interface Science*, 450-454.

Scholz, S. G., Sampaio, D. J., Mangang, M., & Pfleging, W. (2017). Process and parameter optimisation for micro structuring of 3D freeform metallic surfaces: a comparative study of short-pulse (nanosecond) and ultrafast (picosecond, femtosecond) laser ablation. *Proc. of SPIE: Laser-based Micro- and Nanoprocessing XI. 10092.* SPIE.

Silva, E. J., Oliveira, J. F., Salles, B. B., Cardoso, R. S., & Reis, V. R. (2013). Strategies for production of parts textured by grinding using patterned wheels. *CIRP Annals - Manufacturing Technology*, 355-358.

Steinkopf, R., Hartung, J., Kinast, J., Gebhardt, A., & Risse, S. (2015). Structured surfaces on metal optics. *Material Technologies and Applications to Optics, Structures, Components and Sub-Systems II. 9574.* SPIE.

Stepien, P. (2007a). Grinding forces in regular surface texture generation. *International Journal of Machine Tools & Manufacture*, 2098-2110.

Stepien, P. (2007b). Undeformed chip sizes in grinding process of regular surface texture generation. *The Archive of Mechanical Engineering, 54*(3), 235-259.

Stepien, P. (2011). Deterministic and stochastic components of regular surface texture generated by a special grinding process. *Wear 271*, 514-518.

Stout, K. J., & Blunt, L. (2001). A contribution to the debate on surface classifications - random, systematic, unstructured, structured and engineered. *International Journal of Machine Tools & Manufacture*, 2039-2044.

Telang, A. (2014). Static Stiffness Analysis of High Frequency Milling Spindle. *International Journal of Research in Engineering and Technology, 3*, 577-585.

To, S., Zhu, Z., & Zeng, W. (2015). Novel end-fly-cutting-servo system for deterministic generation of hierarchical micro-nanostructures. *CIRP Annals - Manufacturing Technology, 64*, 113-136.

Tong, Z., & Luo, X. (2015). Investigation of focused ion beam induced damage in single crystal diamond tools. *Applied Surface Science, 347*, 727-735.

Wang, J., Jiang, X., Blunt, L. A., Leach, R. K., & Scott, P. J. (2012). Intelligent sampling for the measurement of structured surfaces. *Measurement Science and Technology*.

Wang, W., Liu, B., Jiang, G., Mei, X., Wang, Z., & Wang, K. (2016). Study on hierarchical structured PDMS for surface super-hydrophobicity using imprinting with ultrafast laser structured models. *Applied surface science, 364*, 528-538.

Wegener, K., Hoffmeister, H. W., Karpuschewski, B., Kuster, F., Hahmann, W. C., & Rabiey, M. (2011). Conditioning and monitoring of grinding wheels. *CIRP Annals - Manufacturing Technology*, 757-777.

Xie, X. Z., Chen, G. Y., & Li, L. J. (2004). Dressing of resin-bonded superabrasive grinding wheels by means of acousto-optic Q-switched pulsed Nd:YAG laser. *Optics & Laser Technoloty*, 406-419.

Yan, J., Kaneko, T., Uchida, K., Yoshihara, N., & Kuriyagawa, T. (2010). Fabricating microgrooves with varied cross-sections by electrodischarge machining. *International Journal of Advanced Machining Technology, 50*, 991-1002.

Yan, J., Zhang, Z., Kuriyagawa, T., & Gonda, H. (2010). Fabricating micro-structured surface by using single-crystalline diamond endmill. *International Journal of Advanced Manufacturing Technology, 51*, 957-964.

Zhang, C., & Shin, Y. C. (2002). A novel laser-assisted truing and dressing technique for vitrified CBN wheels. *International Journal of Machine Tools & Manufacture*, 825-835.

Zhang, J., Li, Q., Zhang, H., Cui, Q., Cui, T., Ge, C., . . . Zhang, D. (2017). Fast generation of micro structured surface by applying PCD tools in micro turning. *International Journal of Advanced Manufacturing Technology, 90*, 1165-1176.

Zhang, S. J., To, S., Wang, S. J., & Zhu, Z. W. (2015). A review of surface roughness generation in ultra-precision machining. *International Journal of Machine Tools & Manufacture, 91*, 76-95.

Zhong-Chen, C., Chi Fai, C., Lai Ting, H., & Ming Yu, L. (2017). Theoretical and experimental investigation of surface generation in swing precess bonnet polishing of complex three-dimensional structured surfaces. *Precision Engineering, 50*, 361-371.

Zhu, W.-L., Yang, S., Ju, B.-F., Jiang, J., & Sun, A. (2016). Scanning tunneling microscopy-based on-machine measurement for diamond fly cutting of micro-structured surfaces. *Precision Engineering, 43*, 308-314.

Zhu, W.-L., Zhu, Z., Ren, M., Ehmann, K. F., & Ju, B.-F. (2016). Modeling and analysis of uncertainty in on-machine form characterisation of diamond-machined optical micro-structured surfaces. *Measurement Science and Technology, 27*.